Airborne Optical Systems Testbed: FEMA Support of Puerto Rico's Recovery from Hurricane Maria

Humanitarian Assistance
and Disaster Relief
Systems Group

28 July 2021

Lincoln Laboratory
MASSACHUSETTS INSTITUTE OF TECHNOLOGY
LEXINGTON, MASSACHUSETTS

Massachusetts Institute of Technology
Lincoln Laboratory

Airborne Optical Systems Testbed: FEMA Support of Puerto Rico's Recovery from Hurricane Maria

Humanitarian Assistance and Disaster Relief Systems Group
Group 21

Project Report AOSTB-1

28 July 2021

Lexington   Massachusetts

This page intentionally left blank.

EXECUTIVE SUMMARY

Hurricane Maria struck Puerto Rico on 20 September 2017. This catastrophic storm devastated the island with sustained winds of 155 mph and more than 37 inches of rainfall. As the recovery progressed into early 2018, MIT Lincoln Laboratory (MIT LL) was requested to provide support utilizing the Airborne Optical Systems Testbed, a state-of-the-art Geiger-mode (GM) LIDAR remote sensing platform capable of creating a high-resolution, three-dimensional model of the entire island.

In 30 days, MIT LL collected the vast majority of Puerto Rico's 3,500 square miles, including the islands of Culebra and Vieques. Those data were then processed on the MIT Lincoln Laboratory Super Computer, generating three-dimensional data products that could be leveraged by FEMA to support site inspections.

A significant level of effort was expended to establish methods for turning the amassed data into actionable products. For several months, MIT LL maintained a presence at the Joint Recovery Office (JRO), providing direct support to the Transportation Sector. Together, the Laboratory and FEMA JRO developed a workflow for using the collected GM-LIDAR data to conduct virtual site inspections of roadways damaged by flooding and landslides. MIT LL developed a training program for this workflow and delivered it to more than 100 staff at the JRO. Additional staff at MIT LL conducted virtual site inspections from the Laboratory in Lexington, MA.

Efforts were made to leverage the collected data outside of the original scope, but a combination of factors led to mixed results. These factors included resistance on the part of FEMA staff and challenges with the actual data, such as horizontal georegistration and compatibility of the initially delivered data projections. Despite improvements made to the data, insertion of a vastly new technology into an already complex recovery proved very challenging.

While developing the manual exploitation workflows and trainings, MIT LL was able to better understand the FEMA analysts' needs and began the development of several artificial intelligence/machine-learning (AI/ML) algorithms to automate the exploitation. The rate and volume of data collection for disasters has increased to the point where it is no longer human actionable, so the development of these automated exploitation algorithms is key to making use of emerging technologies.

Through this work, MIT LL has identified numerous challenges that are inherent to using any sensor to support disaster response and recovery. Providing comprehensive analytical input to answer the questions required by FEMA will require different sensor packages with different resolutions, collection rates, and revisit time, and these sensor packages must be paired with corresponding algorithms for exploitation. By taking a systems-level approach, MIT LL has developed a framework to solve many of the identified challenges.

The efforts in Puerto Rico have shown that the application of GM-LIDAR to virtual damage assessments can achieve an improvement in accuracy and efficiency, particularly in similarly wide-scale and catastrophic events. Even greater impact can be achieved with continued development of AI/ML algorithms to automate these virtual damage assessments. However, the success of any future remote sensing-based support of damage assessments will require both the continued adaptation of FEMA policies to leverage this technology and clearly articulated and understood characterization of sensor platforms and accompanying algorithms.

TABLE OF CONTENTS

Page

TABLE OF CONTENTS
(Continued)

Page

LIST OF ILLUSTRATIONS

LIST OF ILLUSTRATIONS
(Continued)

LIST OF ILLUSTRATIONS
(Continued)

LIST OF ILLUSTRATIONS
(Continued)

LIST OF TABLES

This page intentionally left blank.

1. INTRODUCTION

1.1 AOSTB CAPABILITY OVERVIEW

The MIT Lincoln Laboratory (MIT LL) Airborne Optical System Testbed (AOSTB) is a Geiger-mode LIDAR (GM-LIDAR) system capable of rolling on and off an aircraft. Similar to traditional LIDAR systems, the AOSTB sends pulses of laser light from an aircraft to the ground, and records the return time of the reflection of that laser light in order to determine the distance from the aircraft to points on the ground. These distance measurements are then combined with location data to generate a high-resolution, three-dimensional (3D) model of the Earth's surface. The AOSTB differs significantly from traditional LIDAR in that the sensor recording the returning laser light is an advanced avalanche photodiode (APD), which is capable of detecting single photons of light. The high sensitivity of the APD enables the 3D models that are created to be of much higher resolution than traditional LIDAR, and are created much faster than a traditional LIDAR system.

Quickly acquired, high-resolution, accurately measurable 3D models of an area affected by disaster provide a rich dataset for emergency managers to leverage in support of the recovery efforts. Collecting those data shortly after a disaster establishes this rich dataset not only for response, but a permanent data record that can support long-term recovery and future mitigation or planning efforts.
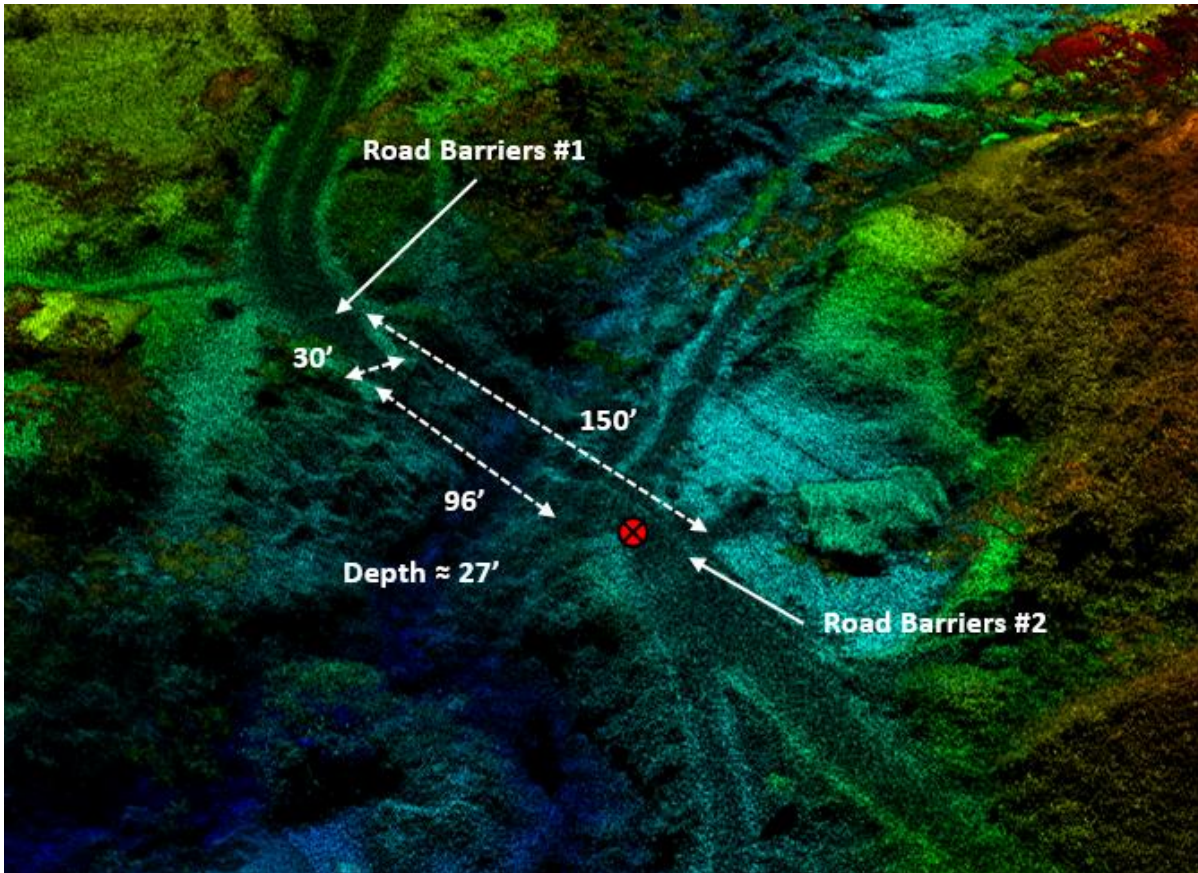
Figure 1. Sample AOSTB data showing PR-770 road washout, annotated with damage measurements.

1.1.1   Data Collection

The roll-on/roll off capability allows the AOSTB to be coupled with the aircraft most appropriate to the mission. For smaller area collections, the AOSTB has been flown on a Twin Otter, and for large-scale collections such as Puerto Rico, a Basler BT-67 modified DC-3 has been used.

The following table shows an overview of the typical data collection parameters.

TABLE 1

Data Collection

Point Spacing/ Resolution	Point Density	Aircraft	Collection Altitude	Aircraft Speed	Area Collection Rate
25 cm	>25 ppm^2	BT-67	10k ft. msl	150 knots	40 mi^2/hour

1.1.2 Data Processing

Supporting these wide-area data collections is a custom data processing pipeline that runs on the MIT Lincoln Laboratory Super Computer (LLSC). This pipeline processes the raw collected data through the typical intermediate data associated with LIDAR, but adds additional data products that are specifically geared towards understanding human activity in a given area. The data are processed into tiles that are roughly 500 m^2 in size. The table below shows the products produced by the MIT LL pipeline:

TABLE 2

Data Products

Name	Data Type	File Type	Ext	Description
HAG	Point Cloud	Binary Point Format	BPF	Height Above Ground: A point cloud where each point has X, Y, and Z values, plus an additional attribute (HAG), which is the point's height above the bare earth/ground surface
L3	Point Cloud	LASer	LAS	LAS files are the typical point-cloud data associated with LIDAR; each point in the data has an X, Y, and Z attributes
BE	Point Cloud	Binary Point Format	BPF	Bare Earth: A point cloud representing only those points determined to be the bare earth/ground surface
DTM	Raster	GeoTiff	TIF	Digital Terrain Model: A rasterized version of the bare earth product
DSM	Raster	GeoTiff	TIF	Digital Surface Model: A rasterized version of the LAS product
RII	Raster	GeoTiff	TIF	Relative Intensity Image: A rasterized representation of the relative intensity of light reflections

1.1.3 Data Resolution

AOSTB collects point cloud data with 25 cm point spacing. This 3D model of the collected area can be measured accurately to within that 25 cm point spacing, with a maximum error of 50 cm. One way to think of the data is creating a model of the Earth using basketball-sized spheres.

Determining the relative quality of the resolution compared to traditional LIDAR collections requires some background on industry standards. The most traditional use of LIDAR is to establish a digital elevation model of an area. The U.S. Geological Survey (USGS) has established the 3D Elevation Program (3DEP), which sets standards for data collection and quality standards for LIDAR collected in support of the 3DEP. Those standards are codified in the USGS LIDAR Base Specification [1]. There are some requirements for LIDAR collected for the 3DEP that cannot be met by utilizing AOSTB in a disaster context. First, some requirements cannot be met due to the fundamental differences between GM-LIDAR and traditional LIDAR. Secondly, the USGS sets forth requirements about the acceptable environmental conditions for a 3DEP collection, specifically excluding the types of conditions most likely encountered in a disaster (e.g., flooding).

Although GM-LIDAR may not currently be applicable to the USGS 3D Elevation Program, the LIDAR base specification does provide some indication of how the AOSTB data quality compares to traditional LIDAR collections in terms of point spacing and point density. The base specification provides "quality levels" for data, ranging from QL0 (highest quality) to QL3 (minimum quality). Two relevant USGS quality levels and corresponding AOSTB performance are shown in TABLE 3.

TABLE 3

USGS 3DEP Quality Levels

Quality Level	Aggregate Nominal Point Spacing (m)	MIT LL AOSTB Point Spacing (m)	Aggregate Nominal Pulse Density (pls/m^2)	MIT LL AOSTB point Density (pls/m^2)
QL0	≤0.35	0.25	≥8.0	≥25

1.1.4 Operational Timing

The AOSTB can collect large areas of high-resolution data quickly, and the MIT LL Super Computer can process that data quickly. For planning purposes, the timeline below illustrates each phase in the typical mission and the associated timing for an area of 250 mi^2.

TABLE 4

Operational Timing for 250 mi²

Aircraft Acquisition	Sensor Installation	Travel to Staging	Flight Time (250 mi²)	Data Transfer (ideal conditions)	Data Processing LLSC	Total Collection/Processing Timing (250 mi²)
Varies	24 hours	24 hours	6 hours	3.5 hours	23.5 hours	33 hours

As indicated in the table, if an aircraft were readily available, the AOSTB could be considered for pre-deployment to an impending disaster (e.g., hurricane) and be useful in the response timeframe by collecting and processing an area of 250 mi² (about the size of Chicago) within the first 36 hours.

After the initial data processing, subsequent analysis can be conducted to automate various damage assessment tasks such as road finding, road damage, and debris volume estimation.

1.2 CAPABILITY SUMMARY

The AOSTB provides a proof of concept, showing that GM-LIDAR can be used to quickly create a high-resolution, measurable 3D model of a wide area after a disaster impact and that those measurable data can be leveraged to support operational and financial decision making during the recovery process.

The algorithms developed for GM-LIDAR provide a pathway towards automating analysis such as road identification and road damage detection at scale. These analytics could enable additional decision-making inputs such as optimized routing for emergency vehicles and detection of isolated communities.

This page intentionally left blank.

2. PUERTO RICO CAMPAIGN NARRATIVE

To support the Federal Emergency Management Agency's (FEMA), MIT Lincoln Laboratory agreed to provide advanced airborne 3D LIDAR sensing capabilities and associated data exploitation to generate data products directly relevant to FEMA's recovery needs in post-Hurricane Maria Puerto Rico. The three goals below were central to this effort and encapsulate the purpose behind MIT LL's support.

1. Demonstrate remote inspection and damage assessment of high-interest target areas and assets through airborne GM-LIDAR remote sensing, as directed by FEMA decision makers.

2. Create a high-resolution 3D baseline model of the Puerto Rico mainland and the islands of Vieques and Culebra to facilitate island-wide recovery planning and monitoring as well as preparedness activities for future disaster response activities.

3. Develop and deliver user-accessible analytics tools and utilities to emergency management analysts and decision makers and provide technical training for these capabilities.

To ensure that MIT LL's efforts were pertinent and timely to FEMA's needs, the MIT LL team worked closely with FEMA's coordinating efforts, managed primarily from FEMA's Joint Field Office in Puerto Rico.

2.1 PUERTO RICO DATA COLLECTION

MIT LL has a long history in the design and development of novel and highly capable airborne sensor systems and, in support of these efforts, operates the MIT Lincoln Laboratory Flight Test Facility (FTF). This FTF maintains and operates a small fleet of aircraft suitable for sensor hardware testing and data collection operations, and up through April 2018, AOSTB activities had utilized an FTF-operated Twin Otter aircraft, capable of ~4-hour sorties and air speeds between 100–150 knots. This type of aircraft is popular around the world, has seen extensive service within the Laboratory's many airborne sensor development activities, and is well suited for small-scale and short-range aircraft needs.

Natural disaster environments experienced by the U.S. routinely extend across thousands of square miles, however, and Hurricane Maria's impact across the entirety of Puerto Rico was no exception. The land area impacted by Hurricane Maria was approximately 3,500 mi^2, and FEMA requested a complete 3D map of the Commonwealth as best possible to facilitate task-oriented analytics for recovery activities. Were a Twin Otter-type aircraft to be used, realistic time estimates for a flight campaign with adequate sensor coverage overlap extended to several months in duration; this timeframe would have extended well in to the following rainy season, reducing the likelihood of completion or operational success. To mitigate this risk and reduce the expected flight campaign completion timeframe, alternative airframes were explored that might yield a sufficient net increase in daily area coverage. 3DEO Inc. (a Massachusetts-based small business that specializes in GM-LIDAR technology and that was created as a Lincoln Laboratory spinoff)

aided MIT LL in identifying and evaluating several candidate alternative airframes against anticipated performance, cost, and availability, and MIT LL ultimately selected a BT-67 operated by Airtec as an airframe for sensor installation and deployment to Puerto Rico. A re-manufactured DC-3 purpose-built by Basler Turbo Conversions for science missions, the BT-67 has been historically used on behalf of USG-sponsored airborne sensing and LIDAR missions in glacier and ice research. MIT LL installed the AOSTB sensor aboard the BT-67 aircraft, conducted a short series of local checkout and calibration flights, and ferried down to Puerto Rico in a single nonstop flight.
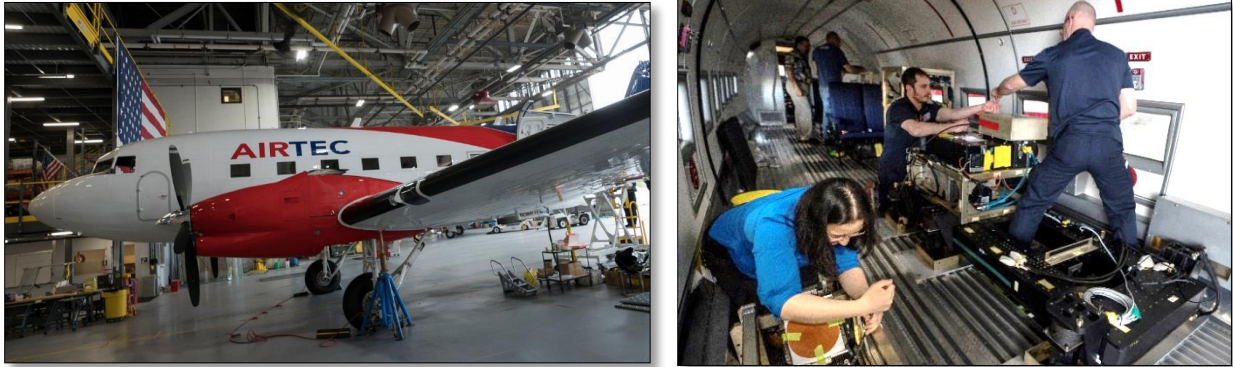
Figure 2. The BT-67 aircraft newly arrived in the MIT LL Flight Test Facility hangar, and Basler and Lincoln Laboratory technical staff performing the sensor installation.
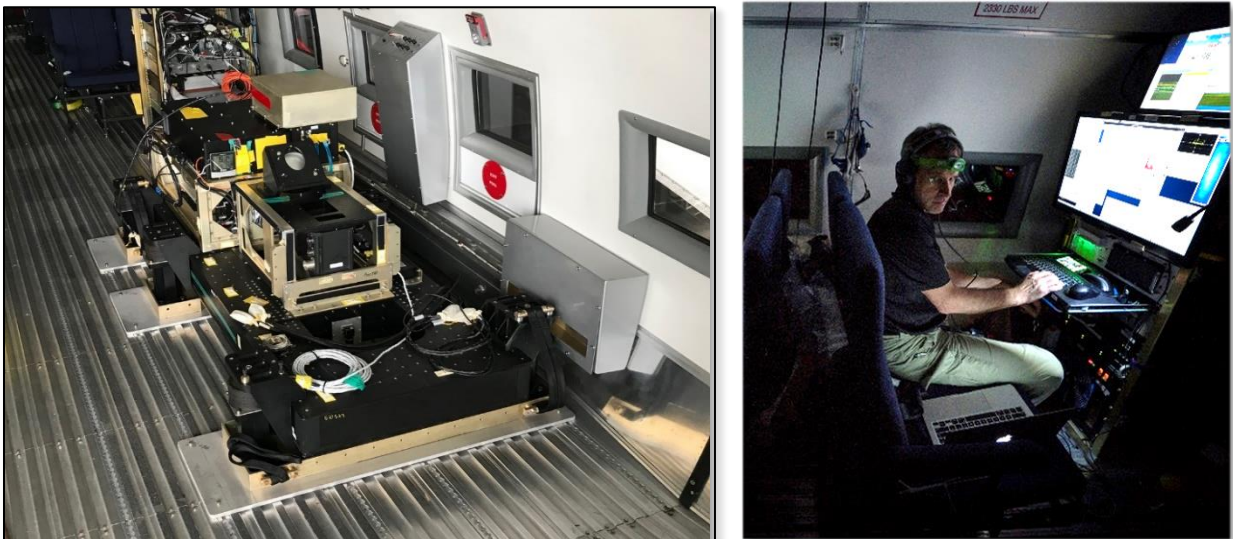
Figure 3. The AOSTB sensor instrument on board the BT-67 aircraft. 3DEO LIDAR engineers played an extensive role in flight planning, mission command, and sensor operation throughout the data collection campaign.

8

The AOSTB utilizes single-photon-sensitive, time-of-flight imaging technology to collect information about the surface characteristics of the land below; this advanced GM-LIDAR system is 10 to 100 times more capable than commercial system available and can collect wide-area, high-resolution, 3D datasets very rapidly. When flown over a disaster site, the system sends out pulses of laser light that bounce off the land and structures below and are collected again by the instrument. The timing of each light pulse's return to the instrument is used to build what researchers call a "point-cloud map," a high-resolution 3D model of the scanned area that depicts the heights of structures and landscape features. GM-LIDAR is uniquely capable of balancing point density, area coverage rate, and foliage penetration, and in these efforts, the instrument and aircraft operating parameters were configured to balance these criteria across the flight campaign.

TABLE 5

Puerto Rico Campaign Summary

Point Spacing/ Resolution	Point Density	Aircraft	Collection Altitude	Aircraft Speed	Area Collection Rate	Sorties	Collection Time
25 cm	25 ppm^2	BT-67	10k ft msl	150 kts	40 mi^2/hour	23	30 days

The effort's first mission was flown the night of 30 May, and the broader campaign extended through June. A total of 23 sorties were flown over approximately 30 days. Throughout the flight campaign, Lincoln Laboratory staff were aided by LIDAR engineers and flight campaign data collection experts at 3DEO. Through the use of the long-endurance BT-67, MIT LL was able to double the per-flight data collection rates, with airtimes per sortie approaching eight hours. Coordination with FEMA's transportation sector for flight mission priorities and status occurred at the FEMA Joint Field Office in Guaynabo, with primary flight and sensor operations based out of Isla Verde Airport near San Juan. This overall team was structured in to two components.

Mission Planning and FEMA Coordination, focused on the FEMA Joint Recovery Office in Guaynabo, PR

- Coordinated and negotiated FEMA priorities
- Liaisoned with external organizations
- Planned and coordinated collection campaign
- Prepared task requests and delivered to flight planners
- Guided analytics development, data products, and reported to FEMA

Flight and Sensor Operations, conducted out of Isla Verde Airport near San Juan

- Refined task requests and translated to flight plans
- Executed sorties
- Quick-turned data quality assessment
  - Transfered data to Lexington for processing and local archive

Flight and sensor personnel roles were carefully defined to ensure safe, consistent, and sustainable operations during the near constant level of activity throughout June 2018:

TABLE 6

Roles and Responsibilities

Role	Responsibility
Collection Manager	Liaison/coordination w/mission planning and data processing
	Flight tasking, planning, staffing, and site operations
Mission Commander (flight crew)	Plan flight and lead sensor flight team
	Coordinate with pilot
	Maintain flight log and lead flight debrief
	Draft and deliver situation report to Collection Manager
Sensor Operator (flight crew)	Ensure sensor scan modes, target details, etc., are loaded and ready
	Prepare and maintain sensor mission readiness
	Operate sensor and data recorder
OBP Operator (flight crew)	Monitor sensor and onboard processor (OBP)
	Trouble-shoot sensor as needed
Standby Operator (flight crew)	Support any flight crew role as needed
	Provide ground support as possible
Data Manager	Offload data
	Initiate and monitor data transfer
Ground Support	Debug sensor issues
	Generate quick-look reports from OBP data
	Support flight crews and data operations

In addition to the above on-site roles, personnel on staff at MIT LL support the nightly sorties, particularly in advanced weather near- or now-casting. Given the time sensitivity of the response and data

collection, it was critical that each sortie be effectively planned and conducted, which required the best possible understanding of island-wide cloud cover. Meteorology specialists at MIT LL provided daily updates to the flight operations team in Puerto Rico, in some cases in the hours and minutes remaining before wheels-up, to ensure that the nightly collection area was well chosen for best visibility and atmospherics.

At wheels-down after each nightly sortie, the collected data were retrieved from the aircraft, error-checked, redundantly backed up locally, and a set of drives either shipped (or hand-carried by staff naturally rotating in and out) to Massachusetts for processing using intensive computational resources. Given the level of destruction in Puerto Rico, electronic means of data transfer were unacceptably slow and unreliable.
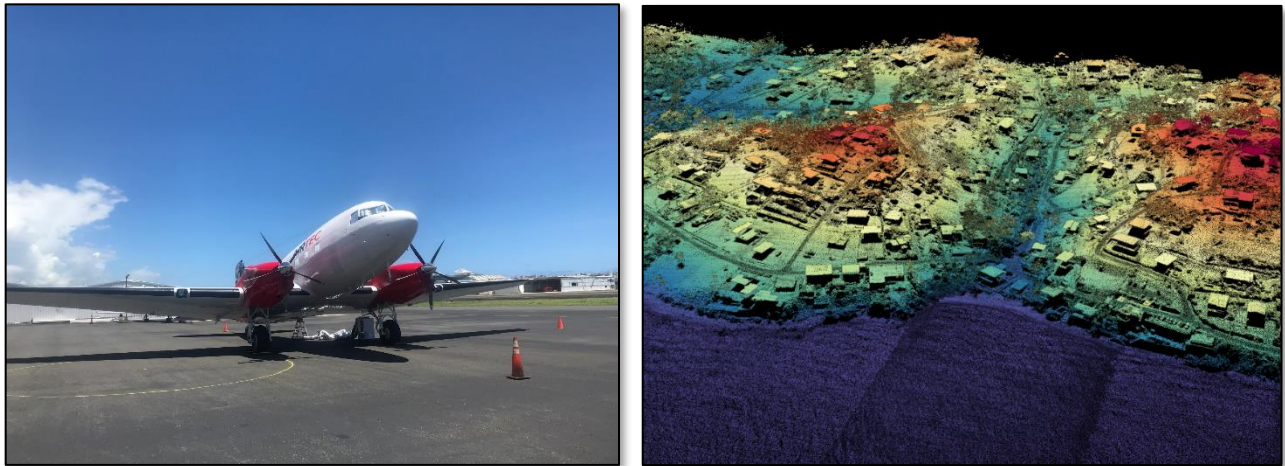
Figure 4. The BT-67 with installed sensor at Isla Verde Airport. The islands of Culebra (shown) and Vieques were some of the first regions of Puerto Rico collected during the campaign.

2.2 DATA PROCESSING

The raw sensor data collected during an AOSTB collection sortie is a series of measurements from 1) the Global Positioning System (GPS) and inertial measurement unit (IMU) to locate and orient the sensor in space, 2) the mirror's direction pointing the laser, and 3) the sensor's measurements of the laser's returns. These various pieces of raw data must be combined, along with other inputs like sensor calibration, to create every point in the resulting GM-LIDAR point cloud. This multi-phased process of combining all these inputs is generally referred to as data processing and performed by our processing pipeline.

The processing pipeline is a custom-built software suite developed by MIT Lincoln Laboratory. It uses a divide and conquer approach to break the collected area into equal-area geospatial buckets. This breaks the workload into tractable pieces and allows us to distribute the work across multiple computer

nodes for high-performance parallel processing. Each bucket in turn has multiple phases of processing, each further refining the resulting GM-LIDAR products.

The general pipeline steps are:

- Combine raw data streams (L0) and break into buckets of noisy point clouds (L05)
- For each bucket:
  - Perform coincidence processing to produce a single-view point cloud (L2)
  - Intelligently aggregate point clouds from multiple line-of-sight-angles to produce aggregated point clouds (L3)
  - Run additional exploitation algorithms to extract data (L4) from aggregated point clouds. Some examples of these L4 products are:
    - Digital Surface Model
    - Digital Terrain Model
    - Bare Earth Model
    - Height Above Ground
    - Feature Extraction

Each of the phases of processing mentioned has numerous parameters to optimize for different operational needs. One example is the software suite provides multiple coincidence processing algorithms, each optimized for different goals. Some algorithms are better suited to foliage penetration, others optimize for image quality and linear features like walls and power lines, and still others optimize for near real-time processing speed. These built-in capabilities are critical to meeting real-world processing requirements.

For the Puerto Rico GM-LIDAR processing, 500 m^2 buckets were used, resulting in ~38,000 buckets to cover the island. Each bucket produced 6 or more L4 products, resulting in more than 228,000 individual product tiles. This processing was performed on the LLSC, offering petaflop-scale processing with more than 41,000 processor cores available. This scale allowed us more flexibility iterating on various processing parameters and approaches. The flexibility of the processing pipeline means a supercomputer is not required. Processing has also been performed on small portable mini-clusters and Amazon Web Services for cloud processing to support various operational limitations and timing requirements.

2.3   DATA DISTRIBUTION

To enable distribution of processed GM-LIDAR data, MIT LL developed and deployed an externally facing web application called VIEWS. To protect against the unauthorized viewing of the data, VIEWS requires users to register for an account via the FEMA-RS-VIEWS-APPROVAL@ll.mit.edu email address. Separate accounts can be created for the three datasets served by the app (e.g., Puerto Rico, North Carolina, and South Carolina). When approved, the user is then granted access to VIEWS (https://fema-rs.hadr.ll.mit.edu/) and can visualize and download GM-LIDAR data and associated data products. VIEWS is shown in Figure 5.
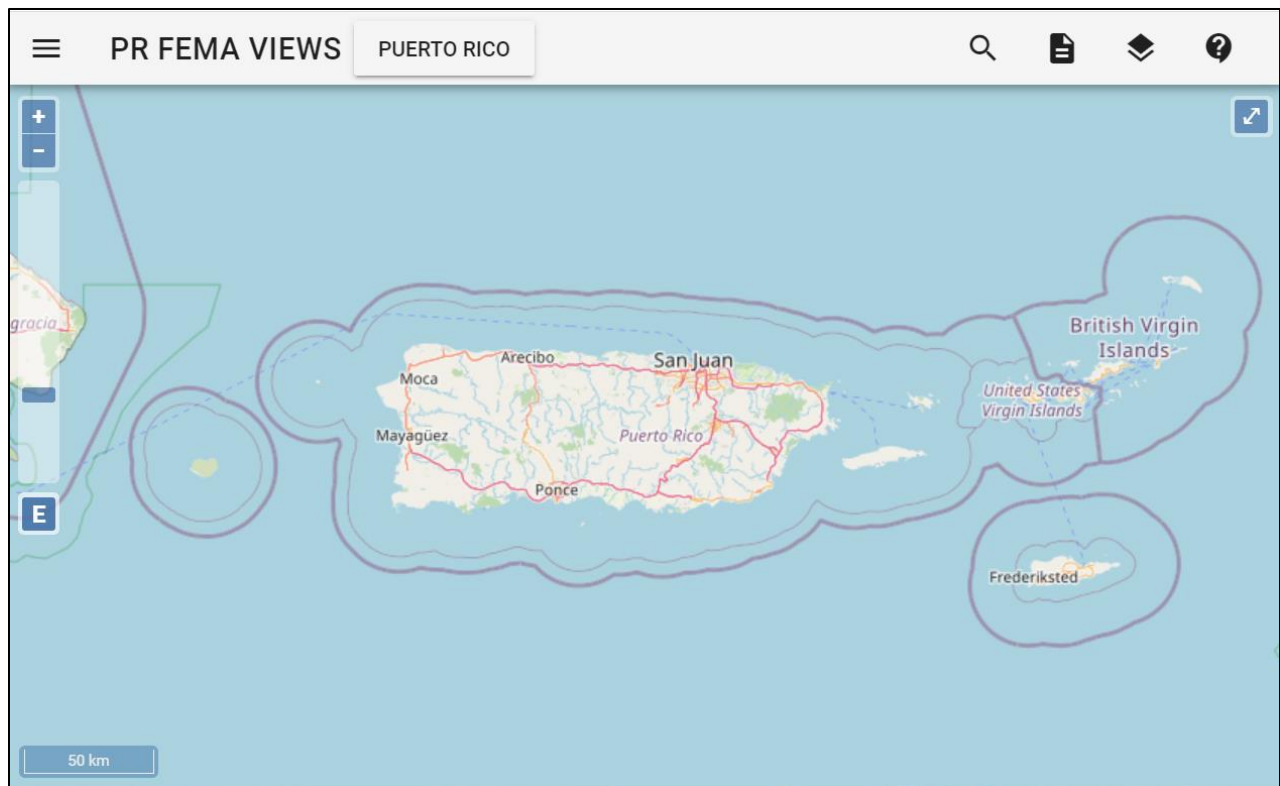
Figure 5. The VIEWS user interface.

Figure 6. The VIEWS control bar.

From left to right, the top control bar as highlighted in Figure 6 contains these controls:

1. A menu that allows access to sortie flight data, map overlays such as live weather satellite data, GM-LIDAR data, the VIEWS help page, and a logout control

2. A selector for the dataset to view (set here to Puerto Rico)

3. A search button that allows the user to search by name for places and landmarks, or by latitude–longitude coordinate

4. A details button

5. A map layers button that allows the user to select from map base layers, including OpenStreetMaps and satellite views

6. A button to send email to the VIEWS team via FEMA-RS-VIEWS-FEEDBACK@ll.mit.edu to suggest features or report bugs

VIEWS also allows the user to see the flight path for each collection sortie (see Figure 7).
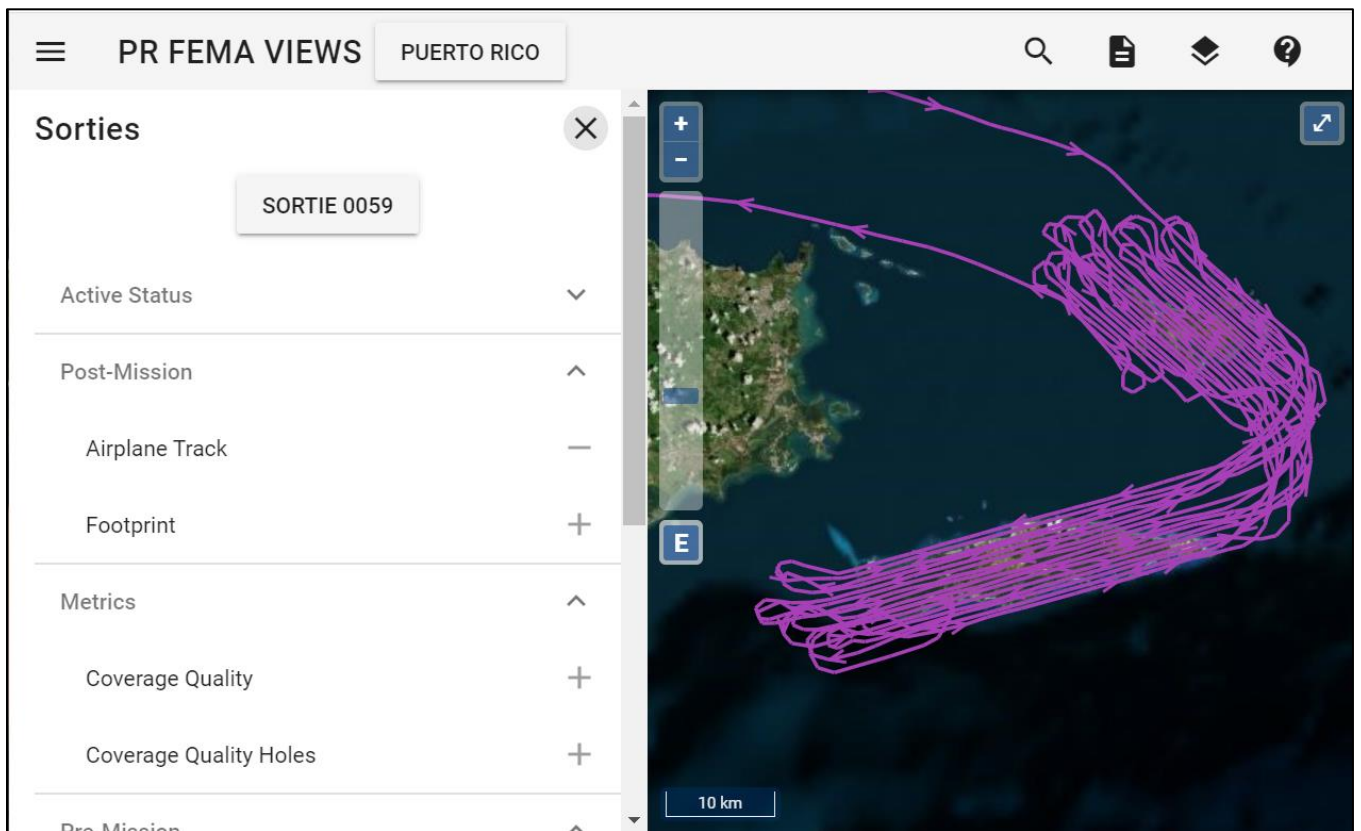
Figure 7. Flight path for one sortie over Culebra and Vieques, shown over a satellite base map.

Through a grid-based interface, the user can select multiple processed tiles and download the corresponding GM-LIDAR point clouds and other generated data products (see Figure 8). Multiple files

are collected into a ZIP archive and automatically downloaded through the web browser. The user can then apply their analytical tools to the local copy of the data.
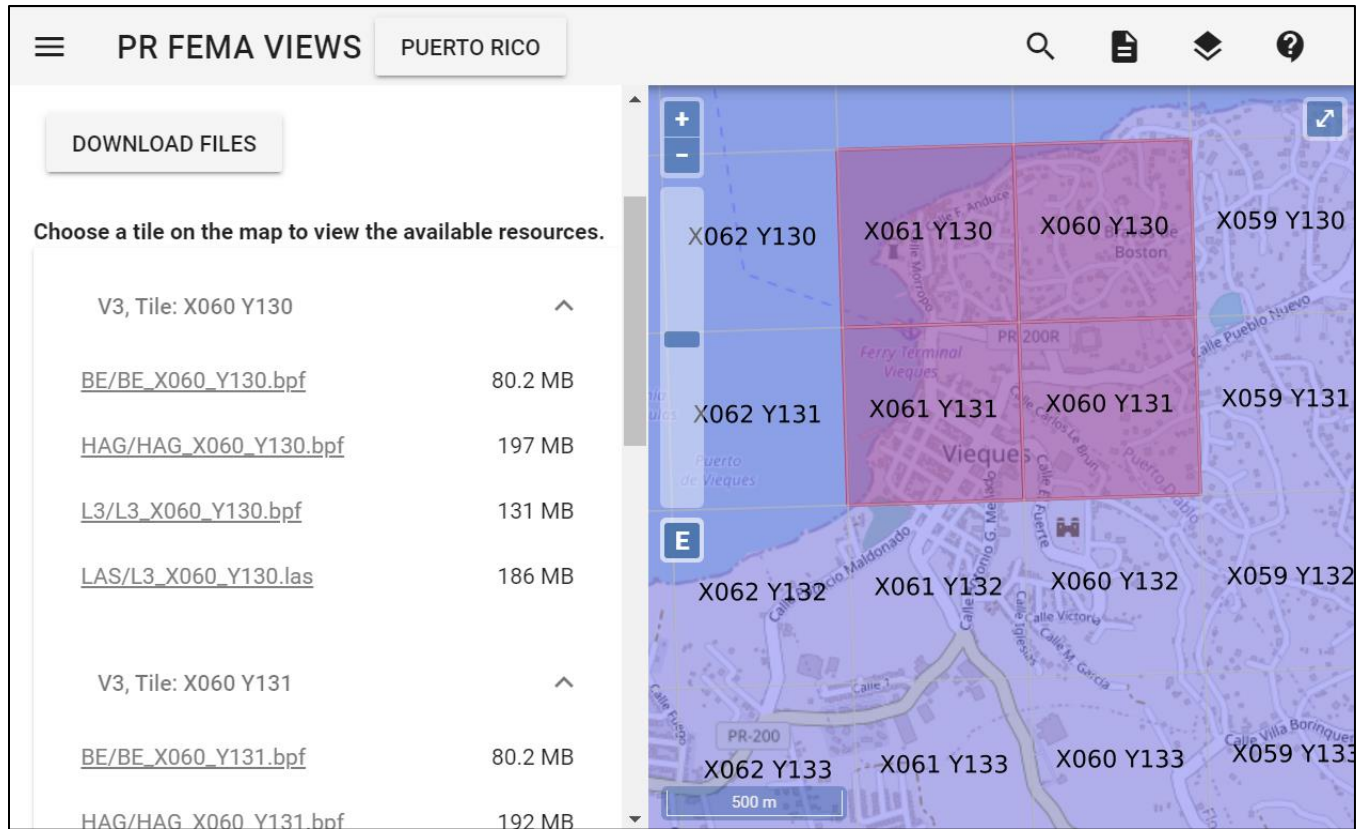
Figure 8. Downloading files for four selected tiles.

2.4 DATA SOCIALIZATION AND REFINEMENT

As use of the GM-LIDAR data extended into use cases beyond the transportation sector, MIT LL established a working group with approximately 25 individuals across 15 government, academic, and industry organizations. Representatives included FEMA, the U.S. Geological Survey (USGS), U.S. Army Corps of Engineers (USACE), and several companies working as contractors to FEMA for the Puerto Rico recovery. The working group provided valuable feedback and identified challenges related to the data that made exploitation to support their particular mission more difficult. MIT LL was able to address many of these challenges through the delivery of a reprocessed dataset for all of Puerto Rico. The major lines of effort are described below.

2.4.1 Horizontal Georegistration

The initial data delivery had suboptimal horizontal georegistration. The spatial relationships of the data were highly accurate internally, but when projecting the GM-LIDAR points to geographic coordinates, the placement was off. The initial dataset was still completely usable for the intended purpose of measuring damage to transportation sector concerns, but it was less useful for correlation with other geographic datasets. This limited further exploitation opportunities.

The discrepancies resulted from the rapid collection methodology over such a large area combined with hardware performance variations. The collection for Puerto Rico was a fast-paced effort, so there were no resources or time available to deploy or identify ground control points ahead of collection flights, a technique often used to achieve better horizontal georegistration accuracy.

In order to improve the horizontal georegistration on a whole-island scale as quickly as possible, MIT LL developed a processing methodology that correlated, in three dimensions, the data collected by AOSTB with a pre-existing LIDAR data collection performed for the USGS. By programmatically correlating major features that were unchanged between the pre-existing LIDAR collection and the AOSTB collection, the geographic coordinates of the pre-existing LIDAR could be adopted.

The end result of this effort was an island-wide dataset that has a horizontal georegistration accurate to within approximately three meters.

2.4.2 Datum and Coordinate System

The initial delivery of point cloud data was in BPF format, using the WGS 84/UTM datum and coordinate system. The vertical reference was in terms of height above ellipsoid. These are the default file formats and projections used for other MIT LL GM-LIDAR missions, but were not typical formats or projections consumed by FEMA analysts. Notable confusion arose around the elevation values, as some geographic features that are clearly above sea level would contain negative values since the ellipsoid approximating the Earth exceeded the actual surface in areas of Puerto Rico.

Through discussions with the working group and the JRO GIS Unit Leader, it was determined that the reprocessed data that would be most digestible by FEMA analysts would be data in the LAS format projected to the NAD83/Puerto Rico State Plane horizontal coordinate system, with a vertical datum referenced to the Puerto Rico specific datum PRVD02 [2].

The LAS format does not support the additional attributes present in the BPF format, such as "Height Above Ground" and "Relative Reflectivity", both of which are very useful for algorithm development, so the revised dataset would still include the BPF format as well.

These changes were all incorporated into Version 3 of the data delivery.

2.4.3 Data Delivery to US Army Corps of Engineers GRiD

Working group participants included representatives from the USACE Geospatial Repository and Data (GRiD) Management System, which is a U.S. government platform for hosting and disseminating point cloud data [3]. A plan was devised to publish all of the MIT LL AOSTB GM-LIDAR data products for Puerto Rico to the USACE GRiD platform. As part of the iterative reprocessing tests used to solve the aforementioned challenges, the data were also delivered to GRiD to identify the compatibility of the data and the best transfer mechanisms.

When Version 3 of the full island dataset was ready, MIT LL published it to its RS-VIEWS platform and provided a copy to the USACE GRiD team, and the full dataset was made publicly accessible on the USACE GRiD platform in June of 2019.

2.4.4 Island-Wide In-Browser Visualization

Both the RS-VIEWS and USACE GRiD systems provide distribution of dense point cloud data that spans large geographic areas by presenting the user with a map of the area containing data and then allowing the user to specify small areas to download. This approach works well for acquiring data for small study areas, but makes wide area exploration and visualization a challenge. The working group members also noted that the map interfaces were difficult for FEMA analysts to identify with and that a more direct, browser-based access to the point cloud data might make them more accessible and understandable.

MIT LL investigated several open source methods for visualizing three-dimensional point clouds through a web browser. The system provided by Entwine and Potree was chosen for the serializable capability of the Entwine format and the existing visualization and analysis tools available with Potree.

Entwine [4] organizes LIDAR point clouds (including GM-LIDAR) into an octree representation called Entwine Point Format (EPT). Similar to tiling two-dimensional imagery with different levels of resolutions to allow for smooth transition between large scale and small scale, this allows for sparse point clouds to be serialized at small scale ("zoomed out"), and more detail point data to be pulled in at larger scales ("zoomed in").

Potree [5] is a JavaScript-based web application that can ingest and visualize EPT data. This open source application also has many out of the box analysis tools.

The entire Puerto Rico dataset, consisting of more than 181 billion points, was converted to EPT format and can be seamlessly explored via web browser. Data can be measured in three dimensions and subsections of data can be exported as standard LAS files.
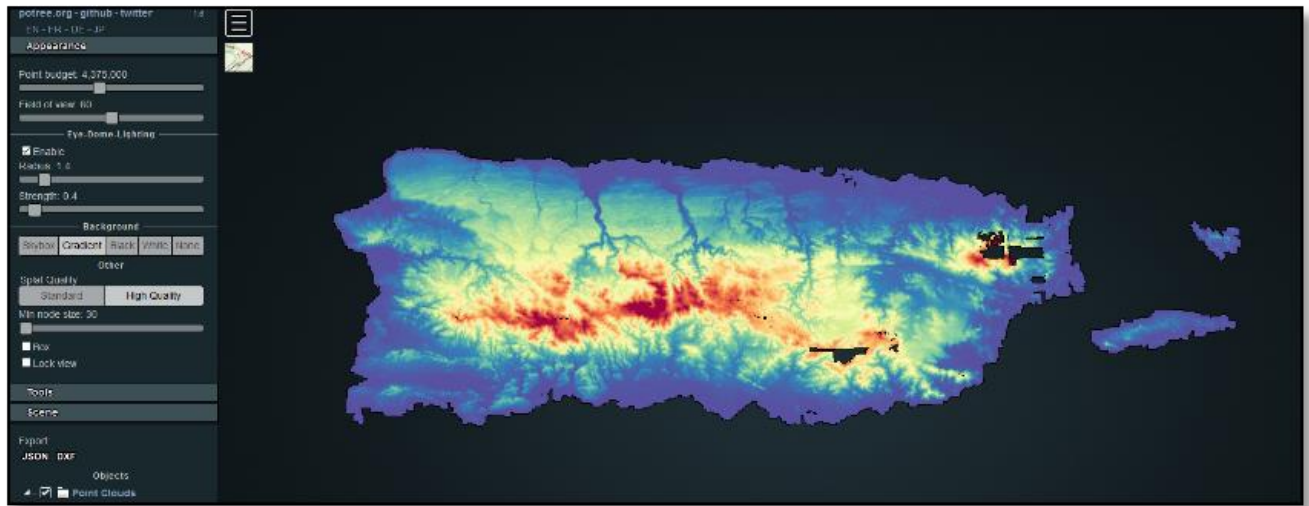
Figure 9. Puerto Rico Entwine/Potree.

There are challenges with the existing Potree application that could be addressed with further software development. For example, the most requested feature from the various users and partners that MIT LL shared the tool with was the ability to navigate to a known location (street address, point of interest name, etc.). Potree does allow for moving the location in view based on coordinates passed on the URL as parameters, but this is not a viable mechanism for most users.

The other gap with Potree is volume calculation. The tool does provide the user with the ability to select a volume using a stretchable cube, but the volume calculated is the volume of that cube and not of any points or voids within the cube. Potree is open source, so both of these features could be added with additional development time.
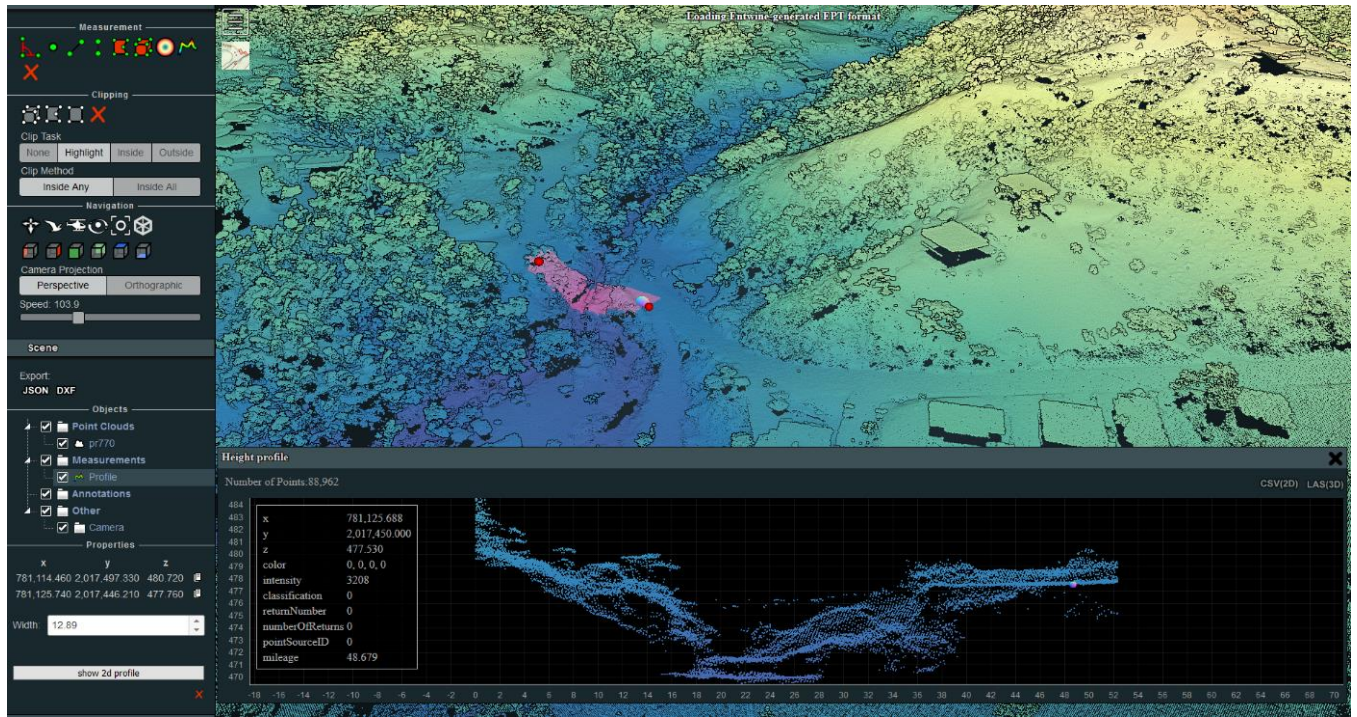
Figure 10. Profile visualization and data export options for damaged roadway.

This page intentionally left blank.

3. DATA EXPLOITATION

3.1   EVALUATED USE CASES

At the request of the JRO leadership, MIT LL created the "LIDAR Sector Fact Sheets" document. This document provides an assessment of how GM-LIDAR could be leveraged to satisfy the reporting requirements for each sector at the JRO.

The fact sheets presented a list of each reporting requirement provided by FEMA and whether that requirement could be informed by GM-LIDAR. In some cases, the applicability of GM-LIDAR to that reporting requirement is very clear and could be described as a "yes" or "no" answer (e.g., measuring the volume of a washed-out roadway). For some reporting requirements, the applicability was unclear or nuanced.

For each sector, the fact sheets include sample images successful use as well as documented limitations to the application of the technology to that sector reporting requirement.

Fact sheets were created for the following sectors and are included as Appendix A: Transportation, Debris, Energy, Communications, Mitigation, Environment Historic Preservation (EHP), Water, Public Building/Housing, Commonwealth, and Natural Culture Resources.

3.2   ROAD DAMAGE FOCUS

The MIT LL program was sponsored by the Transportation Sector. Due to the significant damage sustained by roads and highways throughout Puerto Rico and the resulting impacts to the supply chain of commerce as well as the day-to-day life of Puerto Ricans, the Transportation Sector was keen to have MIT LL focus the algorithm development on road damage. Because the program manager was from the Transportation Sector, MIT LL was able to have more access to persons with domain expertise in the assessment processes and reports for road and bridge damage.

3.2.1   Remote Sensing-Based Sight Inspection Workflow

MIT LL worked collaboratively with FEMA JRO staff to develop a standard remote sensing-based sight inspection workflow using a combination of Google Earth Pro and Quick Terrain Modeler software with optical satellite imagery and 3D GM-LIDAR point cloud data. The virtual sight inspection begins with a reported set of geodetic coordinates, which are entered into RS-VIEWS so that analysts can identify and download the one or more corresponding 500 sq. mi GM-LIDAR tile. Once downloaded, the GM-LIDAR tile is loaded into the Quick Terrain Modeler software for initial assessment and visualization. In this initial assessment, parameters are set for the point cloud such as projection, vertical and horizontal datum, coordinate system, and measurement units to ensure maximum compatibility with FEMA reporting standards and it is visualized by altitude, height above ground, and intensity. Simultaneously, Google Earth

Pro is launched and linked to Quick Terrain Modeler to enable rapid visualization of current and historical optical satellite imagery of the reported location. In GM-LIDAR datasets where vegetation such as tree canopies obscure the reported damage, the 3D GM-LIDAR point cloud is processed to generate a bare-earth digital terrain model, which is then substituted for subsequent measurements in place of the original point cloud. Depending on the type of damage, multiple measurements are made on both the GM-LIDAR and optical satellite data, including length and width of the damage; depth, height, and volume of cavity or debris pile; area; perimeter; and slope. Image chips and high-resolution measurement profiles are exported from both Google Earth and Quick Terrain Modeler into a power point presentation. Where available, pre- and post-disaster images of the damage location are included, and all slides are attributed with standard features such as compass bearing, legends, scale bars, image annotations, and all measurements performed on the GM-LIDAR data. The complete workflow remote sensing-based site inspection was captured in a final webinar made available to FEMA JRO staff along with a detailed field manual that also addressed site inspection edge cases.
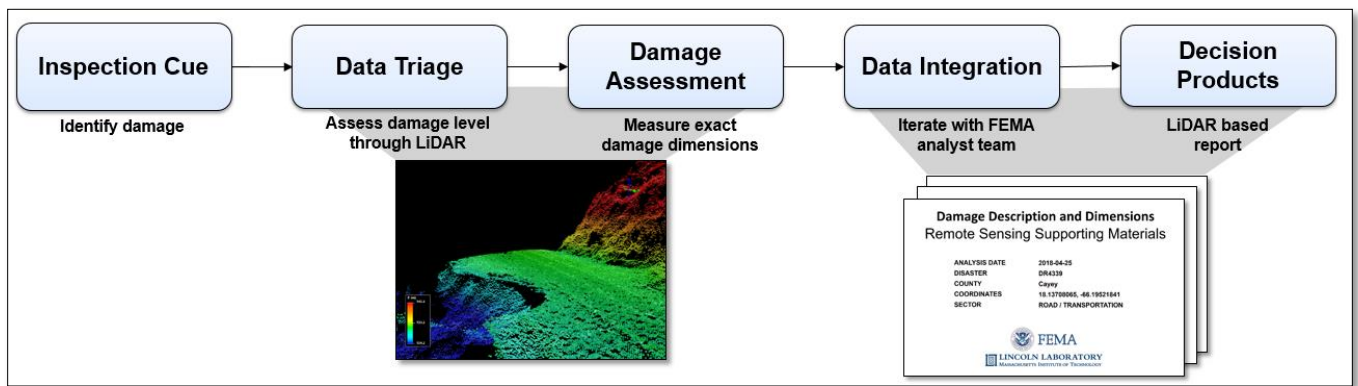
Figure 11. Remote sensing supported site inspection workflow overview.

3.2.2   MIT LL Conducted Manual Exploitation

At the request of the JRO leadership, MIT LL manually created data products including processed GM-LIDAR imagery and analysis of damage to support the damage dimensions and description (DDD) documents within the project worksheet (PW). The sites were chosen by the JRO and included roads, bridges, and park and recreation areas that had known damage. Many of the sites already had completed DDD through FEMA's standard procedure. The MIT LL data products were a proof of concept to show the utility of the data, socialize the products with JRO staff, and to give MIT LL staff a better understanding of the requirements needed to satisfy the DDD. Program manager Travis Johnson identified a group of JRO staff to act as subject matter experts (SME). As the data products were created, MIT LL staff at the JRO would have individual and group meetings with the SMEs to gather feedback on the data products. Through

this iterative process, MIT LL was able to refine the style, annotation, and key data provided on the products. MIT LL provided the JRO with approximately 80 data products with completed manual analysis that could support the DDD in a PW.

Upon receipt of the MIT LL data products, the program manager attempted to continue to socialize the products and solicit feedback from JRO staff. There was significant pushback on the use of GM-LIDAR data to create DDDs and support PWs as there was concern that the use of the data could displace FEMA staff and contractors since the DDDs could be created faster when using technology. There was also concern that few FEMA staff and contractors had experience with 3D point cloud data or the skills to conduct the analysis to create a DDD. MIT LL staff onsite at the JRO and the program manager had numerous conversations to clarify that FEMA staff and contractors would not be displaced because even with GM-LIDAR data, there would still be humans in the process, including those making site visits, as well as training for people to conduct the GM-LIDAR analysis. These conversations were often ignored or met with the responses that working with GM-LIDAR data was not in the person's job description or that the formal FEMA process did not cover the use of creating DDDs from remote sensing.

3.2.3 GM-LIDAR-Based Training Developed and Delivered

Understanding the need to have trained staff to ensure that the JRO could expedite the completion of PWs, MIT LL created a training program, and the initial training consisted of two parts. The first was a lecture-style training to explain GM-LIDAR, the data created, and how they could be used to aid in Puerto Rico's response and recovery. The learning objectives of this two-hour lecture and discussion were to impart an understanding of the data, illustrate the benefits to each of the sectors, and answer questions. This introductory training was delivered to more than 250 staff at the JRO. In addition to offering the training course in Puerto Rico, MIT LL also delivered a series of online trainings to ensure a maximum number of participants, as well as allowing participants from FEMA offices across the island to attend. JRO staff were instructed on how to access GM-LIDAR data through RS-VIEWS and how to visualize, process, and analyze GM-LIDAR data in both ArcGIS and Quick Terrain Modeler. MIT LL created supplementary training material for the workshops, including 3 hours of webinars and a 107-page end-to-end GM-LIDAR processing in Quick Terrain Modeler field manual. Onsite weekly training sessions were conducted on six separate occasions, and webinars were conducted on three separate occasions.

MIT LL ensured that for each class, at least one of the trainers conducting the training was a Spanish speaker. This was to ensure that there would not be a language barrier on the chance that one of the FEMA staff or contractors had a question or issue and preferred to ask or discuss in their native language.

There were a series of challenges to training at the JRO. The first was identifying the appropriate FEMA staff. Because the classes were a significant investment in time, sector leaders were reluctant to release their staff for them. This challenge was amplified because some leaders and staff were unsure of how their respective sector would utilize the data, considering that it was not formally part of the standard FEMA practice. Another challenge with identifying appropriate staff is the transient workforce. Sector leaders would not want to send a person who only had a few months left on their rotation to the trainings

because it would be a sunk-cost investment. There was also the challenge of aptitude in the staff. Most disaster response and recovery professionals are familiar with GIS data products, but do not have a GIS or 3D point cloud data background. Motivating a staff who were already exceptionally busy to learn a new skill proved difficult. There were also logistical challenges in terms of finding appropriate space.

Once staff were identified and space was secured, there were then administrative challenges. This included people not doing the read-ahead work and not following instructions or the many reminders to download software on their computer. This led to a significant delay in getting a class started. There were also professional challenges in terms of people who were assigned but clearly had no interest in participating. Staff would miss large portions of the class or spend significant amounts of time texting and even talking on their phone. This lack of professionalism was demoralizing to the MIT LL instructors and the other participants.

MIT LL would recommend that FEMA should invest in training staff from one of FEMA's ongoing contractors to allow for persistence of the skillset in the work force, as well as formalizing how GM-LIDAR data could support DDDs, PWs, and other FEMA procedures.

3.2.4 Roadside Embankment Failure/Landslide Road Use Case

In spring 2020, MIT LL was asked to review the applicability of the AOSTB GM-LIDAR data to support the analysis of roadside embankment failures caused by landslides during Hurricane Maria. There were several challenges FEMA presented: the ongoing pandemic precluded site inspectors from traveling to sites, many of the sites were likely overgrown with vegetation since nearly three years had passed since the hurricane, and the FEMA-recorded locations of the landslides were known to have accuracy issues. The AOSTB GM-LIDAR data represented a high-resolution, volumetric dataset that captured the damage for review, even three years later.

To address these challenges, MIT LL developed a course of action in coordination with the Transportation and Municipality sectors:

1. Apply the MIT LL landslide prediction algorithm to the Orocovis area of Puerto Rico

2. Analyze the correlation of predicted landslide locations with the FEMA-reported roadside embankment failure locations; this included a FEMA-provided scale for confidence in the coordinate's accuracy

3. If the analysis showed that the predicted landslide locations could be used as a cue to analysts to hone in on the damage, then MIT LL would develop a custom training program for analysts to generate a remote sensing-based DDD for the sites

The results of the analysis to determine correlation of landslide prediction sites and FEMA-reported sites indicated that of the 50 sites provided by FEMA, only 4 sites were deemed potentially challenging. These sites were known to have uncertain coordinates recorded by FEMA, and the nearest predicted

landslide was site within 500 meters. The other 46 sites had predicted landslide locations within 100 meters or had coordinates that were known to be highly accurate.
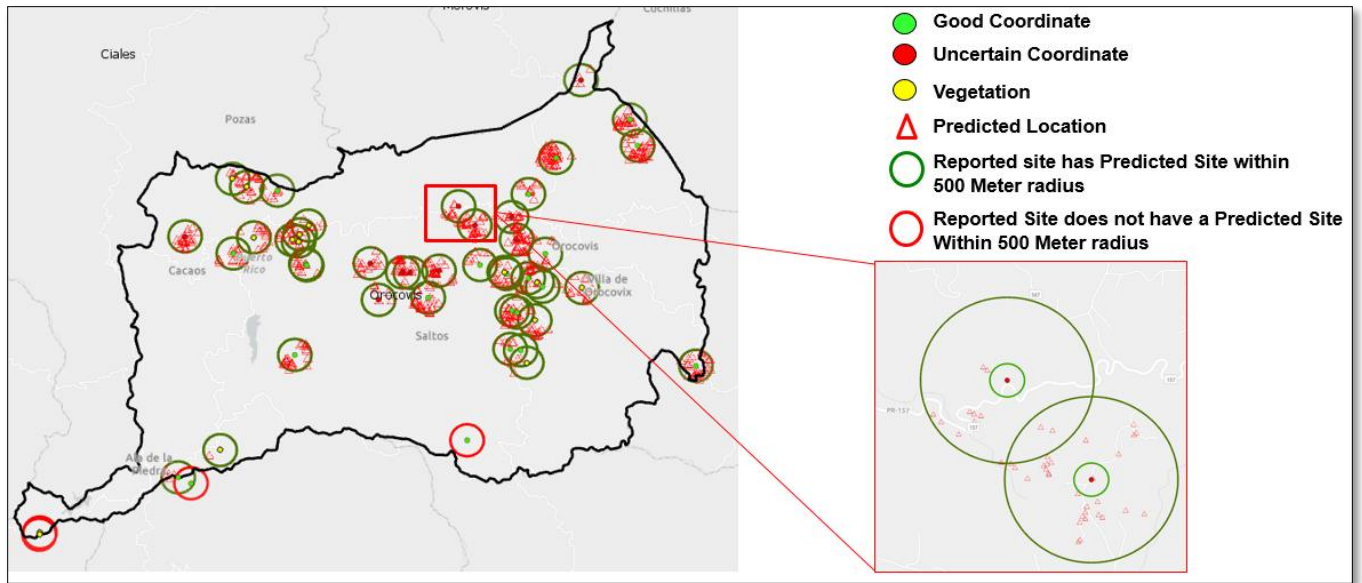
Figure 12. MIT LL landslide prediction, FEMA coordinate confidence, and spatial correlation

Given the likelihood of success, MIT LL developed and delivered a custom training program for a cadre of site inspectors identified by the Municipality sector. The training consisted of self-paced video tutorials for using VIEWS to acquire the data and QT Modeler to analyze the data. The video training was combined with virtual meetings with the site inspectors to answer questions and provided feedback on their classroom practice DDDs.
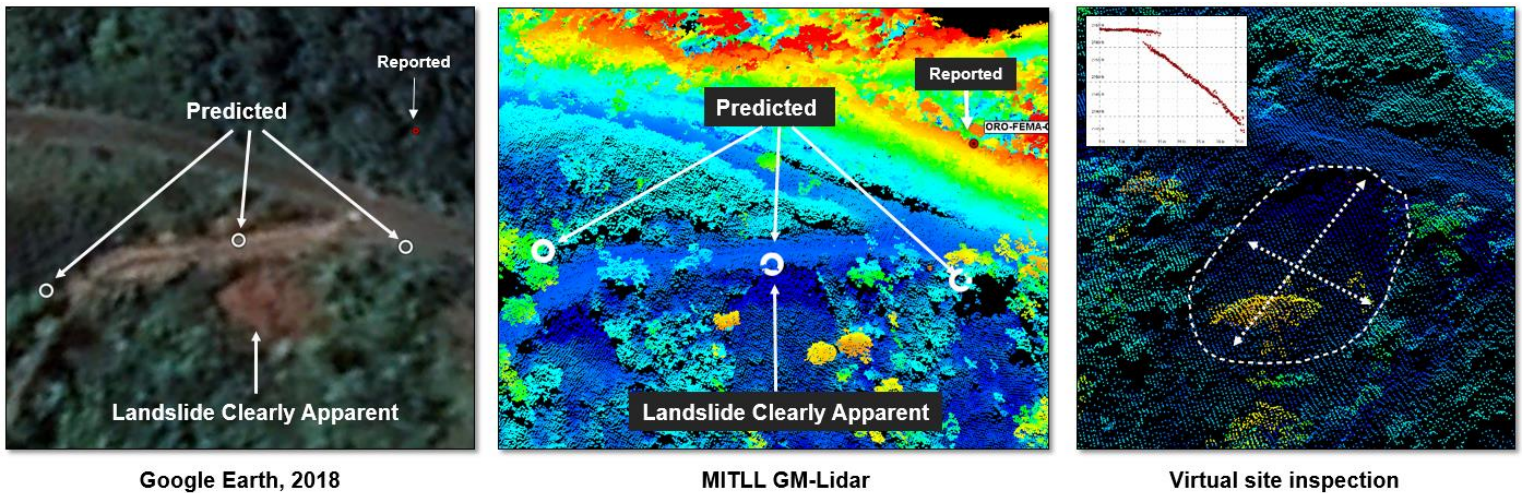
Figure 13. Sample workflow: predicted locations provide cues to correlate a reported landslide with actual damage. Viewing the same data in the GM-LIDAR allows for a virtual site inspection.

All of the predicted landslide locations and proximity buffers were provided to the site inspection team as a Google Earth KMZ file.

3.3 EFFICIENCIES ANALYSIS

Conducting virtual damage assessments using remote sensing data such as GM-LIDAR can increase efficiency in recovery operations in several ways. Each site inspection is unique and may take a variable amount of time, making it difficult to conduct a quantitative analysis. However, there are commonalities across site inspections that can be made more efficient by incorporating GM-LIDAR. For example, analysis of the data prior to conducting an in-person site inspection can inform the team of any obvious access issues, such as other landslides or road damage. Analysis of the data can also inform the team of potential measurement issues given the terrain and characteristics of the site. This pre-site awareness can help the team plan out their measurement strategy and possibly inform what specialized equipment they may need. For sites with particularly challenging measurements, such as very deep holes or steep grades, the team may choose to conduct those measurements using only the data. In some cases, site inspectors may return to the JRO and, while reviewing their data, determine that they need to revisit the site in order to confirm a measurement or record a measurement that was missed. In these cases, the GM-LIDAR analysis could be used to virtually revisit the site.

A source for significant efficiency increase would be for analysts to conduct virtual assessments for most of the site and provide those results to a field team that travels to the site to quickly confirm key measurements. These virtual inspections could be done remotely by FEMA staff or contractors outside of the disaster impact area. Distributing the analysis outside of the disaster and across time zones allows for

26

near continuous work that is done by analysts who are not subjected to the physical and mental stress of a disaster environment. Such a remote team also allows the onsite inspectors to focus their efforts on safety and confirmation.

For each step in the site inspection process, GM-LIDAR offers a tool for potentially increasing the efficiency. Table 7 outlines these steps and a qualitative interpretation of improvements through GM-LIDAR incorporation.

TABLE 7
Inspection Efficiency Improvements

Task/Type	Traditional	GM-LIDAR Supported	GM-LIDAR Focused	GM-LIDAR Complete
Orient to site	Map of location and coordinates	Visualize the site in 3D, looking for access or safety issues	Virtual remote teams use GM-LIDAR to conduct initial assessments of several sites and provide to field tea	Virtual remote or JRO teams use GM-LIDAR to conduct full assessments of sites
Travel to pick up FEMA vehicle	Groups of 2–4	Groups of 2–4	Groups of 2	One analyst per site
Travel to site	Site access may be difficult or dangerous, delaying inspection	Path is selected based on safety analysis from data	Path is selected based on safety analysis from data	Not required
Inspect site	Accurate measurements may not be possible due to physical constraints Measurement time is variable depending on site characteristics and site inspection team	Dangerous measurements taken from data Measurement time is variable depending on site characteristics and site inspection team	Quickly verify key measurements recorded in GM-LIDAR assessment Measurement time is minimal, conducting only a small number of validating measurements	Conduct total virtual site inspection and measurements for DDD
Return to drop off FEMA vehicle	Required	Required	Required	Not Required
Return to JRO	Required	Required	Required	Not Required
Verify field observations	Recording errors or missing measurements	If needed, revisits can be done virtually by JRO teams or remote teams	GM-LIDAR data validated by field measurements	Quality assurance process involves

	require revisiting the site		If needed, revisits can be done virtually by JRO teams or remote teams	analysts checking each other's work
Complete paperwork for PW	Required	Required	Required	Required

Table Key:

Common/Baseline Efforts	Improved Efficiency	Greater Improved Efficiency

3.4 IMMERSIVE VISUALIZATION AND TOOLS

Exploring 3D data through 2D interfaces can be a challenge for some users. In order to fully demonstrate the capability of a high-resolution, 3D dataset, MIT LL built a prototype virtual reality-based toolset for conducting virtual site inspections.

Using the GM-LIDAR data collected by AOSTB, the team used the Unity [6] video game engine to construct an immersive and interactive virtual world surrounding a well-known road damage site. The site could be explored using commercial off-the-shelf VR headsets, and custom in-world tools were created to support a virtual site inspection. The colors and images of the virtual world are video game textures, but the underlying data for terrain, roads, and structures are entirely based on GM-LIDAR data from AOSTB.

In the virtual environment, the site inspector is able to explore the entire area from any vantage point or height and conduct precise measurements using the provided tools. Geotagged photos can be displayed within the system, combining real-world imagery and perspective with the virtual rendering.

In the sample images below, an MIT LL analyst familiar with the virtual reality system went through the site inspection measurement process using the virtual site. The simplicity of the interface allows for pointing at one location with a natural hand gesture, and then pointing to another location and recording that distance. All of the measurements are based on the underlying GM-LIDAR data and so are very accurate.

In the case of the sample area PR-770, an analyst familiar with using the virtual tools and somewhat familiar with the location and damage ahead of time was able to conduct the virtual site inspection in around three minutes.

Figure 14. Virtual reality rendering of PR-770 damage area, showing a geotagged photo taken from the same perspective during an in-person site inspection.
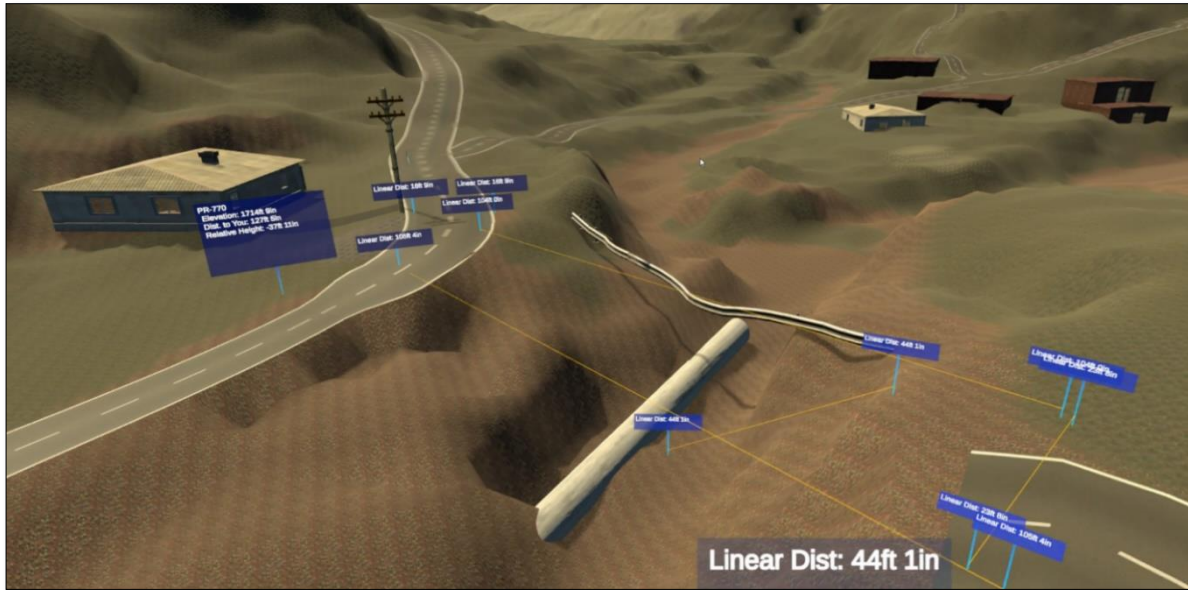
Figure 15. Site inspection conducted in virtual reality in three minutes.

3.5 EXAMPLE PARTNER USE CASES

Over the course of the program, there were instances where other agencies took an interest in the data for uses that the initial collection had not foreseen. The richness of the dataset continues to provide new use cases and reinforces the value of collecting data soon after a disaster. Two examples are described here.

3.5.1 NIST Wind Tunnel Modeling of Hospitals

The National Institute of Standards (NIST) contacted MIT LL asking for the GM-LIDAR data surrounding the areas of a set of hospitals and antenna towers in Puerto Rico that are located at the top of a mountain ridge to support wind tunnel modeling [7]. The Laboratory was able to deliver data for two of the requested hospitals. Unfortunately, the other hospitals and radio antennas were located in an area that had data quality issues. **Figure 17** shows the data provided for one of the hospitals.
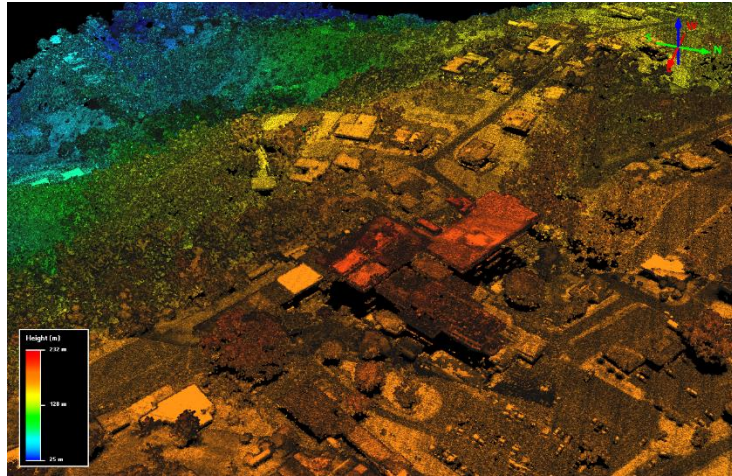
Figure 16. Hilltop hospital for NIST study.

3.5.2   Arecibo Observatory

In December 2020, the Arecibo Observatory collapsed. As the second-largest radio telescope in the world, the loss of this scientific instrument was significant. MIT LL was able to provide the observatory the GM-LIDAR collected after Hurricane Maria, and it is the hope of both MIT LL and the Arecibo Observatory that the data will assist with the reconstruction efforts.
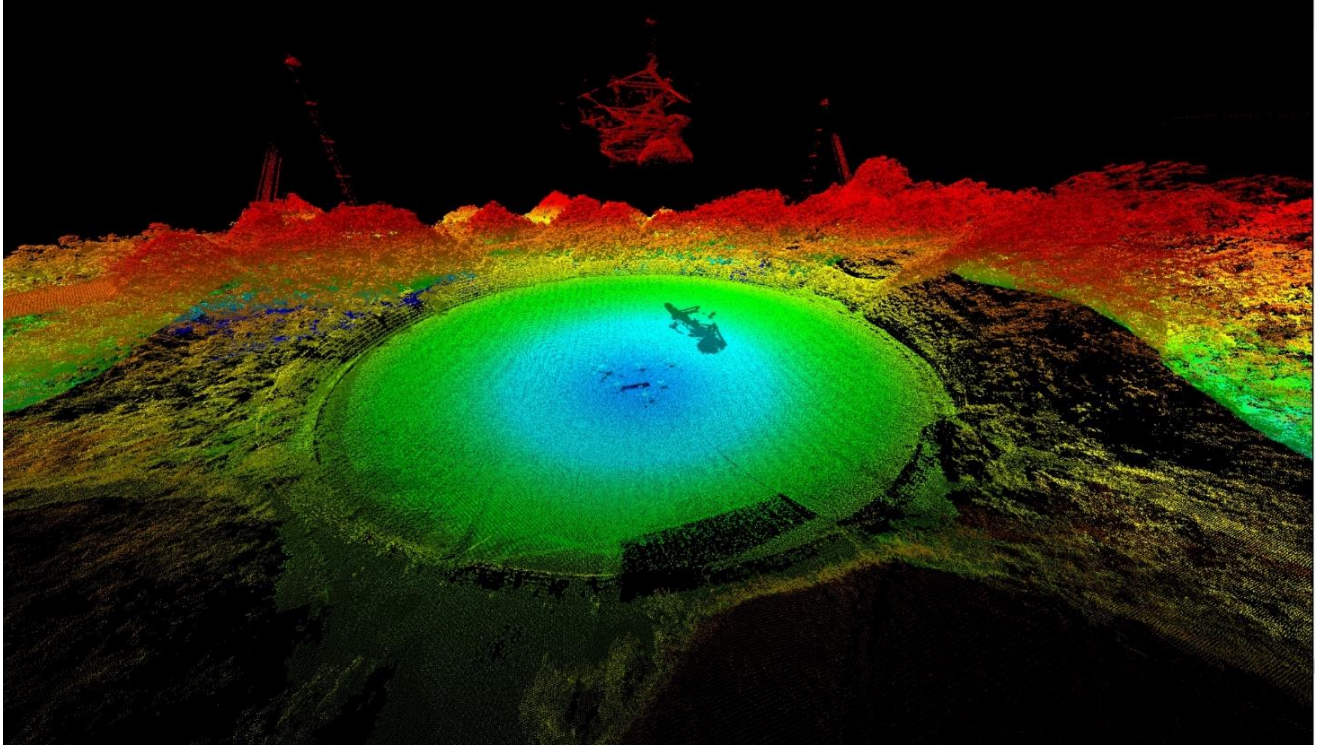
Figure 17. Arecibo Observatory shown with elevation and relative reflectivity color ramp.

4. AUTOMATED ANALYSIS

Automated analysis of AOSTB data can provide significant time and cost savings after catastrophic events. In parallel with the manual data exploitation efforts, MIT LL has developed several algorithms to support disaster recovery. The top-level goals for the automation efforts in Puerto Rico were:

1. Detect roads

2. Detect damage in those roads

3. Calculate point-to-point routing based on undamaged roads

4. Detect structures

The manual exploitation efforts provided invaluable input into the requirements for each of these automated analyses. This section provides a cursory overview of each of these lines of effort. It is intended to provide enough detail to understand the concept and operational applicability. Separate documents are provided that describe each of the algorithms in sufficient detail for them to be replicated.

4.1 ROAD WIDTH ESTIMATION

4.1.1 Overview

The purpose of this algorithm is to identify the extent of roads with the intended extension that the output be used to find road damage and rubble on the road shoulder. Operationally, this algorithm provides a critical first step for automating transportation-related analyses. In addition to enabling the detection of road damage, complex operations could be developed by identifying an entire road network within the AOSTB GM-LIDAR over hundreds of square miles. Sample complex operations include, but are not limited to, point-to-point routing based on road damage and the detection of communities that are isolated due to surrounding road damage.

4.1.2 Workflow

As shown in the workflow overview in Figure 18, the input is a GM-LIDAR dataset consisting of x, y, and z coordinates, along with the relative reflectivity, signal-to-noise ratio, significance ratio, and confidence. From the coordinates, additional parameters are calculated for each point, specifically the height above ground and 11 attributes describing the geometry and reflectivity of the point cloud. This collection of values is operated on by a convolutional neural network with an output layer that produces probabilities of points being located on a road. These probabilities are noisy, so a follow-on step uses known road centerlines from Open Street Maps to remove false detections and estimate true road widths.
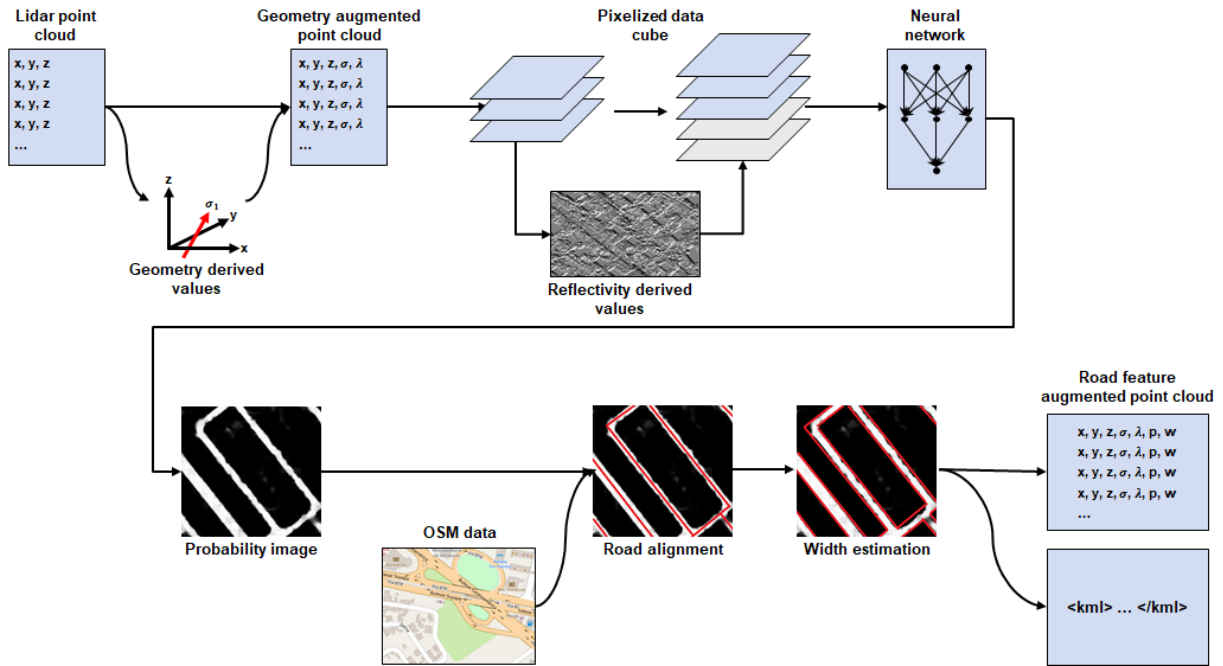
Figure 18. Road width estimation workflow overview.

4.1.3 Output

This algorithm produces two main outputs:

1. A KML [7] file with information about each road segment location along with the segment width

2. A BPF [8] GM-LIDAR tile with the points labeled according to their probability of being road points and our estimate of road extent

4.1.4 Results

To evaluate the performance of this algorithm, we used truthed tiles, but ones that were not part of the set used to train the neural network. In this case, a total of five truthed tiles were evaluated using the complete pipeline and the output compared to the truth. Since we have the ability to choose the threshold at which an edge is declared, we can look at the range of potential accuracies produced by varying this parameter. The ROC curve in Figure 19 shows how changing the cutoff alters the false positive and true positive rates.
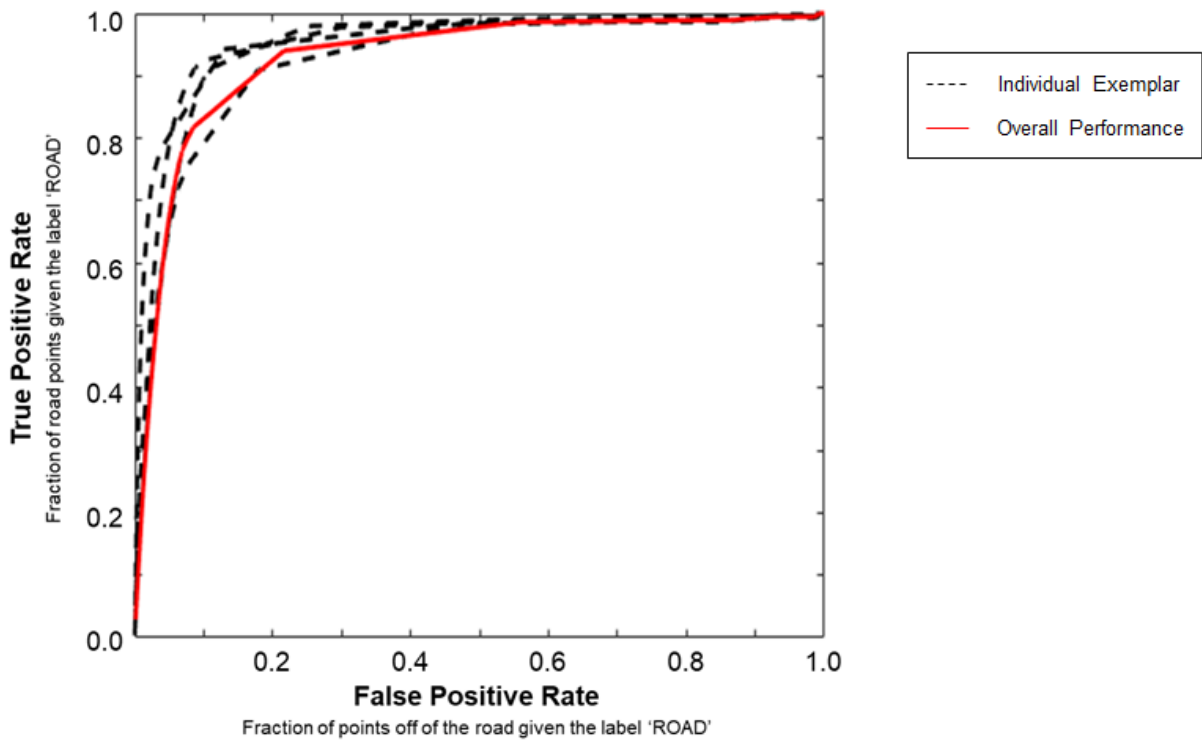
Figure 19. Road width estimation ROC curve.

This shows that if we are willing to accept a 10% false positive rate, then we will account for 80% of road points. Given that some of the point labeled as 'NOT ROAD' are likely crosswalks and cars on the road, this appears to be a sound method for determining road width.

4.2   ROAD DAMAGE

4.2.1   Overview

The purpose of this algorithm is to detect sites of road surface damage. The algorithm utilizes the output of the road width estimation algorithm and reports sites with locally anomalous surface geometries. In lieu of an abundance of ground truth data for road damage in GM-LIDAR, this unsupervised algorithm is both explainable and relatively robust to variations in data quality and landscape characteristics.

4.2.2   Workflow

The input is a GM-LIDAR dataset consisting of x, y, and z coordinates, along with the relative reflectivity, signal-to-noise ratio, significance ratio, and confidence. Using these attributes, an additional

set of eigenvalue-based geometric features using k=6-point neighbors were calculated. A classification of whether a point was on a road was an additional feature, drawn from the aforementioned road detection algorithm output. Anomaly detection within the 500 m^2 area point cloud tiles was performed and sites were attributed a damage score. This score is an estimate of damage volume weighted by an indication of how anomalous the site is relative to the remaining data in the tile.


```
Tile point cloud data      →   Classification of road and non-   →   Filter points with           →   Gaussian fit; filter data above
(Area=500m^2)                  road points using Road                'onRoad'==True and with          fixed Mahalanobis distance
                               Detection Algorithm                   'HeightAboveGround' < .75m       threshold
```

```
Euclidean clustering using fixed   →   Calculate cluster centroid   →   Combine into final product:
parameters: minimum points             locations and generate           CSV or KML of detected
in a cluster=50, maximum               damage score:                    damage locations with
distance to be included in a           ∑HeightAboveGround*Mahala         associated damage score
cluster=.75m                           nobis distance
```

Figure 20. Road surface anomaly detection algorithm workflow overview.

4.2.3 Output

This algorithm produces a CSV or KML [7] file generated from the centroid of each cluster of points nominated as potential damage sites, along with the associated damage score.

4.2.4 Results

A visual comparison of the output of this algorithm with a known road damage site in Puerto Rico due to Hurricane Maria is detailed in Figure 21. As a proxy for output of the road detection algorithm, roads were manually labeled in this example.

The leftmost images are pre-storm and post-storm imagery that show significant flooding and related road damage at the site. The output of the road damage detection algorithm for candidate damage locations is shown at the lower right, with yellow pushpins indicating potential damage. One can compare the output to the human-annotated image of GM-LIDAR at the top right.
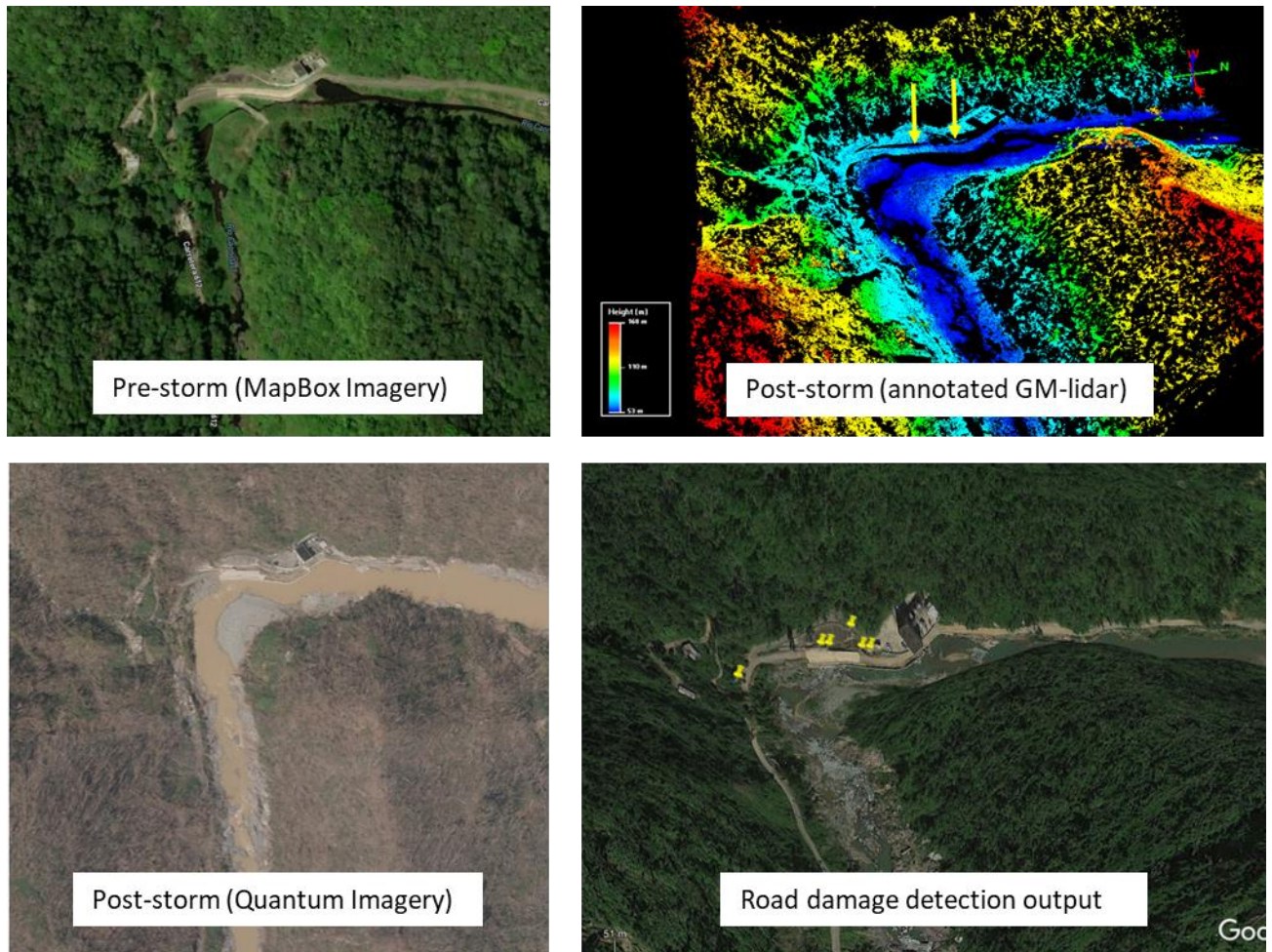
Figure 21. Road damage detection sample.

There are insufficient data to calculate an algorithm performance ROC curve at this time.

4.3 ROAD NAVIGABILITY

In addition to identifying road damage for the purposes of repair efforts, the damage log can be used as an input to a program that finds routes for ingress/egress in the affected area.

4.3.1 Overview

The purpose of the road navigability method is to find paths from one set of points (sources) to another set of points (sinks) that avoid the damage identified through the road damage algorithm. This can mean

routing that simply takes parallel roads, which are slightly less efficient; routes that go through parking lots and other hard surfaces; or in the most extreme cases, through flat areas such as fields. Which routes are considered acceptable is dependent on the type of vehicles that are being considered and their specific capabilities.

In the immediate aftermath of a disaster, there is a need for individuals to evacuate the area and for emergency responders to enter. However, the typical pathways they would have employed may have become damaged or blocked as part of the disaster. As such, a method that provides directions under the constraints of this damage is beneficial.

4.3.2   Workflow

This method uses both the road information from OSM and the GM-LIDAR point cloud characterization. These two datasets provide complimentary features that are needed to quickly find routes that are also efficient. The most rapid computation of routes is accomplished using the road definition because it has far fewer points than the GM-LIDAR that need to be considered. The GM-LIDAR point cloud, on the other hand, has information about the topology of the world that is needed for finding routes that do not strictly stick to roads.

Before road navigability is computed, the roads and road damage need to be identified using the previously described methods. The road probability from the road-finding method is used in road navigability to identify areas that are similar to roads such as parking lots that should be considered during the routing process.

All routing in this method is done using a weighted *A** algorithm, though it will be applied to different graphs. This function is notated as $A^*(p, p', G)$ and returns a list of points $P = (p_1 = p, p_2, p_3, \ldots, p_k = p')$. In this case, the weighting between points will be equal to their Euclidean distance. However, when routing on the GM-LIDAR point cloud, these weights will be multiplied by factors associated with their difference in elevation and probability of being a road.

The algorithm starts by finding the path between a starting point and an ending point on the OSM data. This should be familiar to anyone who has used online driving directions. Once this route is established, we determine how reachable each of the waypoints on that route are using the GM-LIDAR point cloud. Some of the initial waypoints may prove to be unreachable and will be discarded.

In order to perform routing on the GM-LIDAR point cloud, we have to provide it with a graph structure. This is accomplished by finding the nearest *k* points to each point and connecting them with an edge.
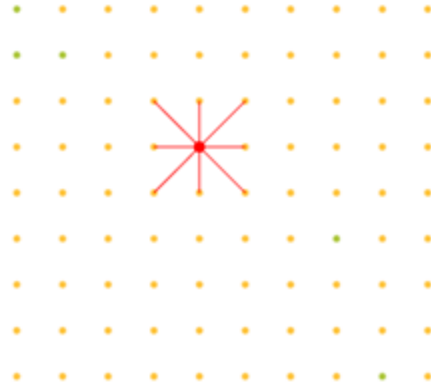
Figure 22. A point in the GM-LIDAR point cloud along with connections to the eight closest neighbors. Applying this methodology to all of the points in the set creates a graph.

Consider the entire road graph from OSM as a weighted graph $G_r = (V_r, E_r, W_r)$ and the graph induced on the point cloud as $G_L = (V_L, E_L, W_L)$, where V is a set of vertices, E is a set of edges and W is the set of weights on the edges. We will use a projection operator, $\pi(\cdot)$, that takes a point in the set of OSM vertices and returns the nearest point in the GM-LIDAR point cloud set. The star projection operator $\pi^*(\cdot)$ finds the nearest point, which is also a point identified as a road in the road detection method.

One critical aspect of routing is the proper application of a weighting scheme. Weights on the OSM graph are calculated as the Euclidean length of the edges. The GM-LIDAR point cloud contains significant more information, so more can be done with the weights. For our purposes, we use the scheme $W = d \cdot ((1 - p) + \delta_r + D + z^c)$ where d is the Euclidean distance, p is the probability assigned by the road detection algorithm, δ_r is whether or not the points are identified as roads by the road detection algorithm, D is the cost associated with damage as identified in the road damage process (may be infinite), and z^c is the difference in elevation between the points raised to some amplifying power. This scheme has the effect of making the weight on edges between points that are very likely roads to be close to zero.

Start with the optimal path $P = A^*(p, p', G_r)$. Then, find the path $P_1 = A^*(\pi^*(p_1), \pi^*(p_2), G_L)$. If this path exists, then we can more to $P_2 = A^*(\pi^*(p_2), \pi^*(p_3), G_L)$. Otherwise, the point is not accessible and we have to check $P_1 = A^*(\pi^*(p_1), \pi^*(p_{2+i}), G_L)$ for increasing i until a path is found. As we move down the chain, this process has to be repeated for each segment.

4.3.3 Output

This process produces a list of points in the GM-LIDAR space that a traveler would take to get from one point to another. It is able to do this in an efficient manner by only looking at local points instead of

trying to route over the entire point cloud. It fuses the information from GM-LIDAR detection with the routes calculated on the more efficient OSM representation.

4.3.4   Results

The output can be visualized on the GM-LIDAR point cloud. These maps could be downloaded to personal devices of emergency workers entering the area.
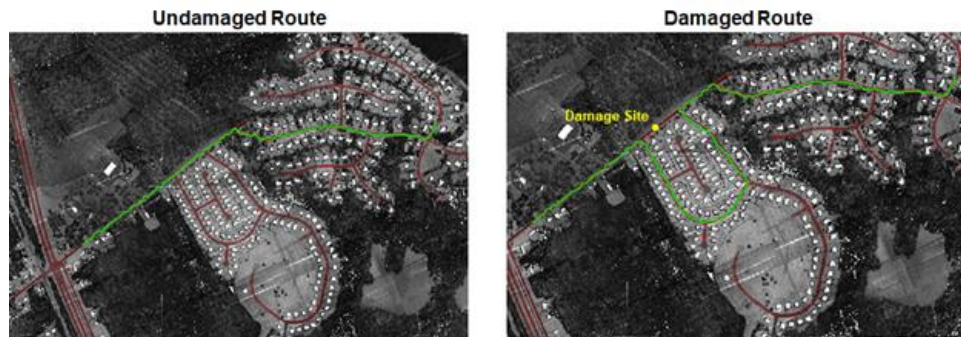

Figure 23. The most efficient route on the undamaged road (left), and routing around a damaged site placed in the path of the most efficient route (right).

In Figure 23 above, the route is colored in green and roads are in red. The left image shows an efficient route, whereas the right image shows how a damage site is routed around using this process. As can be seen, there is a significant detour, but it tends to stay on the roads. This is the result of the weighting methods employed that makes the costs of roads very low. A different weighting scheme could potentially route through the front yards of the houses bordering the damage site.

Further development should focus around developing the weighting scheme to meet the needs of responders. This would involve assessing the capabilities of response vehicles and matching them to the sensed differences in the environment. For example, curbs need to be weighted in a manner consummate with the ability for them to be climbed by the vehicles being employed in the response.

Another direction for development that builds on this capability is the identification of isolated areas. Some remote cities are serviced only by a single or small number of roads, and if these become severed, there is no way in or out. Quickly identifying this condition is critical to the planning of response efforts, as it will take extra effort to reach these stranded communities.

This capability can also be extended to efficient routing for the delivery of supplies. If the sources are ports and sinks are potential aid distribution points, then routes can be found to efficiently deliver the aid to where it is needed. Finding particularly long routes could also inform the need for the selection of a different distribution point.

4.4 STRUCTURE DETECTION

The purpose of this algorithm is to determine the feasibility of identifying building structures in a GM-LIDAR point cloud for the future purpose of enabling building damage detection at scale for catastrophic disasters. Research was conducted into numerous existing methods of semantic segmentation of point cloud data, and the "Semantic Classification of 3D Point Clouds with Multiscale Spherical Neighborhoods" [9] was selected to be adapted to AOSTB data, and extended for structure detection.

4.4.1 Workflow

The input is a GM-LIDAR dataset consisting of x, y, and z coordinates, along with the relative reflectivity, signal-to-noise ratio, significance ratio, and confidence. Using these attributes, an additional set of geometric features are calculated using various neighborhood scales surrounding each point. This augmented point cloud is then classified utilizing a trained random forest model. The resulting labels suffer from a large false positive rate, which is addressed by post-processing the positive points with a K-nearest neighbors filter followed by an agglomerative clustering filter to remove unstructured noise in the labels. Only clusters with a sufficiently large number of points are retained. The process is illustrated in Figure 24.
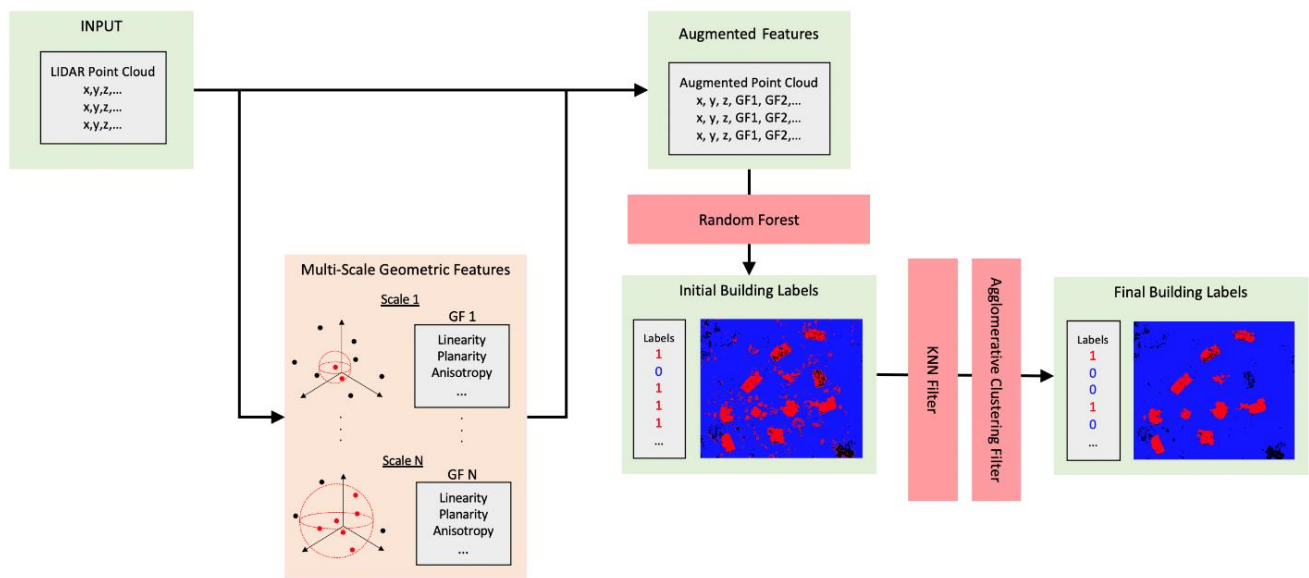

Figure 24. Building detection workflow overview.

41

4.4.2 Output

The output of the algorithm is a BPF file of the original GM-LIDAR point cloud with an attribute representing the pointwise building label classification.

4.4.3 Results

The initial ROC curve of the unfiltered random forest classifier results show that the model is able to capture almost all building points below a false positive rate of 0.10; however, because of the large class imbalance in favor of non-building points, this still amounts to many misclassified points relative to the number of building points.
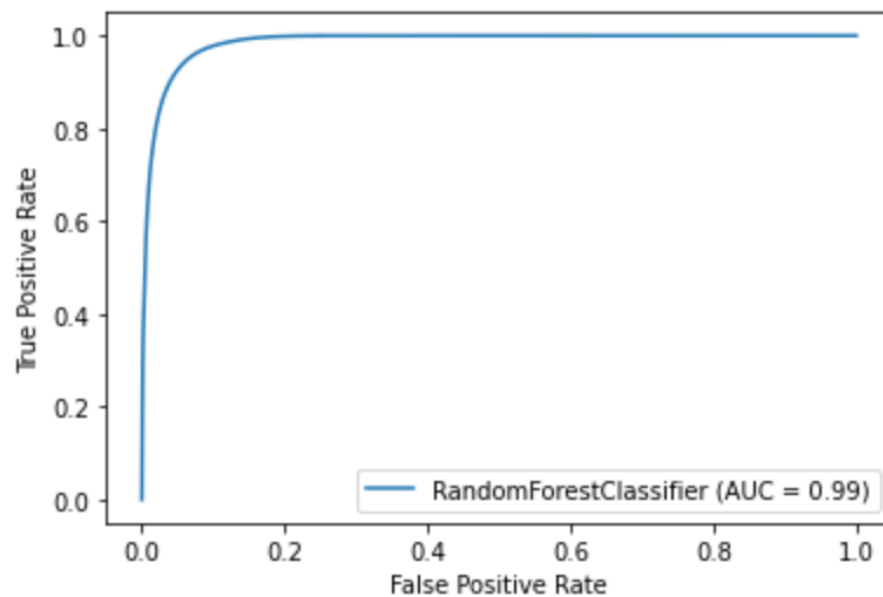
Figure 25. ROC curve parameterized by random forest estimator vote threshold for classification.

Provisional results of the post-filtered class assignments are contained to a qualitative analysis. Generally, it was found that the truth masks do not capture all buildings present in the GM-LIDAR scene and falsely label foliage above the building footprint as part of the building. The trained model can discern these points and, in some cases, performs better than the hand-truthed data.
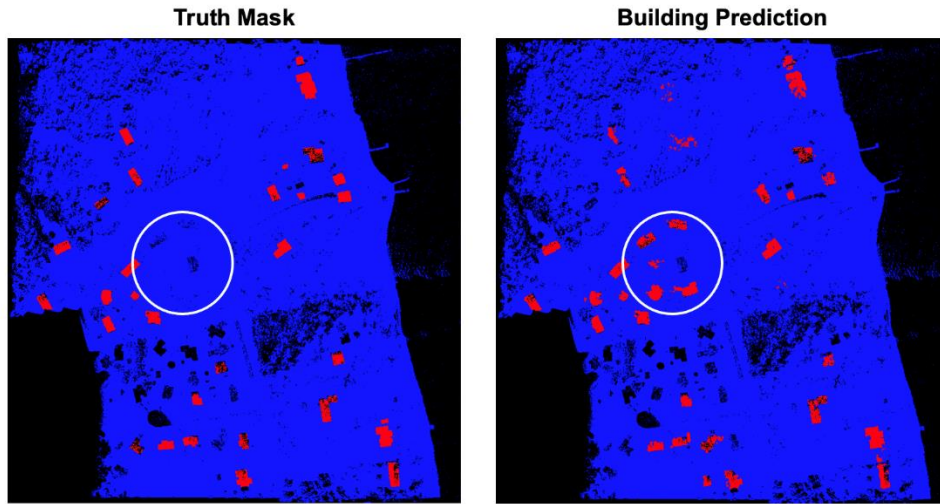
Figure 26. Top view comparing truth mask with final building prediction. Circled in white are various buildings unmarked in the truth mask, but captured by the model.
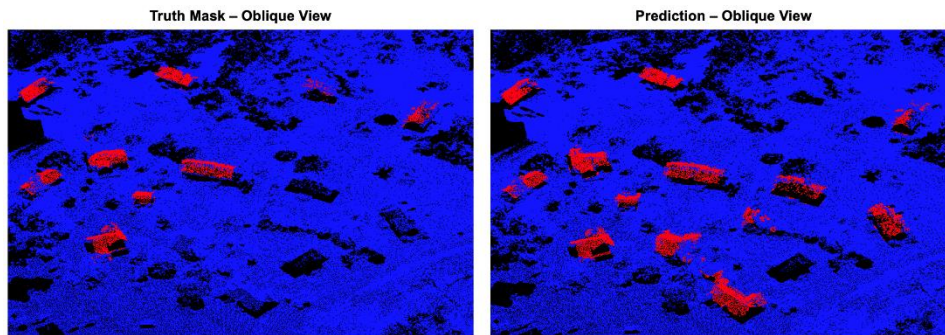
Figure 27. Oblique view of truth mask and final prediction.

Although results are promising, there are significant challenges to expanding this methodology to identifying building damage. The first challenge is in collecting and annotating truth data. Earthquake damage is structurally different from hurricane damage and examples of each (or any other "type" of damage) should be collected before the model can be expected to identify such features. Another challenge lies in the nature of the data collected. GM-LIDAR alone is limiting in that the algorithm can only leverage the raw point cloud with limited reflectivity data. Current machine-learning algorithms on strict point clouds perform worse than those with color features. Therefore, it is recommended that for both building detection

and future damage detection, RGB data or even hyperspectral data should be co-collected with points to provide an additional discriminating feature.

5. OPERATIONAL CAPABILITY UPDATES (JUNE 2019 CAMPAIGN)

Although the AOSTB GM-LIDAR system had been used previously for smaller-scale tests, the work in Puerto Rico was the first attempt to use this system at scale. In doing so, a number of specific shortcoming and opportunities for improvement were identified and addressed as part of the June campaign preparation. In doing so, we were able to perform an end-to-end workflow demonstration to provide predictable timelines from wheels-up to usable data products in hand. When selecting targets for our tests, we worked with the state of Rhode Island to select target areas that, while still meeting all of our test criteria, could also be used by them for urban planning, urban forest assessments, and coastline analysis.

5.1 CAMPAIGN OVERVIEW

A number of sensor hardware and software upgrades were performed to improve sensor stability and reliability, and to ultimately achieve predictable, timely, and actionable data product generation. The first hardware change was aimed at addressing image quality issues observed in the Puerto Rico data. Upon careful examination of the sensor hardware, a number of laboratory-grade optical mounts were found to be potentially responsible for image blurring and warping when used in high vibration environments, such as aircraft. These mounts, along with the IMU mount, were replaced with significantly more rigid elements.

The next hardware change was the installation of a new transmitter (laser), which increased output power by 300%. The increase in output power allows for faster scanning at higher altitudes, increasing the area coverage rate as well as point density. With this increase in laser power came an opportunity to explore daytime operations. For this, an additional narrow bandpass spectral filter and oven assembly were installed into the system, which prevented most sunlight into making its way into our receiver system and significantly reduced noise attributable to sunlight. Although nighttime data collection is still preferred for optimal quality, daytime operations are now a viable option.

During the flight campaigns, operators also observed the transmit beam would occasionally shift (likely due to thermal flexing of the mounts in a cabin without environmental controls) and sometimes nearly completely miss the receiver. To address this, we incorporated new opto-mechanical (piezo) control elements for the transmit optics, which allow the operator to physically move the transmit beam from a software control panel on the operator workstation. This was an important safety improvement, as fatigued operators no longer have to get out of their seats, walk over to the optical bench, unscrew and remove the optical enclosure cover, and physically twist knobs to move the beam back into view.

Operating over mountainous terrain in Puerto Rico, sensor operators noted the difficulty in maintaining an optimal "range gate", where the receiver system is told to start being sensitive to photons and when to stop. At the beginning of the range gate, each pixel is sensitized, or "armed". Once armed, it is sensitive to any photon returns or other source of noise (e.g., thermal, spectral). Upon absorbing the energy from a surface-reflected photon or from a phonon or other source of noise, the pixel is said to have

"fired" and takes some amount of time before it can be re-armed. This period of time is called "dead time". In an ideal world, pixels are all armed just before the terrain (range gate is opened), and the range gate is closed just after below the terrain, so that you reset and re-arm as fast as possible. The wider the range gate, the more potential you have for a noisy image.

When an operator is manually adjusting range gating, as was the case for the Puerto Rico data collection, the gate must be kept wide enough to account for human reaction time, trying to keep up with a rapidly changing range histogram with its own software delays. Automatic range gating was added as a capability for the June test campaign and enables the AOSTB to collect cleaner, crisper, data over any types of terrain. It also alleviates a significant source of operator fatigue.

Lastly, a long-wave infrared (LWIR) contextual imager was added, offering a nighttime thermal imaging capability that can provide an additional thermal contextual overlay to the 3D imagery. Beyond incorporating this as a standalone capability, the imagery has not yet been used for furthering exploitation of GM-LIDAR data or for the creation of fused products.

All of the improvements and changes were thoroughly tested as part of the June campaign to ensure that the system would be ready for another data collection effort of at least similar scale to the Puerto Rico campaign.

5.2 ROAD DAMAGE

The road damage detection algorithm was run on the set of Massachusetts GM-LIDAR data from the campaign. As a proxy for the output of automated road detection, data that weren't within parcel data and within water body boundaries were classified as road data.

The resulting distribution of damage scores is shown in Figure 28.
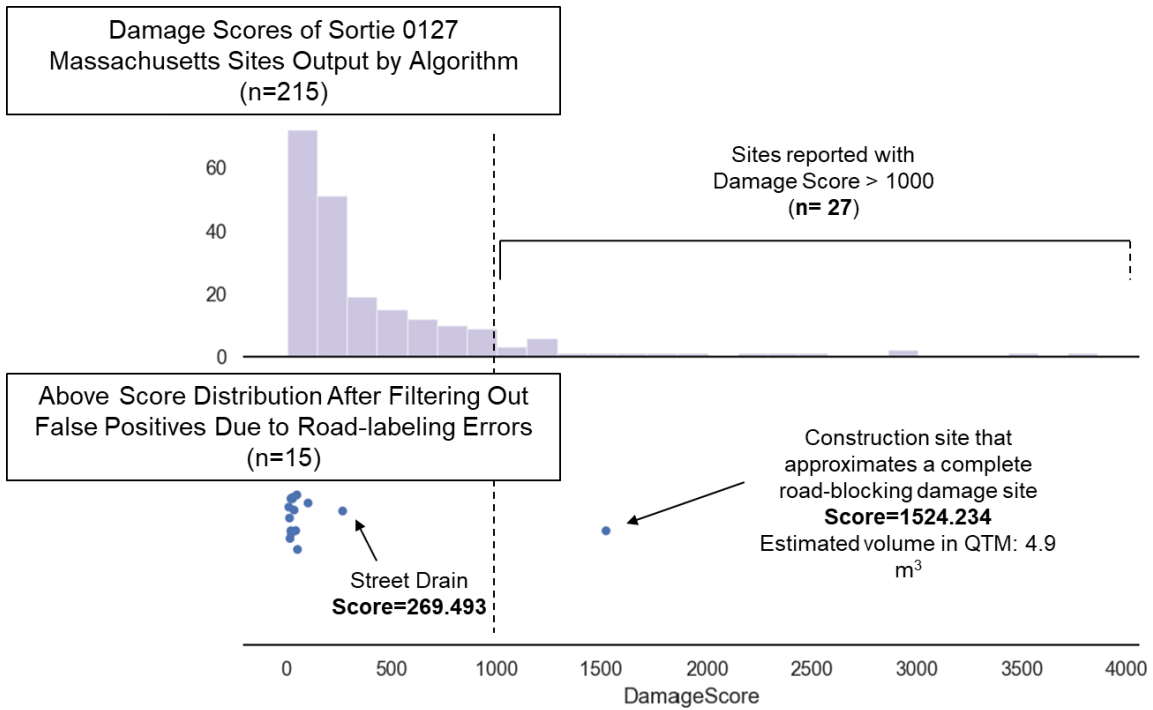
Figure 28. Damage score distribution.

Removing false positives due to errors in road classification in this early version of a road detection algorithm, we plot the lower graph of the distributions of damage scores.

An investigation of the highest-scoring site in this set revealed that this location lined up with a road reclaiming site in Bedford, MA, at the time of the campaign.

Figure 29. Road construction detected by algorithm.

The campaign thus provided not only early validation for this approach to road damage detection, but also demonstrated the reliance of the algorithm on accurate classification of roads. Several shortcomings of the parcel data-based approach were addressed by the current road detection algorithm.

5.3   AIRPORT-BASED GEOREGISTRATION VALIDATION

Determining and improving the horizontal georegistration accuracy of data collected in a disaster timeframe was a challenge during the Puerto Rico campaign. For the Operational Capability test campaign, MIT LL developed a methodology for consideration to address these challenges.

Traditional LIDAR collections often rely on establishing a matrix of ground control points throughout the study area. The ground control points are features that will be clearly visible in the collected data that are surveyed to a high degree of accuracy prior to data collection. This approach does require time-consuming field work ahead of the LIDAR collection, which is not likely possible during a disaster response or recovery, limited both by timeframe and access to the field. There are also existing control points established by USGS and the Continuously Operating Reference Stations (CORS) [10] established by NOAA; however, these points are not guaranteed to be located within the collection area or discernable in GM-LIDAR data.

MIT LL investigated using GIS vector data for road centerlines as a reference guide; however, there is significant variance in horizontal accuracy of road centerlines, making this approach not reliably scalable across the U.S.

The proposed approach is to use airport centerlines as a quick reference for horizontal georegistration accuracy. Per FAA Advisory Circular 150-5300-18C [11], airport centerlines must be surveyed to within 1 ft (~30 cm). This provides a defined reference that is clearly visible in GM-LIDAR due to the relative reflectivity data clearly depicting runway centerline paint. The ubiquity of even small airports indicates a high likelihood that one or more airport will be in the collection area. At minimum, the collecting aircraft will fly over one airport at the beginning and end of any given sortie (takeoff/landing).

Automated scripts were developed that extract airport runway centerline data from a database of all airport GIS data, generate a vector data file that contained a centerline with additional lines spaced at 0.5 m from that centerline for those airports, and collect the processed GM-LIDAR tiles that spatially overlap the airports. This enables a very fast manual check of horizontal georegistration. A sample of this output is shown in Figure 30.
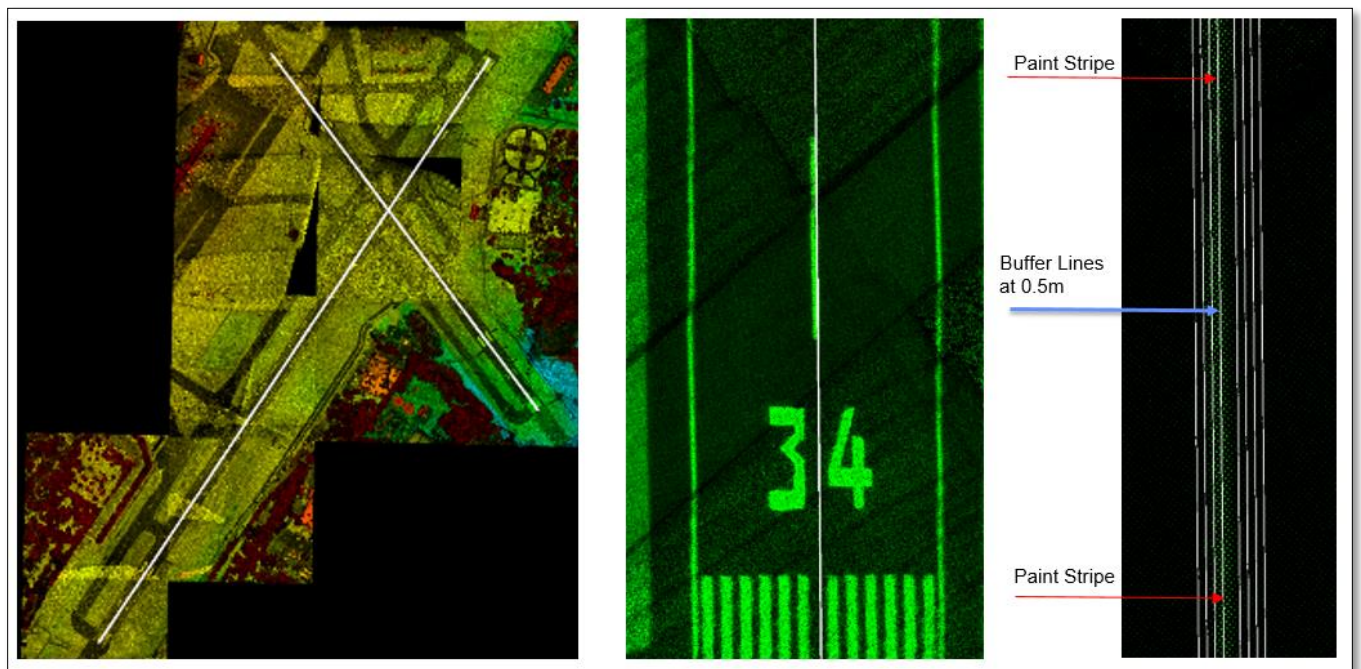

Figure 30. Airport runway centerline with 0.5 m intervals shows roughly 0.5 m offset from GM-LIDAR.

Future development could use the relative reflectivity of the airport centerline to automate a calculation of variation from the georeferenced centerline vector data. Airports typically include more than one runway with differing orientations, which could theoretically provide a reasonable set of references across the AOI to determine transformation matrices to shift the data as needed to improve the registration.

5.4   OPERATIONAL TIMING

An effort was made during this capability test to establish a baseline for data collection and data processing. The sortie that was selected covered an area of 250 square miles, corresponding to the size of a study area in Puerto Rico being evaluated by other laboratories involved in FEMA's Remote Sensing Innovation Working Group. A running time log was recorded for each step of the sortie, starting with aircraft engine start and ending with notification that road damage analytics had completed.

Based on this sortie, the planning numbers for collecting, transferring and processing a 250 square mile AOI is roughly 33 hours, followed by 2–3 hours of additional algorithms, for a total of 36 hours.

There are two caveats to these planning numbers:

1. The data transfer was performed under ideal conditions with near co-location of the aircraft and a high-speed data transfer to the MIT Lincoln Laboratory Super Computer. Operational conditions may have longer data transfer times.

2.   The road damage analytics that were executed for this sortie used an early version of the algorithm. Current versions perform substantially more analysis, so will take longer to complete.

As shown in Figure 31, additional time should be allocated to acquiring the appropriate aircraft for the mission and installing the sensor onto that aircraft.
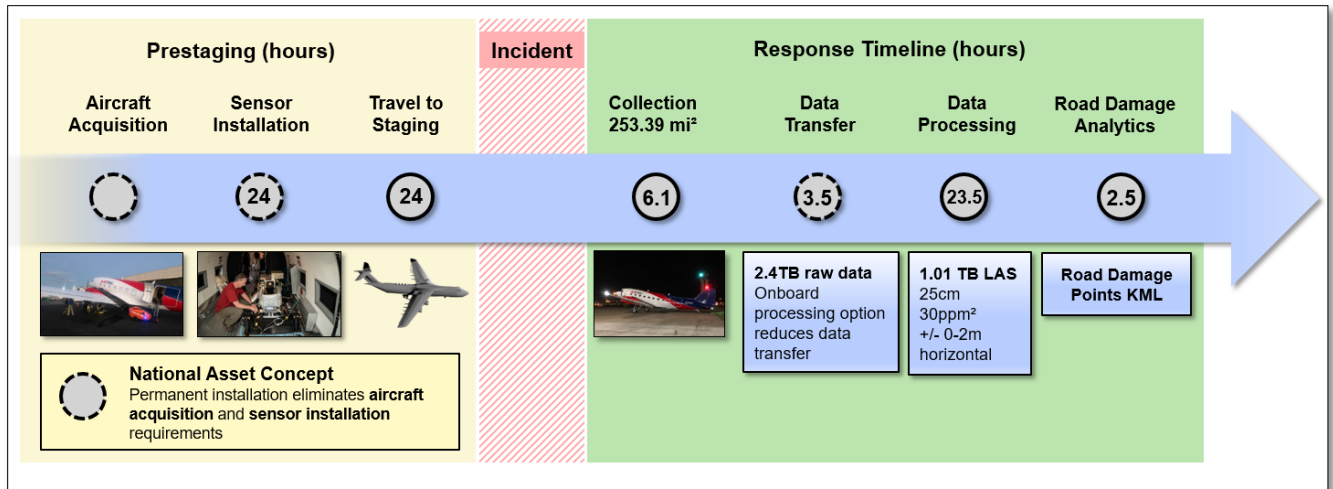
Figure 31. AOSTB execution timeline.

5.5   RESULTS

The operational capability test demonstrated successful corrections to several lessons learned during the Puerto Rico collection. For example, the horizontal georegistration was greatly improved and automatic range gating allows for collection of widely varied terrain.

This page intentionally left blank.

6. FRAMEWORK FOR REMOTE SENSING BASED DISASTER RELIEF

The work performed by MIT LL in support of FEMA's recovery efforts in Puerto Rico after Hurricane Maria identified significant challenges to effective application of remotely sensed data to support disaster recovery needs. The challenges were both technical and organizational in nature. Further compounding these challenges, the landscape of remote sensing support for disaster response and recovery continues to expand rapidly, with numerous academic, government, and industry organizations developing both manual and automated exploitation systems using all available sensing modalities.

A well-known standard process for leveraging remote sensing for information is the tasking, collection, processing, exploitation, and dissemination (TCPED) chain. Although this methodology works well for intelligence, surveillance, and reconnaissance (ISR), MIT LL recommends modifying the chain for use by the emergency management community in order to leverage the myriad sensing modalities and analytics under development.

1. **Determine Area of Impact/Interest (AOI)**—Geographically bounding the disaster impact area helps to identify the best available remote sensing systems for the event. Additionally, by understanding what exists within the AOI, emergency managers can further refine mission requirements. For example, disasters occurring within dense urban areas will have different requirements than a disaster occurring in a less populated or concentrated industrial area.

2. **Mission Tasking**—This step in the chain is similar to the tasking and collection phased of TCPED, but should be guided by emergency management requirements in the AOI. Determining which remote sensing platform should be tasked, given the AOI and the requirements is a substantial challenge. Satellite imagery can be slowed by orbit times and weather conditions, and aircraft-based sensors can be slowed by proximity to the AOI and their area collection rate. With some exceptions, a typical approach is to simply collect any and all available imagery.

3. **Analysis and Distribution**—In this proposed process chain, analysis refers to the automated or crowd-sourced damage detection within imagery by multiple teams and organizations. The distribution portion of this phase refers to each of the analyzing organizations sharing their results.

4. **Validate, Aggregate, and Disseminate**—With numerous academic, government, and industry partners producing automated damage detections using artificial intelligence and machine learning (AI/ML), the volume of output easily overwhelms the emergency management analyst. Establishing a method for validating the results of experimental algorithms, aggregating those results with thematically similar analyses, and disseminating the combined data as authoritative is critical. For example, if there are several organizations conducting automated virtual building damage assessments using AI/ML, each using different algorithms that run against different imagery sources, and each covering partially overlapping geographic areas, there must be a

mechanism for combining and de-conflicting that data into a single stream of validated damage assessments.

5. **Feed Decisions**—The final step of this analysis chain is to provide actionable data directly to the relevant emergency management analysts across federal, state, territory, tribal, county, and local governments.

To enable the success for such a modified decision analysis chain, MIT LL has developed an open standards framework for remote sensing-based disaster response and recovery decision support. This framework provides a template for the emergency management community to engage with industry and the research and development community to best identify how remotely sensed data can support disaster information and analytical needs. The framework has five components.

1. **Define Requirements**—Define quantitative requirements for each FEMA Lifeline component.

2. **Characterize Systems**—Use a standardized method for characterizing remote sensing platforms and algorithms together as a system in terms of their applicability to the defined requirements.

3. **Mission Tasking Guidance**—Developed by comparing the specifics of a disaster event with relevant requirements and spatiotemporally available systems that meet those requirements.

4. **ERSLA**—Use a standard format for communicating analytical results. MIT LL has drafted the Emergency Remote Sensing Language (ERSLA) specification to meet this need.

5. **ERSAT**—Provide a toolset for validating, aggregating, and disseminating analyses. MIT LL has developed the Emergency Remote Sensing Tool prototype to demonstrate this proof of concept.

Each component is described in detail below.

6.1   DEFINE QUANTITATIVE REQUIREMENTS

Perhaps the most significant challenge encountered when applying remotely sensed imagery to the disaster recovery context is the lack of quantitative requirements. Requests from the emergency management community can lack the detail required, phrased such as "We need to find road damage", whereas the quantitative details that can answer that question in the way that is most useful to the operation have not been defined.

To illustrate what is meant by defining quantitative requirements, consider this road navigability example:

Guided by roadway requirements [12] and significant interaction with JRO Transportation Sector site inspectors, we can describe road navigability as being a combination of damage to the roadway and impediments blocking the roadway. As shown in Figure 32, we define several levels of access to the road,

from fully passable to no access. Describing the level of access addresses the nuances to road damage post-disaster; where a roadway may not be fully intact, but it can still be used for emergency use by first responders or with limited capacity by local residents. What dictates the level of navigability can be categorized into damage or impediment. The size of damage and the location or distribution of the damage within the roadway both affect the ability to traverse the road. Impediments may include debris such as fallen trees or flooding. Similar to damage the impediment size, depth, and location on the road determines whether the road can be navigated by vehicles.
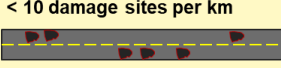
Passable Category	Damage Width	Damage Distribution	Debris Obstruction	Water Inundation
Fully Passable	<10% of road width (0.6m)	< 5 damage sites per km	< 10% of road width (0.6m)	< 2 inches
Partially Obstructed	<20% of road width (1.2m)	< 10 damage sites per km	< 20% of road width (1.2m)	< 4 inches
Limited Access	<40% of road width (2.4m)	< 10 damage sites per 0.5km	< 40% of road width (2.4m)	< 6 inches
No Access	>60% of road width (3.6m)	>10 damage sites per 0.5km	> 60% of road width (3.6m)	> 6 inches

Figure 32. Road navigability detection requirements.

To truly understand the navigability of a road network, the emergency manager needs to know the size, location, and distribution of damage sites; the size and location of debris blocking the road; and the size, location, and depth of floodwaters covering the roadway.

MIT LL recommends that FEMA engage in a detailed requirements analysis that spans all components of the FEMA Community Lifelines.

6.2   SYSTEM CHARACTERIZATION

Remote sensing systems must be characterized in such a way that their applicability to emergency management requirements is clear. Such characterization allows for the emergency management community to determine the most applicable systems as part of mission tasking.

In many other remote sensing-based information support contexts, the match of a sensor platform to the requirements can be articulated relatively easily as a single matrix in a spreadsheet. However, incorporating the combination of a sensor platform and one or more AI/ML algorithms for automating observations introduces a level of complexity that cannot be easily represented in two dimensions. MIT LL

reviewed numerous approaches to visualizing system capabilities across several disparate attributes, including multidimensional matrices, and determined that the spider chart is most appropriate.

For illustration purposes, the following example breaks down each attribute recommended into five levels of performance. Each attribute has different values and scales, but are binned into these five levels for consistency and correlation to the requirements. The requirements described in the previous section would be specific ranges for each attribute.

In TABLE 8, this example set of system performance characteristics are related to the corresponding requirements of a system that can collect 300 mi^2 with an 85% probability of detection of the observation in question, process those data, and detect the damage type in question with 85% or better accuracy, meeting an operational need of a total of 96 hours or less. Note that the values are ordered differently so that the first value represents the least desirable/lowest performance, as though each attribute were rated on a scale from 1–5.

TABLE 8
System Performance and Requirements

Attribute	Description	Range of Values	Required (samples)
Probability of detection	Can the sensor detect the observation required? Determination based on sensor resolution	0–50: None 51–75: Minimal 76–85: Low 86–90: Moderate 86–100: High	85 or better
Revisit Time	How often this can sensor revisit a given AOI	96 hours 72 hours 48 hours 24 hours 12 hours	48 hours
Next Availability	How soon the sensor can conduct the first collection over the AOI	96 hours 72 hours 48 hours 24 hours 12 hours	48 hours
Area Collection Rate	Rate at which the AOI can be captured	100 mi^2/day 200 mi^2/day 300 mi^2/day 400 mi^2/day 500 mi^2/day	200 mi^2/day

Data Processing Time	Length of time required to process data; suggested units are hours per area collected; should include time required to run AI/ML algorithms and deliver output	96 hours/250 mi^2 72 hours/250 mi^2 48 hours/250 mi^2 36 hours/250 mi^2 24 hours/250 mi^2	48 hours/ 250 mi^2
Algorithm Performance	How well the AI/ML algorithm associated with the requirement performs; suggested units are a decimal representation of the AUC of a ROC curve; this metric shows an algorithms performance in terms of true positives vs. false positives	0–0.5: Not better than chance 0.51–0.75: Evolving 0.76–0.85: Good 0.85–0.9: Very Good 0.91–1.0: Exceptional	Very good

Tabular presentation of these requirements can be difficult to interpret quickly. Presenting the data in spider chart form allows for a quick visualization of the requirements. Furthermore, any given system of sensor and algorithm can be overlaid onto the requirements, and the appropriateness of that combination to the requirement at hand can be very quickly visualized.

Shown in Figure 33, each of the attributes are a vertex of the spider chart. The values of each attribute's requirement are depicted on a 1–5 scale, creating a shape. Overlaid as the dashed orange line are the performance values of the MIT LL AOSTB to show how well that particular system can meet the requirements.

In this particular case, the example is showing the actual requirements and performance for "road finding", extracting the road network from an AOSTB collected GM point cloud. Note that the AOSTB well exceeds all of these requirements except for availability. Until AOSTB transitions to an operational tool, there may be some delay in deploying the asset, and visualizing the performance vs. requirements in this way can bring that to the attention of mission tasking.

Figure 33. Spider chart depiction of requirements vs. system performance.

6.3 MISSION TASKING GUIDANCE

After quantitative requirements are clearly defined and systems comprised of sensors and algorithms are characterized in terms of their applicability to those requirements, sophisticated mission tasking can occur.

Considering the road navigability example, the total answer to "are the roads passable?" is the composition of road damage, damage distribution, debris obstructions, and water inundation. Each of these observation requirements are satisfied with different systems of sensors combined with algorithms.

A notional example is shown in Figure 34. Each component observation that informs road navigability is satisfied with a different system of sensor and algorithm. The visual correlation of system performance to requirements provides an easily interpreted guide.
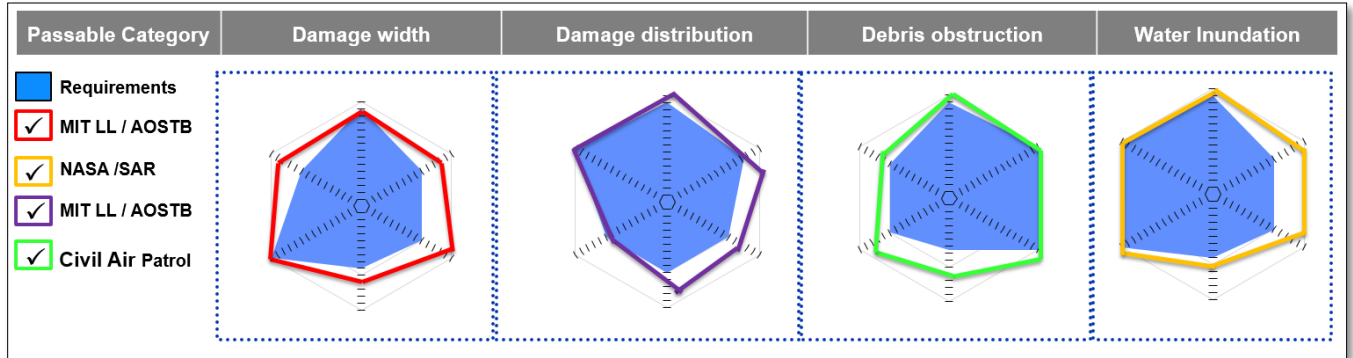

Figure 34. Notional depiction of multi-system mission tasking to determine road navigability.

The ultimate implementation of this framework would enable real-time mission tasking based on the observed or modeled conditions of the disaster. The first mission assigned could be to further scope the subsequent missions by identifying which FEMA Lifeline components exist within the AOI. The results of such missions could be the recommendation of which predetermined systems can meet the observation requirements, and furthermore identify which of those assets are most readily available and viable given the disaster location, environmental conditions such as cloud cover, and the day and time of the event.

It is important to note that the solution for road navigability (as well as other FEMA Community Lifeline components) will likely require multiple systems. As such, the output from these systems must be in a standardized format so that they can be easily aggregated and ingested by the emergency management community. To meet this need, the Emergency Remote Sensing Language (ERSLA) is described in the next section.

6.4   COMMON FORMAT FOR COMMUNICATING OBSERVATIONS (ERSLA)

Appropriate disaster response relies on timely and accurate information to provide a clear picture of the current situation. This information may take many forms to include reports, graphics, and analysis products. Some may start as geospatial data collected from an imaging sensor, such as an airborne GM-LIDAR platform. Regardless of the source, data analysis should only contain the information needed to develop a coherent picture of the current situation. Additionally, this analysis should be formatted to be easily integrated into the disaster response planning workflow.

After evaluating several existing message communication formats used in disaster response and management, military communications, and general network messaging technology, we found that no single format existed that adequately captured sensor analysis for use in disaster response. In response, we developed an extensible markup language (XML)-based hybrid of an existing format. We call this new message format Extended Remote Sensing Language (ERSLA).

The ERSLA message format was derived largely from the cursor on target (CoT) message format [13]. The CoT was designed to succinctly convey information regarding a point, a volume associated with that point, and attributes associated with that combination. This type of terse description and its associated format is valuable for emergency management in order to convey information about locations or entities that have been affected or damaged.

By using an XML format, this new message type can be inserted into other XML-based disaster response messages, such as the Emergency Data Exchange Language (EDXL) [14], where appropriate. Not only can ERSLA be used to communicate sensor analysis results from various remote sensing and analysis systems, it can also be used to capture information based on social media-sourced data and analysis. ERSLA can also be used to ingest the results of surveys, to include the type of geo-referenced information collected by the DDD or the CERT Damage Assessment Form. The extensible nature of ERSLA enables ingestion of future geo-referenced sensor and survey data.

The lightweight, low bandwidth nature of ERSLA messages supports the potential for digitally communicating damage observations from sensing aircraft while still in flight. The standardized format enables partners developing AI/ML algorithms to adjust the schema of their output.

6.4.1 General Format

ERSLA's XML format enables the message contents to be self-describing. This, in turn, enables other tools to generate or parse an ERSLA message. The message is designed to convey those aspects from imagery or other "sensor" analysis products that are relevant for Humanitarian Assistance and Disaster Relief (HADR). The ERSLA message will contain attributes from a base message schema specification and, if appropriate, from a details sub-schema specification. The sub-schema is used to elaborate on the information contained in the base schema. Additionally, the ERSLA message shall be populated with a required set of attributes; these will be denoted by the value of YES in the Required in Initial Message field portion of the Attribute specification.

For example, if the message is only describing information about a point, the ERSLA message will only provide the location of that point in the base portion of the message, along with the other salient non-spatial aspects of the message. If, however, the geometry associated with the ERSLA message is a line or a polygon, then the message organization becomes more complex. The base message still contains the point information associated with the center of the more complex geometry. Additional, geometry information held in the details sub-schema. Such message organization facilitates message parsing to support various

levels of analysis. The full draft specification for ERSLA, including message organization and definitions, can be found in Appendix B.

6.5 VALIDATING AND AGGREGATING OBSERVATIONS (ERSAT)

6.5.1 Overview

As described in the first three steps of this framework, the solution for fully satisfying requirements will likely require observations derived from multiple modes of sensing. The ERSLA messaging approach enables these observations to be combined into a comprehensive representation of each observation. The explosion in AI/ML efforts to identifying damage in disaster contexts introduces the potential for powerful automation, but there is a need to validate the automated results and to aggregate them with the results from other systems.

To accomplish this portion of the open standards framework, MIT LL has developed a prototype software toolset named the Emergency Remote Sensing Analysis Tool (ERSAT). The primary use case of this application is for analysts to view and validate damage observations from AI/ML algorithms that have been executed against remotely sensed data and communicated via ERSLA message. The tool is intended to give the analyst the ability to view an observation, not only in the context of the imagery originally used to generate the observation, but also with other imagery or data sources that may provide the analyst with the needed understanding of the observation to determine if it is valid or not.
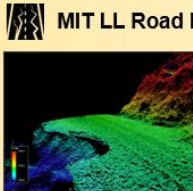
As ERSLA messages are ingested from multiple sources, the links to the original imagery sources are cataloged by ERSAT, building an internal library of imagery that could be leveraged to support observation validation. After a few observations, the analyst may develop a level of trust with the algorithm's output and validate the remaining observations. The ERSAT system will allow analysts to validate the data based on the reported performance of an AI/ML algorithm if that performance falls within the agency's acceptable risk threshold.

The *Entity* attribute specified by the ERSLA messages correspond to the types of things observed, such as roads or structures. For any message that is validated by an analyst, those data is added to a GIS REST service published by ERSAT.

ERSAT is designed to ingest ERSLA messages, but the architecture allows for the development of micro-services that could ingest data from other GIS data sources such as REST services, KML, or ESRI Shapefiles, so long as those data sources matched the ERSLA schema.

Continuing with the road navigability example, if road damage is derived from MIT LL algorithms executed against GM-LIDAR data and road flooding is communicated via algorithms executed against synthetic aperture radar data, the valid output from those two data sources are published as a common "road status" service that can be ingest by emergency management analysts at any level of government.
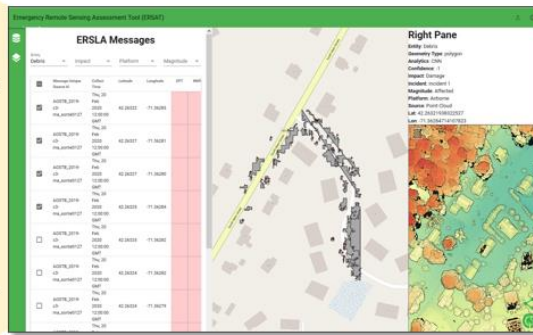
Figure 35. ERSLA/ERSAT analysis workflow.

6.5.2 Technical Implementation

ERSAT is a robust, distributed system that uses the latest web technologies in order to enable users to visualizes and assess remote sensing data in a modern web browser. Through the use of open source applications, ERSAT is well equipped to handle all types of future software requirements. Components consist of:

- **Keycloak** [15]: all communication channels and data access are behind this open source identity and access system; this will position ERSAT for future support for users with various levels of access and privileges

- **GeoServer** [16]: the well-known open source geospatial data server allows GIS data to be shared across other web mapping services in a variety of industry standard formats, enabling distribution of data to all emergency managers involved in the disaster

- **PostgreSQL** [17]: all data are saved and organized in the well-known open source relational database application PostgreSQL.

- **NGINX** [18]: "Engine X" is an open source HTTP and reverse proxy server

The architecture allows users to review all of the information gathered from analysis products and would provide a singular location for storing, viewing, and analysis. The communication between the components of ERSAT is via an application programming interface (API) that positions the tool well for expanded capabilities and potential integration with other systems.

All of these component applications are also able to be deployed on a multitude of software environments such as CentOS [19], Ubuntu [20], and even Amazon Elastic Compute Cloud (EC2) [21] instances. By doing so, FEMA could deploy ERSAT to Amazon EC2 and train partners or crowd source organizations on its use.

ERSAT is a prototype application and a fully deployable enterprise system would require additional development.
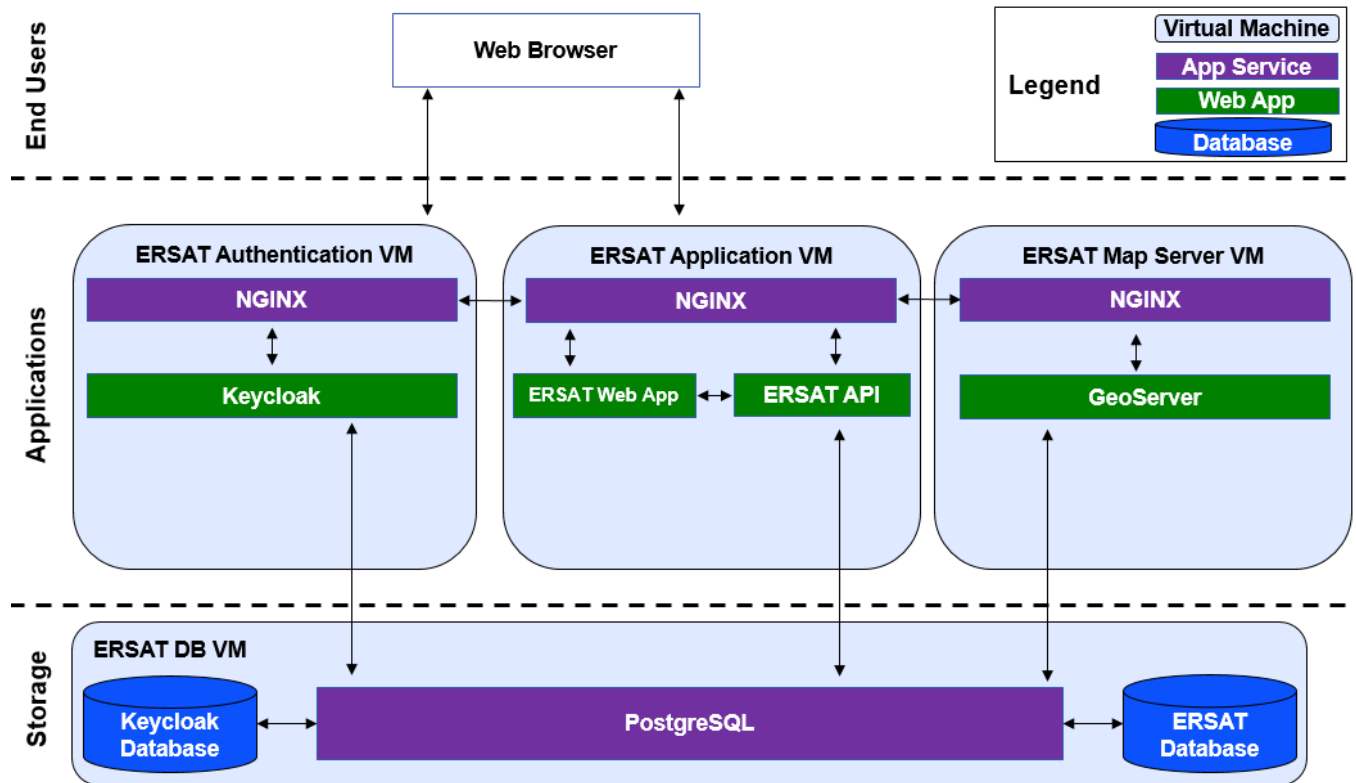

Figure 36. ERSAT architecture.

This page intentionally left blank.

7. RECOMMENDATIONS

This section presents a summary of MIT LL recommendations based on the laboratory's experience supporting FEMA at the Joint Recovery Office in Puerto Rico in the context of extensive experience supporting federal agencies across numerous mission areas.

7.1 NORMALIZE REMOTE SENSING-SUPPORTED DAMAGE ASSESSMENTS

There are numerous benefits to using remotely sensed data to support damage assessments. MIT LL recommends that FEMA leadership continue to support the research and development of remote sensing support of disasters and continue to introduce the technology into FEMA program areas.

When properly applied and exploited, remote sensing has the capacity to increase operational efficiencies by speeding response and recovery times while also reducing overall costs. By collecting imagery immediately after a disaster, including a high-resolution 3D model derived from GM-LIDAR, FEMA establishes a permanent record of the state of damage for an AOI. This permanent record can be used for to support response, long-term recovery, and mitigation against future disasters.

Attempting to inject new technology into high-stress, time-sensitive operations can detract from the success of the technology. To alleviate this, MIT LL recommends that FEMA continue to explore remote sensing, including GM-LIDAR, during steady state.

7.2 EXPAND TRAINING PROGRAMS TO FEMA CONTRACTORS

The transient nature of the FEMA workforce presents significant challenges in terms of training staff on new technology and programs. One strategy that MIT LL recommends is to augment the training of FEMA staff by training additional analysts within the contract companies that support FEMA. Establishing a cadre of analysts who are familiar with a new technology exploitation methodology, such as the GM-LIDAR remote sensing damage assessment workflow, provides continuity to the program effort that can better adapt to the turnover of FEMA personnel.

7.3 ADOPT THE REMOTE SENSING FRAMEWORK

FEMA Headquarters established the FEMA Remote Sensing Innovation Working Group in 2019, bringing together several national laboratories working on the broader challenge of incorporating observations from remote sensing into the FEMA mission space, including the exploitation of AI/ML assessments. This collaborative group is a great step towards effective use of remote sensing to support FEMA.

MIT LL recommends that FEMA work with the other national laboratories within the Remote Sensing Innovation Working Group to adopt the remote sensing framework presented in this document in

order to establish a structured, end-to-end systems approach that will result in providing standards, tools, and techniques that support not only FEMA and its mission, but also state, tribal, territory, and local emergency management.

7.3.1   Requirements Definition

FEMA has been working towards defining requirements related to remote sensing. MIT LL recommends that those efforts continue, but be expanded to include quantitative representations of each FEMA Community Lifeline component. Given the interdependent nature for FEMA program requirements and overlap with state, tribal, territory, and local requirements, the remote sensing requirements definition effort should be done as an agency-wide, detailed systems analysis.

7.3.2   Systems Characterization

FEMA Headquarters has been cataloging the remote sensing assets available to them on a routine basis, such as the Civil Air Patrol (CAP). MIT LL recommends that the system cataloging efforts be extended to include a combination of the sensor and accompanying AI/ML exploitation algorithms.

For example, an effort underway by FEMA that leverages the CAP using a camera system to collect 3D imagery, and then uses an AI/ML algorithm to estimate structural damage presents an immediate opportunity to shift the system characterizations. MIT LL recommends that this system be characterized using the same methodology used to characterize the AOSTB GM-LIDAR system, as described in Section 6.2.

Establishing a standard way to characterize sensors coupled with AI/ML algorithms as combined systems will assist the emergency management community greatly in evaluating the most appropriate tools available to them.

7.3.3   Mission Tasking Guidance

MIT LL recommends that FEMA use the detailed requirements gathered and system characterizations to inform their current mission tasking plans. The systems characterization can be used to engage program areas within FEMA to focus conversations on requirements gathering, and during response or recovery operations to help guide collection priorities.

Given the experimental nature of AI/ML exploitation algorithms and emerging sensor systems, the mission tasking guidance should also include experimental missions conducted by the laboratories involved in the FEMA Remote Sensing Innovation Working Group.

7.3.4   ERSLA

The explosion of AI/ML algorithms under development to support disaster relief generates a deluge of data during a disaster. MIT LL recommends that FEMA continue to work with MIT LL and the FEMA

Remote Sensing Innovation Working Group to evolve the draft Emergency Remote Sensing Language (ERSLA) and adopt this standard as the way for disparate AI/ML algorithms to communicate their results.

7.3.5 ERSAT

The effective and timely utilization of myriad data sources and AI/ML outputs that have varying degrees of accuracy and confidence requires a software toolset to validate, aggregate, and re-disseminate those data. To demonstrate the utility of such a toolset, MIT LL built ERSAT, a prototype system capable of displaying 2D imagery and 3D datasets such as GM-LIDAR and analytics resulting from exploiting those datasets.

MIT LL recommends the FEMA continue developing such a capability, following a model similar to the CAP Imagery Uploader, that can be accessed by state or local emergency managers for events that do not result in a federal declaration. A fully capable enterprise system will require additional funding and development time.

This page intentionally left blank.

8. AOSTB FUTURE

Leveraging lessons learned from the work in support of Puerto Rico's recovery from Hurricane Maria, MIT LL collaborated with Ohio State University's Battelle Center for Science, Engineering, and Public Policy to develop a proposal for the establishment of a National Sensing Asset to more effectively anticipate, monitor, and respond to natural and manmade disasters. This program would establish a dedicated, airborne, remote sensing platform that would provide cutting-edge technology to all FEMA regions. The program would function as a network, ensuring efficient collection of the right information, at the right time, and in the right place. The program would be multi-agency and multi-sector:

- Research and development related to sensing technology will leverage innovations from national labs, federally funded research and development centers (FFRDCs), academia, and the private sector;

- Deployment will be conducted by the National Guard in coordination with FEMA and state Emergency Management Agencies (EMAs);

- A robust data science operation will complement the technological backbone and will leverage organizations such as the Department of Defense's Joint Artificial Intelligence Center (JAIC) and the National Geospatial Intelligence Agency (NGA).

Importantly, the National Sensing Asset would be continuously operational. In periods without disaster scenarios, the program would conduct vulnerability assessments that can inform risk mitigation activities. This is critically important, as underserved communities often face disproportionate harm from natural disasters. During disasters, the National Sensing Asset would a trusted mechanism for collecting critical information and provide the data analytics required to sufficiently support decision makers. Following disaster scenarios, the program will reduce the time required to support communities that need supporting resources.

The National Sensing Asset would constitute a structured mechanism through for stakeholders to collaborate, innovate, and prepare in advance of disasters. Similarly, it would present a streamlined process for the acquisition of data during and after disaster scenarios. However, perhaps the most important aspect of the program is that it would provide a dedicated mechanism for the translation of data into insights for decision makers. This will be conducted through a dedicated data science team that is coupled to each geographic node of the National Sensing Asset network. The data science team will integrate knowledge from across academic, private sector, and government agency partners, including cutting-edge advancements in AI/ML. These teams will also define common standards for geospatial data and ensure interoperability across the National Sensing Asset data and other sources such as satellites and unmanned aerial vehicles (UAVs).

In addition to protecting our critical infrastructure, the National Sensing Asset would offer a significant workforce development opportunity. FEMA Corps is an example of service training through our

federal disaster response infrastructure, and has demonstrated a pathway for programs such as the National Sensing Asset. A specialized track of FEMA Corps could be established, focused specifically on geospatial intelligence that would be synergistic with programmatic elements discussed above such as interaction with the National Guard. Participants could conduct liaison activities between academic organizations, federal agencies, and the operational core of the National Sensing Asset, and develop highly transferable skills in data analytics, communication, and leadership. Engagement with the Corporation for National and Community Service in this manner is consistent with the concept of a National Service Reserve Corps, which has been proposed as a pathway to civic engagement, education opportunities, and economic stability for recent college graduates. As our nation recovers from the dual threat of a pandemic and an economic recession and looks ahead to the risks posed by disasters of increasing severity and frequency, this program would train the highly skilled, adaptive workforce needed to combat these challenges.

APPENDIX A. GM-LIDAR SECTOR FACT SHEETS

The following fact sheets were produced to illustrate potential use cases for each sector at the Puerto Rico Joint Recovery Office (JRO). Some examples were derived from previous MIT LL GM-LIDAR missions and some samples were derived from the Puerto Rico AOSTB mission. The fact sheets cover sectors for: Transportation, Debris, Energy, Communications, Mitigation, Environment Historic Preservation (EHP), Water, Public Building/Housing, Commonwealth, and Natural Culture Resources.

LIDAR Capabilities: Transportation

- Road condition/damage assessment
- Length, width, depth, and volume of damage areas
- Bridge condition/damage assessment
- Guard rails missing/damaged

LIDAR Limitations: Transportation

- Small or shallow damage areas such as cracks and potholes
- Debris around bridges may not be apparent in GM-LIDAR data
- Damaged or missing guard rails may be difficult to see in the data, but may be inferred from surrounding damage.
- Damage assessments enhanced with cues from visual data (Vexcel, Google Earth)

Reporting Requirements	GM-LIDAR Applicable	Notes
Road condition/damage assessment	Yes	Visual detection and/or confirmation of road damage (Figure 37)
Cracks in roads	No	Cracks and small potholes not detected in GM-LIDAR data
Missing roads	Yes	Washouts easily detected from change in elevation of the road surface (Figure 38)
Road shoulders missing	Yes	Shoulder damage detected from elevation change compared to main road surface
Landslide	Yes	Road bed washout even with asphalt/concrete road surface remaining intact detected by elevation change (Figure 38)
Bridge condition/damage assessment	Yes	Visual identification of missing or damaged bridges (Figure 39)

Debris around bridges	Possible	Larger debris piles resulting from washup on bridge pilings visually identified, volume measurements possible; debris under bridges cannot be seen
Missing bridges or pieces of the bridge	Yes	Lengths of damaged sections measured directly from GM-LIDAR data (Figure 39)
Missing guard rails	Possible	Not always obvious in GM-LIDAR data, but may be inferred from surrounding damage assessments
Guard rails hanging off a road	Possible	Not always obvious in GM-LIDAR data, but may be inferred from surrounding damage assessments or additional imagery (Figure 38)

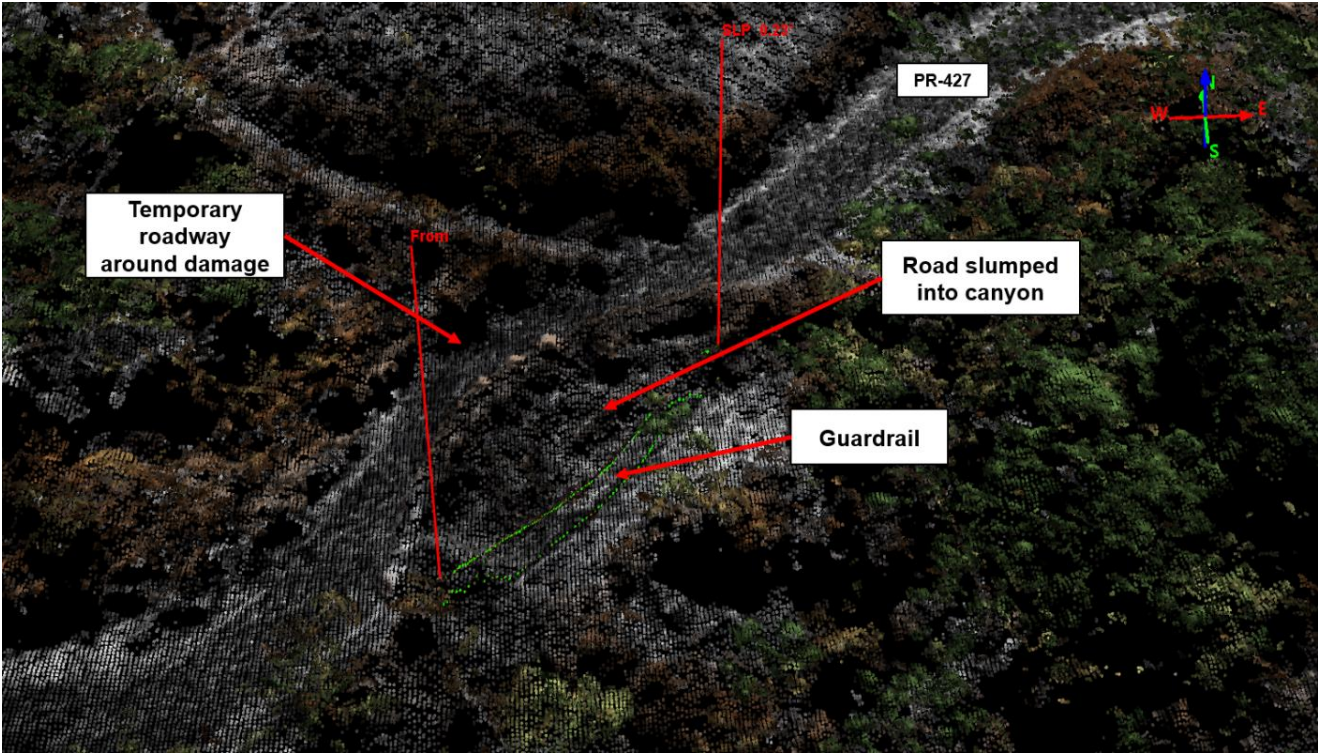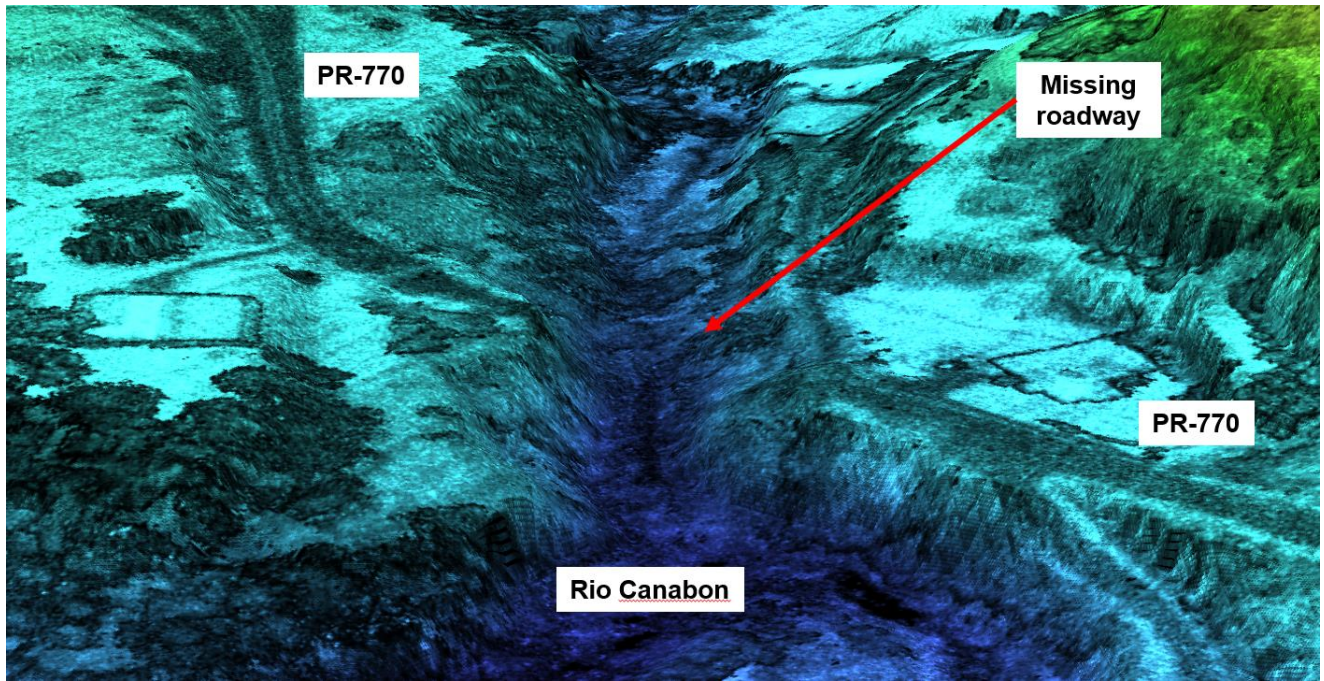**PAST SUCCESSFUL USE CASES: TRANSPORTATION SECTOR**

Figure 37. Missing roadway.

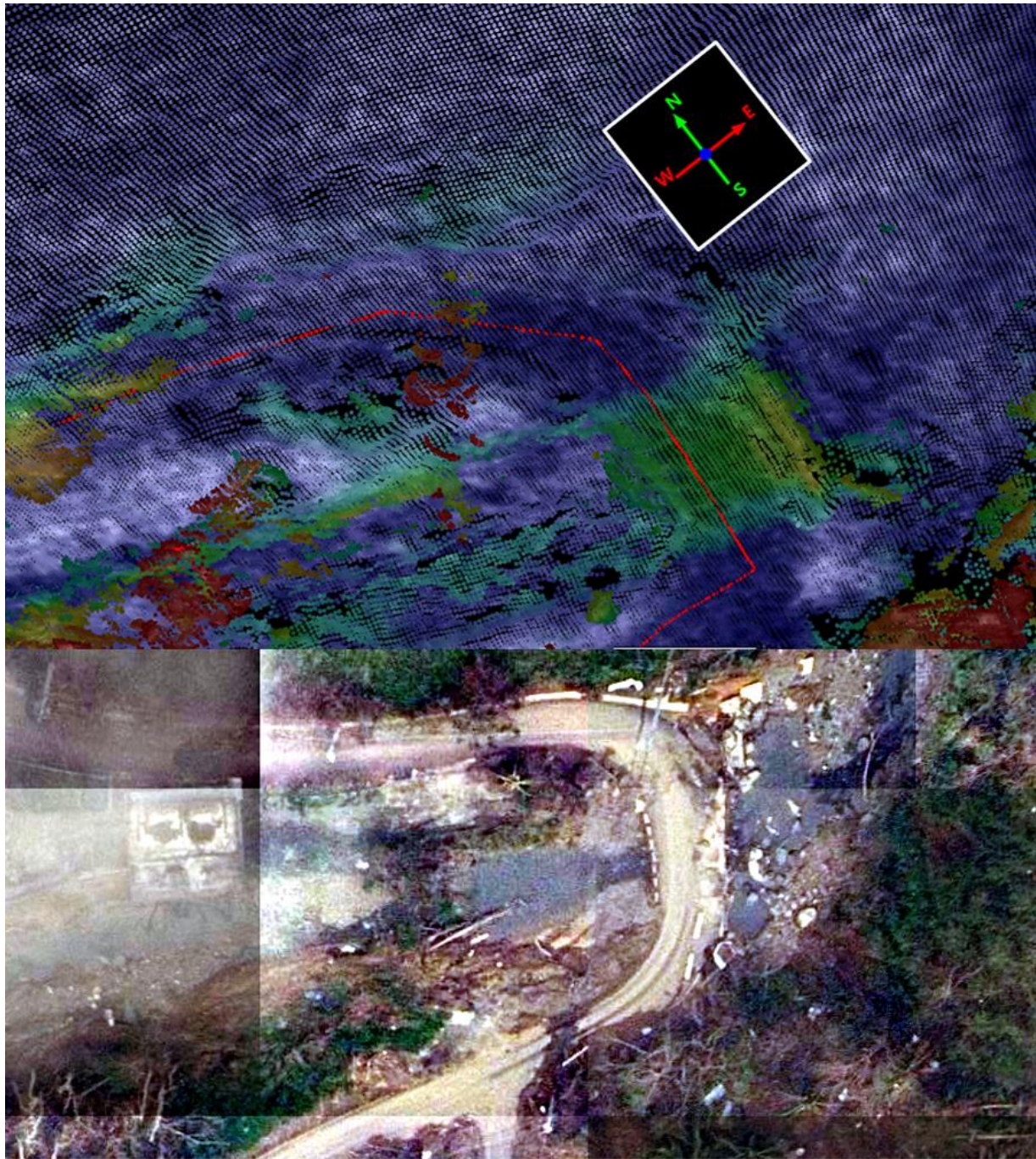*Figure 38. Landslide/road slumped into canyon. Guard rail seen in GM-LIDAR data.*

Figure 39. Bridge damage: LIDAR (top), Vexcel Visual (bottom).

Debris-Related GM-LIDAR Capabilities

- Locating debris piles along roads, water's edge
- Quantity estimations of debris
  - Length
  - Height
  - Width
  - Volume

Debris-Related GM-LIDAR Limitations

- Cannot detect debris under surface of water
- Small shrubs and non-debris objects may falsely be identified as debris piles, but these false positives may be mitigated using pre-event site data

| Reporting Requirements	GM-LIDAR Applicable	Notes
Locations of debris piles along roads	Yes	• Visual identification • Measurements
Debris piles around bridges (sides of bridges, along the water's edge/around a bridge abutment or footings)	Yes/ Possible	• Visual identification • Measurements • Limitations: cannot penetrate water or detect debris under bridge

PAST SUCCESSFUL USE CASES: DEBRIS
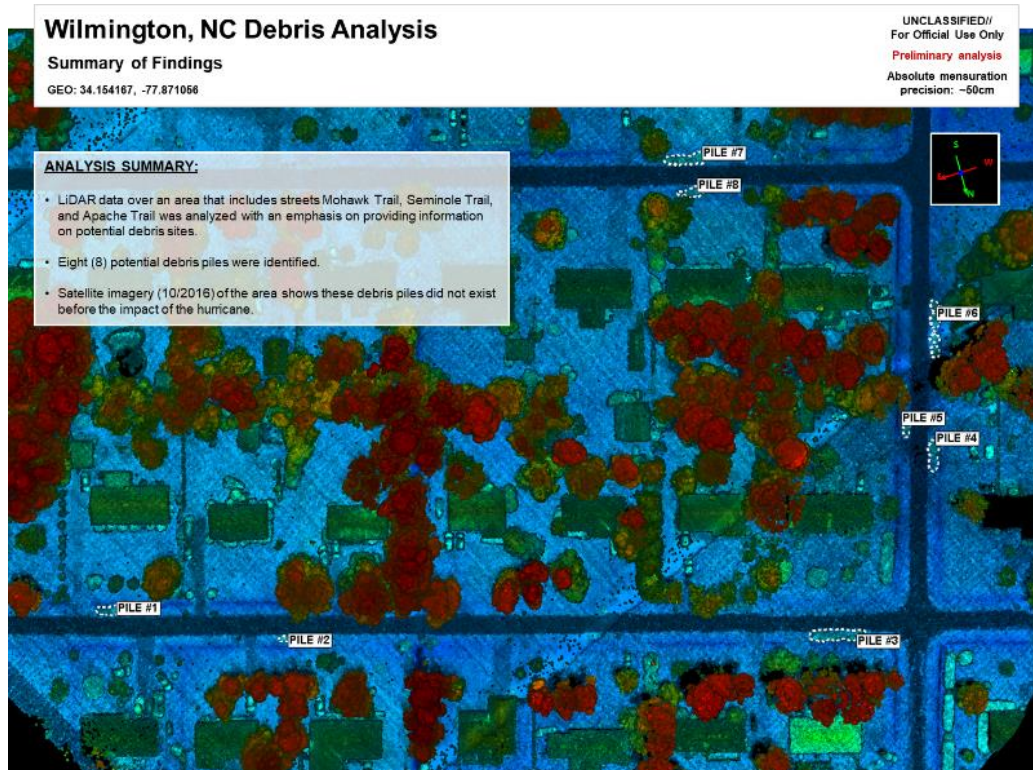
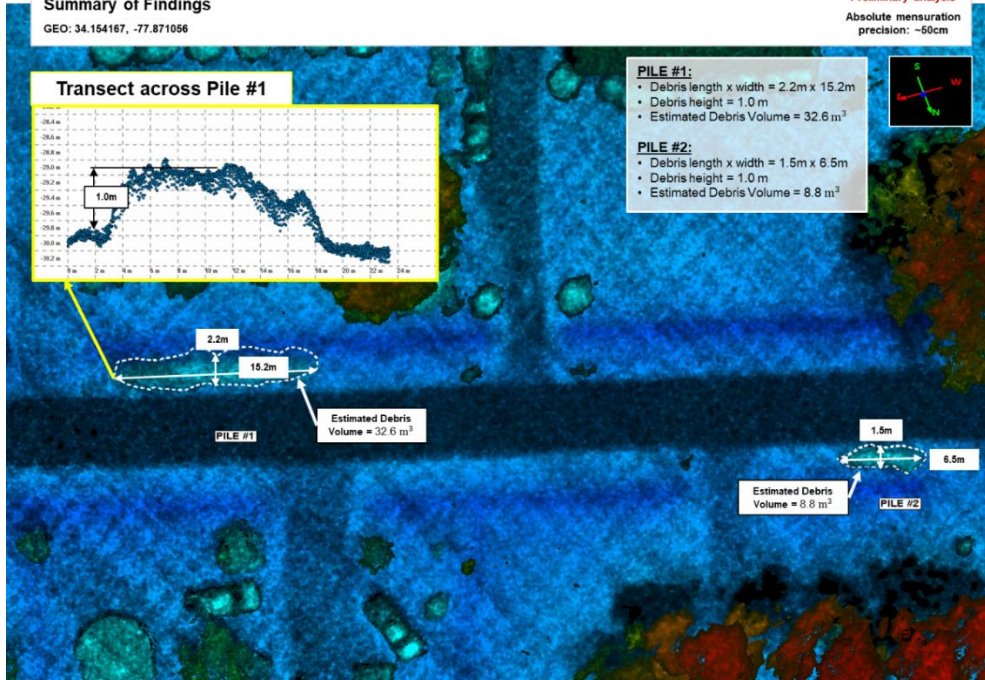*Figure 40. Identification of debris piles in Wilmington, NC.*

Figure 41. Mensuration of debris piles for debris quantity (volumetric) estimation.

GM-LIDAR Capabilities: Energy

- Infrastructure condition/damage assessment
- Downed towers

GM-LIDAR Limitations: Energy

- Power lines on ground not visible in GM-LIDAR data
- Some types of infrastructure damage may not appear in GM-LIDAR data, e.g., blown transformers or substations

| Reporting Requirements	GM-LIDAR Applicable	Notes
Transmission lines	Yes	Visual identification of downed lines, if not fully on ground (See **Figure 42**)
Power poles	Possible	Large support tower damage detected in GM-LIDAR data
Substations	Yes	Major damage to substations visible (See Figure 42)
Power lines on the ground/in a road	No	Completely downed lines have the same elevation as the ground and are not detectable
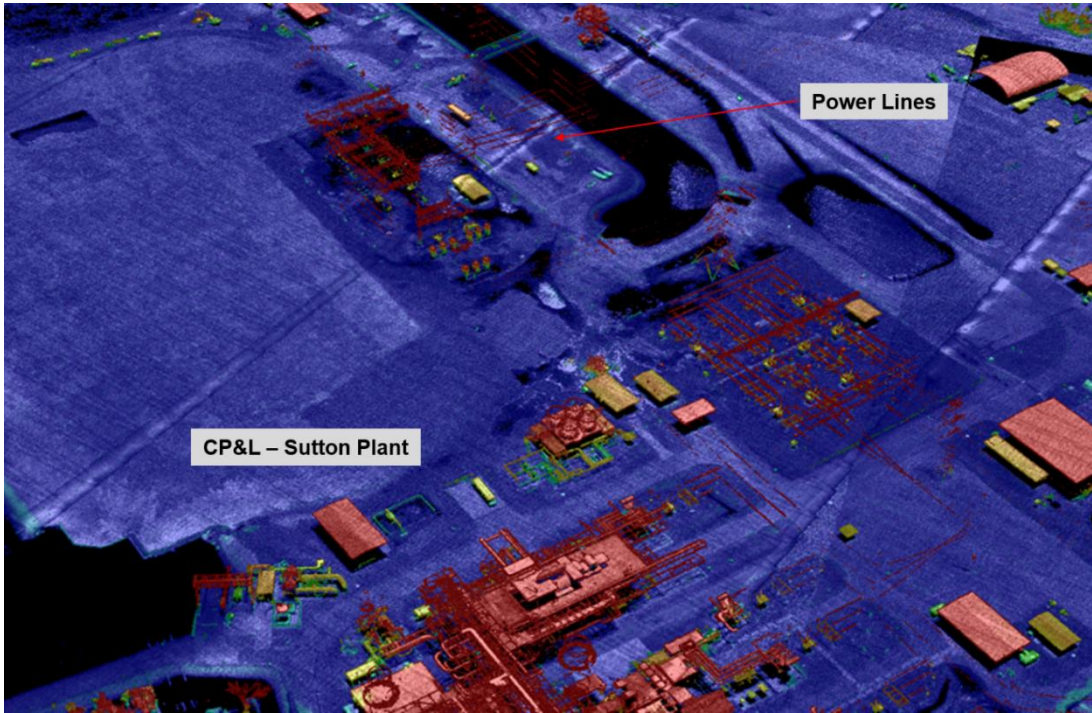
Figure 42. Power plant and lines.

GM-LIDAR Capabilities: Communications

- Visual identification of pole, tower, or lines (see Figure 43)
- Visualize cross section of pole, tower, or lines (see Figure 44)
- Measurements: length, width, height, volume
- Visual detection of major damage

GM-LIDAR Limitations: Communications

- Narrow vertical structures may have lower point density and be more difficult to see
- Low point density could be misinterpreted as damage (e.g., missing tower)
- Precise georegistration over broad areas is in progress

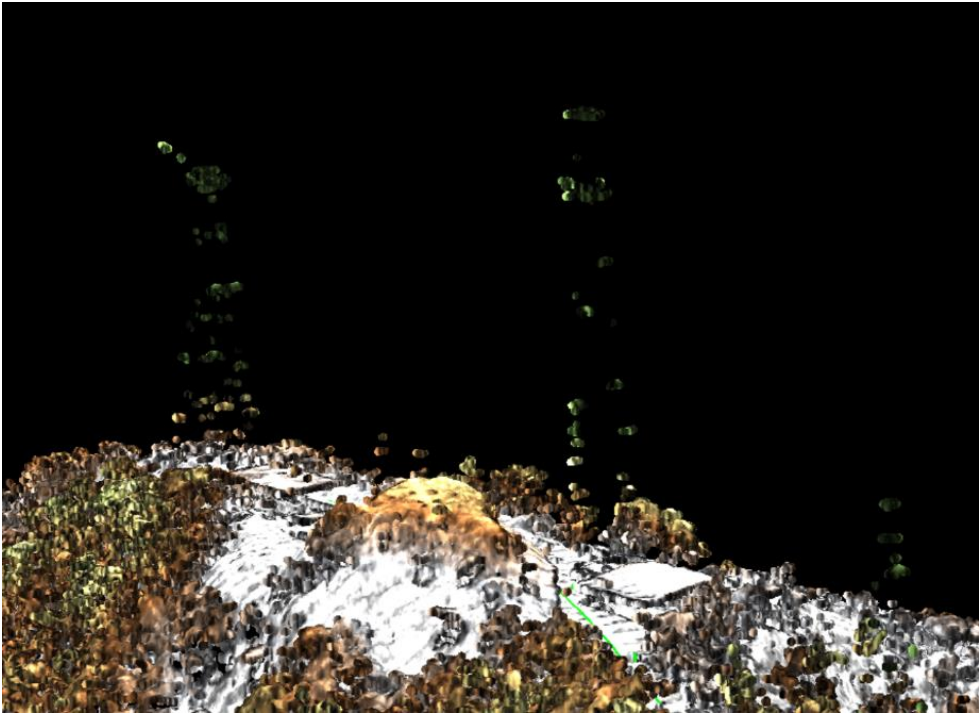| Reporting Requirements	GM-LIDAR Applicable	Notes
Telephone poles, lines	Yes	Use may be limited by low point density
Communications towers	Yes	Use may be limited by low point density

PAST SUCCESSFUL USE CASES: COMMUNICATIONS SECTOR

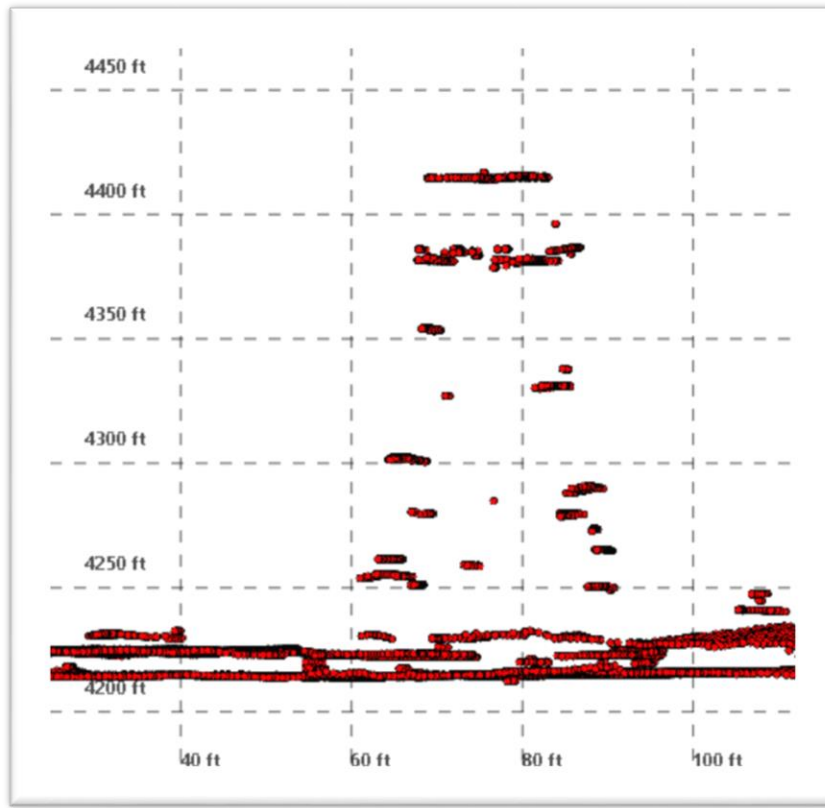*Figure 43. Visualization of communications tower.*

Figure 44. Cross section of communications tower.

Mitigation Sector GM-LIDAR Fact Sheet

GM-LIDAR Capabilities: Landslides

- Visual identification of landslide (see Figure 45)
- Measurements of landslide site (see Figure 46)
    - Length
    - Width
    - Height
    - Estimated volume of fill
- Profile and cross section analysis of landslide
- Slope analysis for landslide detection and potential landslides

GM-LIDAR Limitations: Landslides

- Landslides with small area of impact may not be easily detected
- Significant foliage may obscure landslide site or prevent detection

Reporting Requirements	GM-LIDAR Applicable	Notes
Landslides—existing or recent	Yes	• Visual detection, confirmation and characterization of landslides • GM-LIDAR identification improved with supplementary satellite imagery
Analysis for landslide detection/landslide analysis for potential landslides	Yes	• Measurements of landslide site • Slope analysis for landslide detection and potential landslides

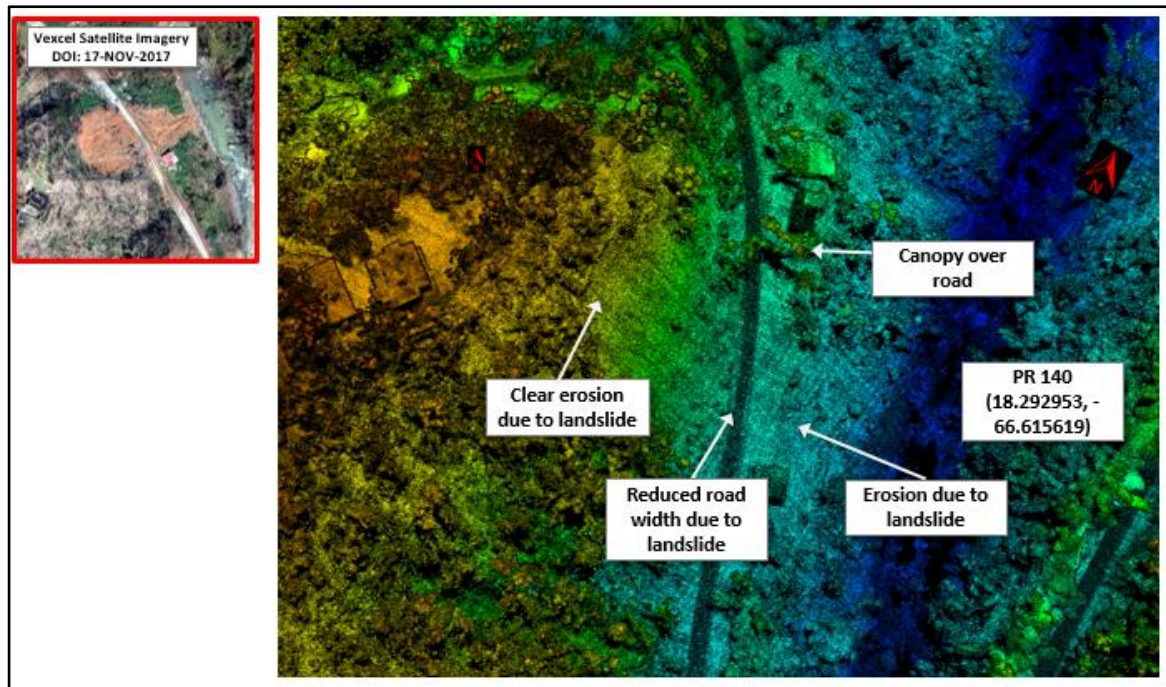**PAST SUCCESSFUL USE CASES: MITIGATION SECTOR**

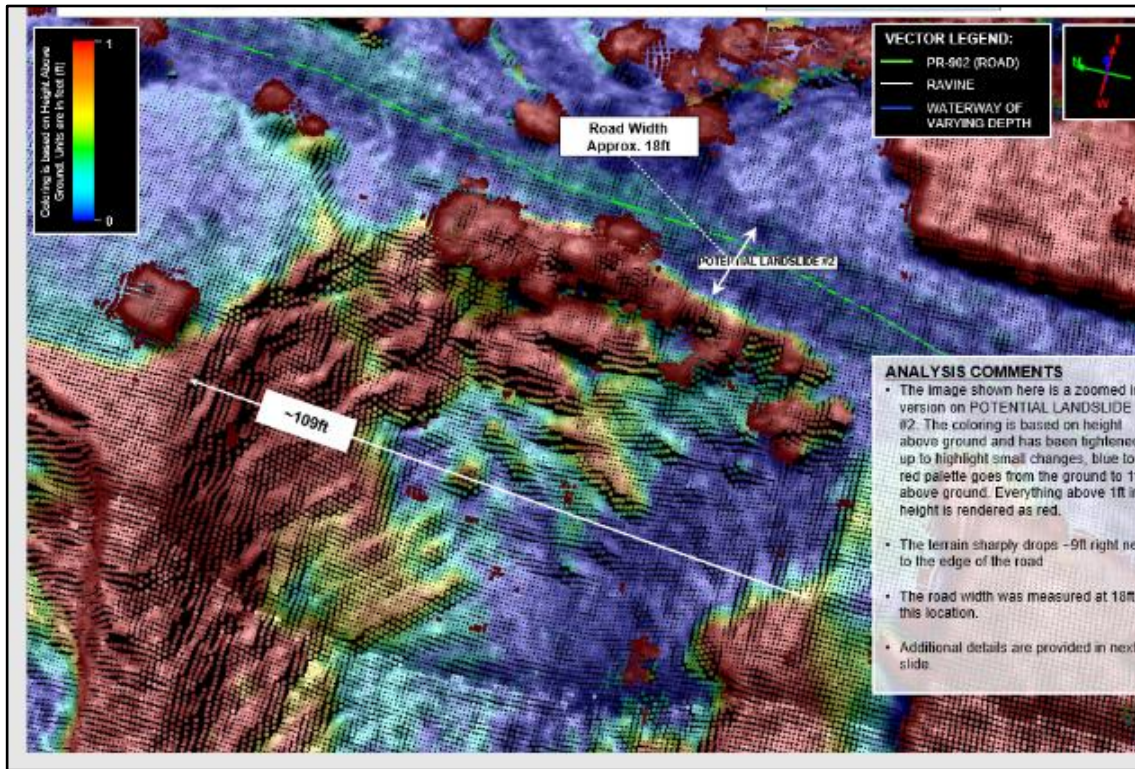*Figure 45. Visual detection, confirmation, and characterization of landslide.*

Figure 46. Mensuration of landslides.

Environmental/Historic Preservation (EHP) Sector GM-LIDAR Fact Sheet

GM-LIDAR Capabilities: Coastal

- Visual identification of coastline/shoreline/beach (see Figure 47)
- Measurements of coastal site and potential breakwater(s) sites
    - Length
    - Width
    - Height
    - Volume
- Profile and cross-section analysis of coastline/shoreline/beach (see Figure 2)
- Slope analysis
- Change detection (depending on data availability)

GM-LIDAR Limitations: Coastal

- GM-LIDAR unable to penetrate water
- Slope or height changes that are small may not easily be detected (<25cm)
- Current data georegistration accuracy may not be high enough to compare with pre-event imagery, GM-LIDAR, or GIS vector data

Reporting Requirements	GM-LIDAR Applicable	Notes
Coastal/shoreline/beach	Yes	• Visual identification
Change detection pre/post storm	Yes	• Depending on data availability
Erosion	Yes	• Visual identification and measurements
Locations for potentially building breakwater(s)	Yes	• Would require engineering input on construction

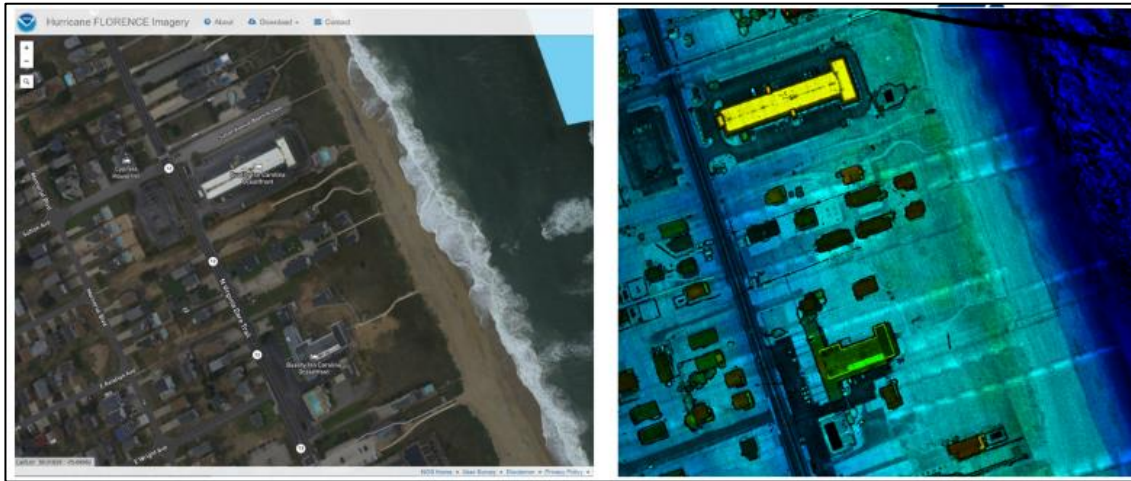**PAST SUCCESSFUL USE CASES: COASTAL**

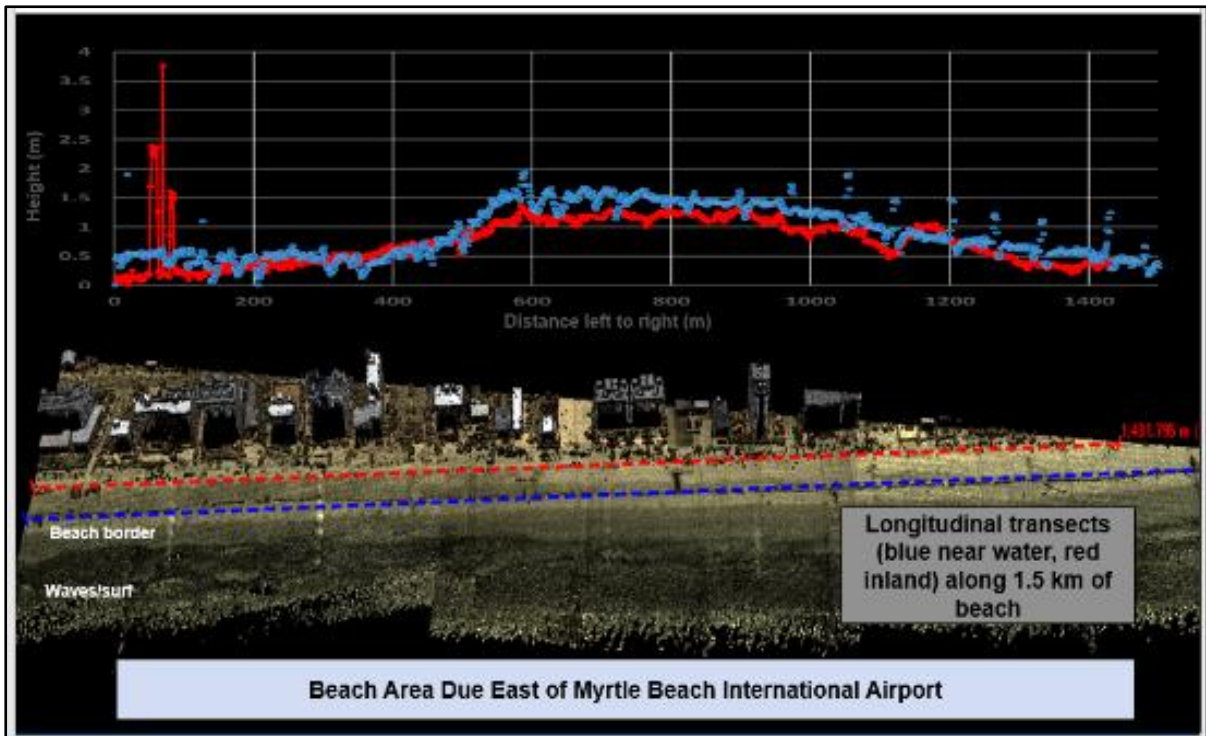*Figure 47. Visual detection, confirmation and characterization of shoreline.*

Figure 48. Profile and cross section analysis.

Water Sector GM-LIDAR Fact Sheet

GM-LIDAR Capabilities: Water Sector

- Visual identification of water and wastewater related infrastructure
- Visual identification of damage to water and wastewater related infrastructure
- Measurements of infrastructure, damage, or water features
    - Length
    - Width
    - Height
    - Volume
- Slope analysis for landslide detection and potential landslides

GM-LIDAR Limitations: Water Sector

- Cannot penetrate water
- Precise georegistration over broad areas is in progress

Reporting Requirements	GM-LIDAR Applicable	Notes
Dam status	Yes	Damage detection and measurement demonstrated with Guajataca Lake Spillway damage assessment (**Figure 49**)
Watershed update	Yes	
Identify water features (lakes, ponds, rivers, streams)	Yes	Detection of water features would be based on visually identifying areas of data voids (black areas) that indicate standing water
Landslides monitoring/density and location analysis.	Possible	Landslide detection and sizing is definitely possible, but continuous monitoring of landslides would require repeated data collections
Effects of landslides on water/waste water infrastructure and water supplies.	Possible	Visual identification of where landslide intersects with waterways; best when combined with vector data for identifying locations of infrastructure and waterways
Volume of landslide sediment impacting downstream water supply reservoirs	Possible	Can only measure volumes above water line
Canal assessment: identify damage and sinkholes	Yes	Assessment limited to damage above waterline of a canal
Effect of river meander's lateral movement on water intakes	Yes	Best supported with combination of vector GIS data showing locations of water intakes

|		
Above-ground pipeline damage	Possible	Cannot likely see damage on underside of pipeline
Water flow detection for damaged above ground pipelines	Possible	If water flow is significant enough to be discernable from background
Debris volume measurement on land	Yes	
Volumetric measurement for debris floating in reservoirs	Possible	Volume could be calculated for debris above water line, but not debris below water line
Exact coordinates per facility (water/ waste water, pump station, water tank, etc.)	Possible	Accuracy of coordinates would depend on overall georegistration accuracy and may vary by some number of meters
Bathymetry/sedimentation rates at PRASA reservoirs	No	
Water levels on systems served by DNRE or municipalities flood control pump stations	No	
Identification of sewage water plumes in rivers and reservoirs	No	

PAST SUCCESSFUL USE CASES: WATER SECTOR
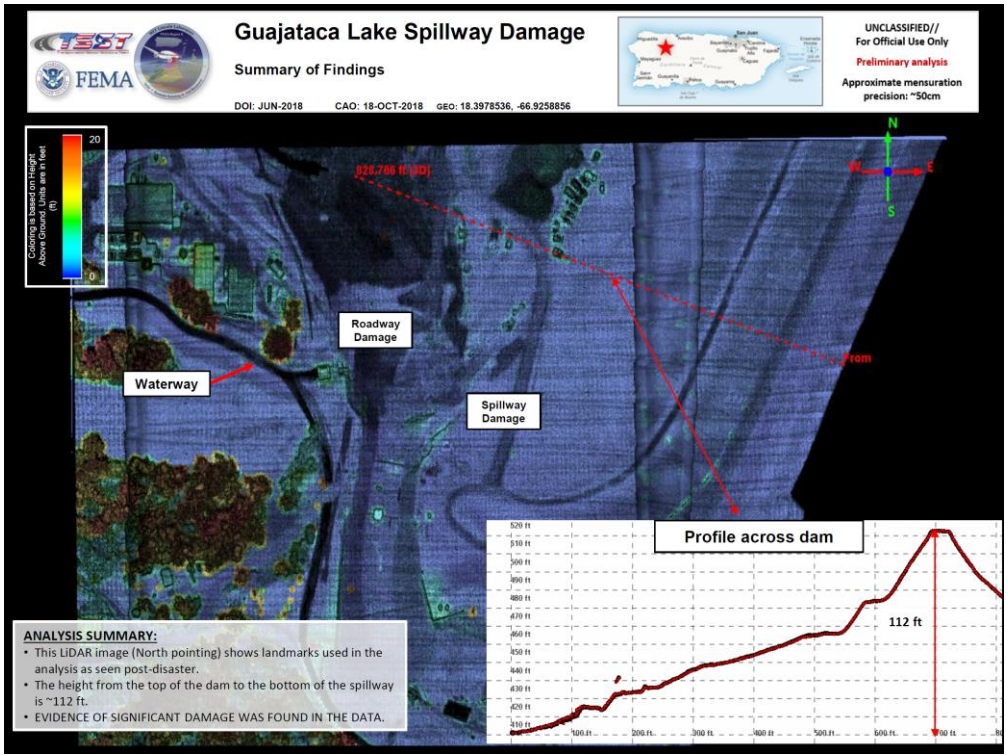
Figure 49. Guajataca Lake spillway damage.
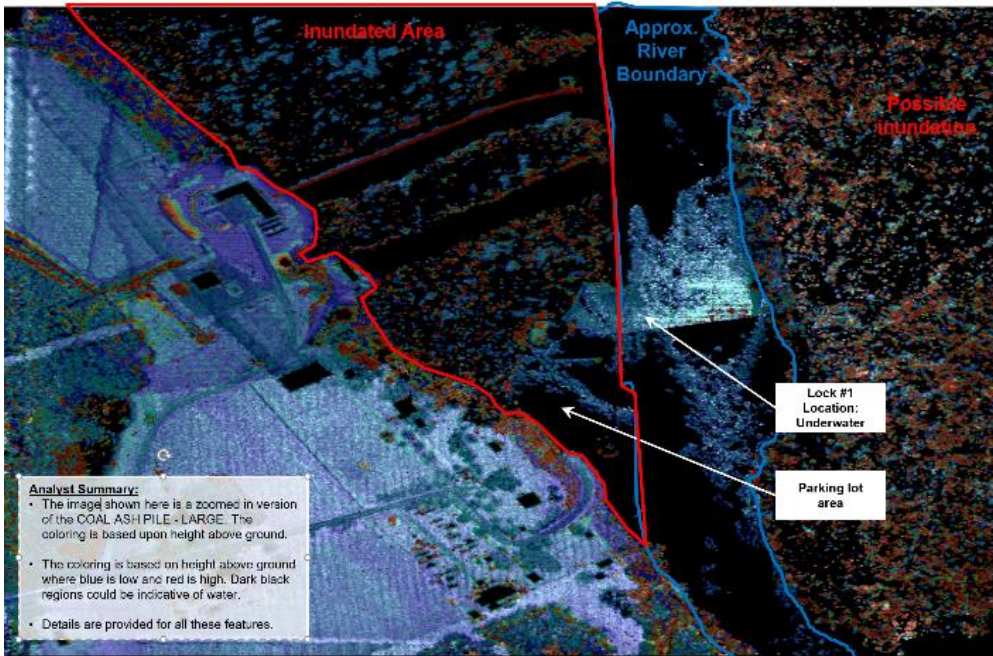
Figure 50. Water inundation visible.
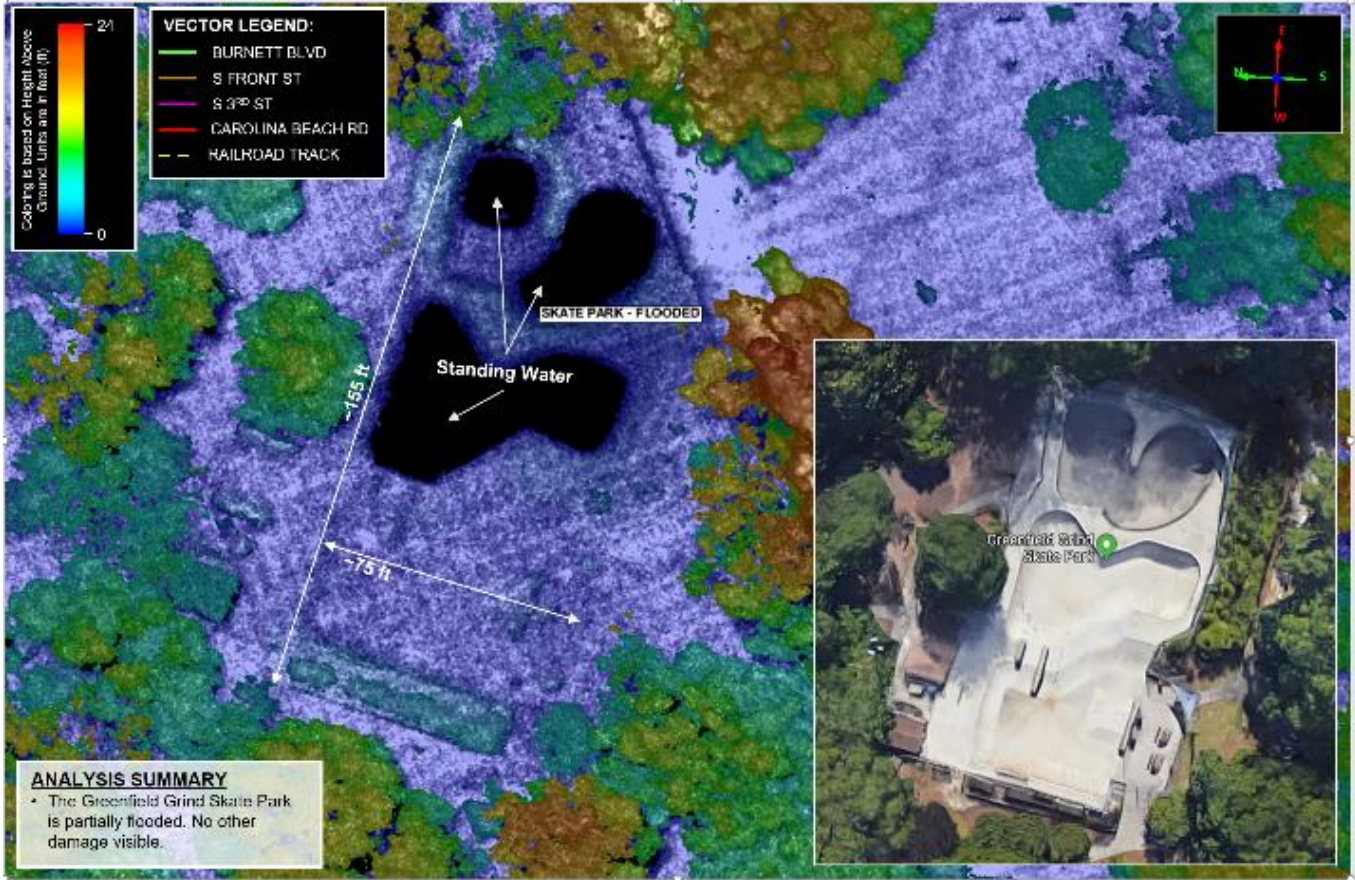
Figure 51. Standing water visible.

Public Building/Housing Sector GM-LIDAR Fact Sheet

Public Building-Related GM-LIDAR Capabilities

- Locating damaged/missing roofs
- Assessing damage to roofs
    - Length/width measurements of damage, height above ground of roof
- Identifying and quantifying total number of damaged buildings
- Measurement of buildings
    - Length, width, height measurements

Public Building-Related GM-LIDAR Limitations

- Cannot detect damage under (intact) roof
- Cannot detect damage smaller than .25 m in area
- Cannot detect damage under waterline in flooded area

Reporting Requirements	GM-LIDAR Applicable	Notes
Damaged/missing roofs	Yes	• Visual detection and/or confirmation • Measurements
Destroyed buildings	Yes	• Visual identification • Measurements
Total number of assets (buildings)	Yes	• Visual identification and quantification of damaged sites
Parcel identification (tax assessment)	No	• Can provide location of damaged sites to later look up parcel identification number
Measurements of buildings	Yes	• Height above ground, length/width/area of roof
Measurement of flood-level damage	No	• Cannot sense objects under waterline or inside structures

USE CASES: PUBLIC BUILDING/ HOUSING SECTOR
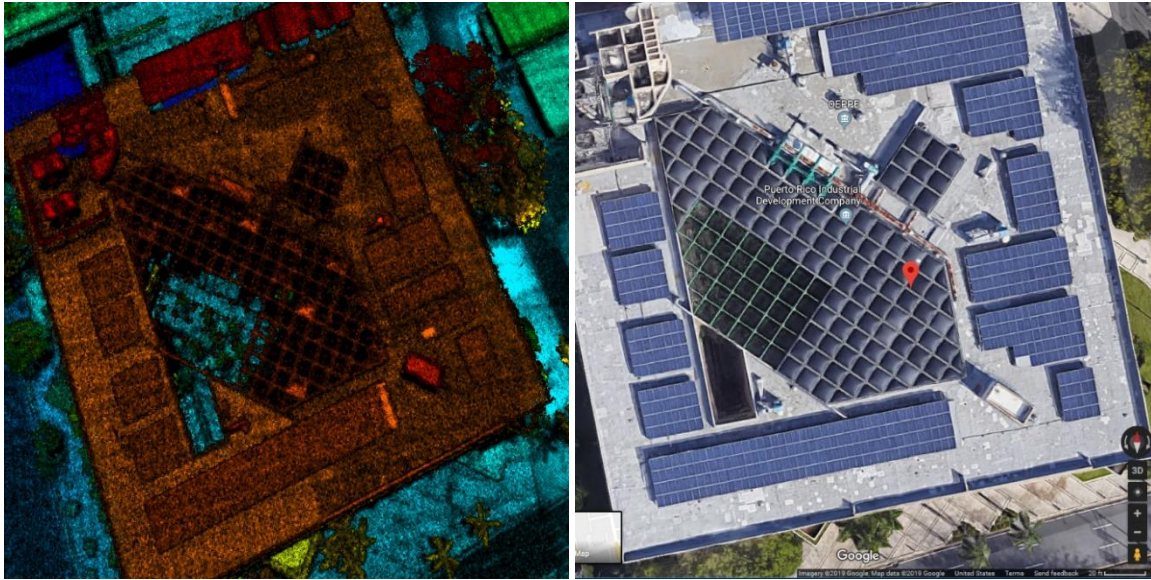
Figure 52. Identification of industrial building in Puerto Rico in post-hurricane GM-LIDAR point cloud (left). Comparing to Google Earth pre-disaster event imagery (right), we assess roof damage.
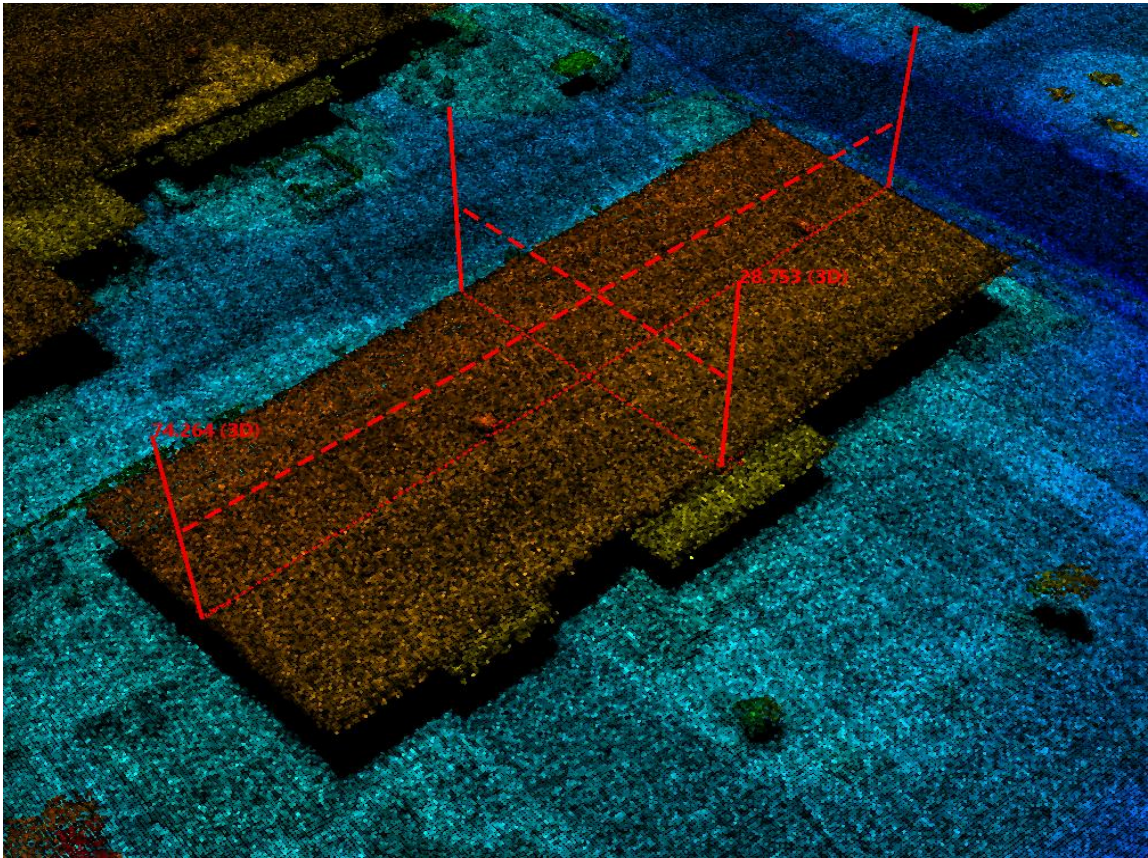
Figure 53. Example measurement of dimensions of intact roof.
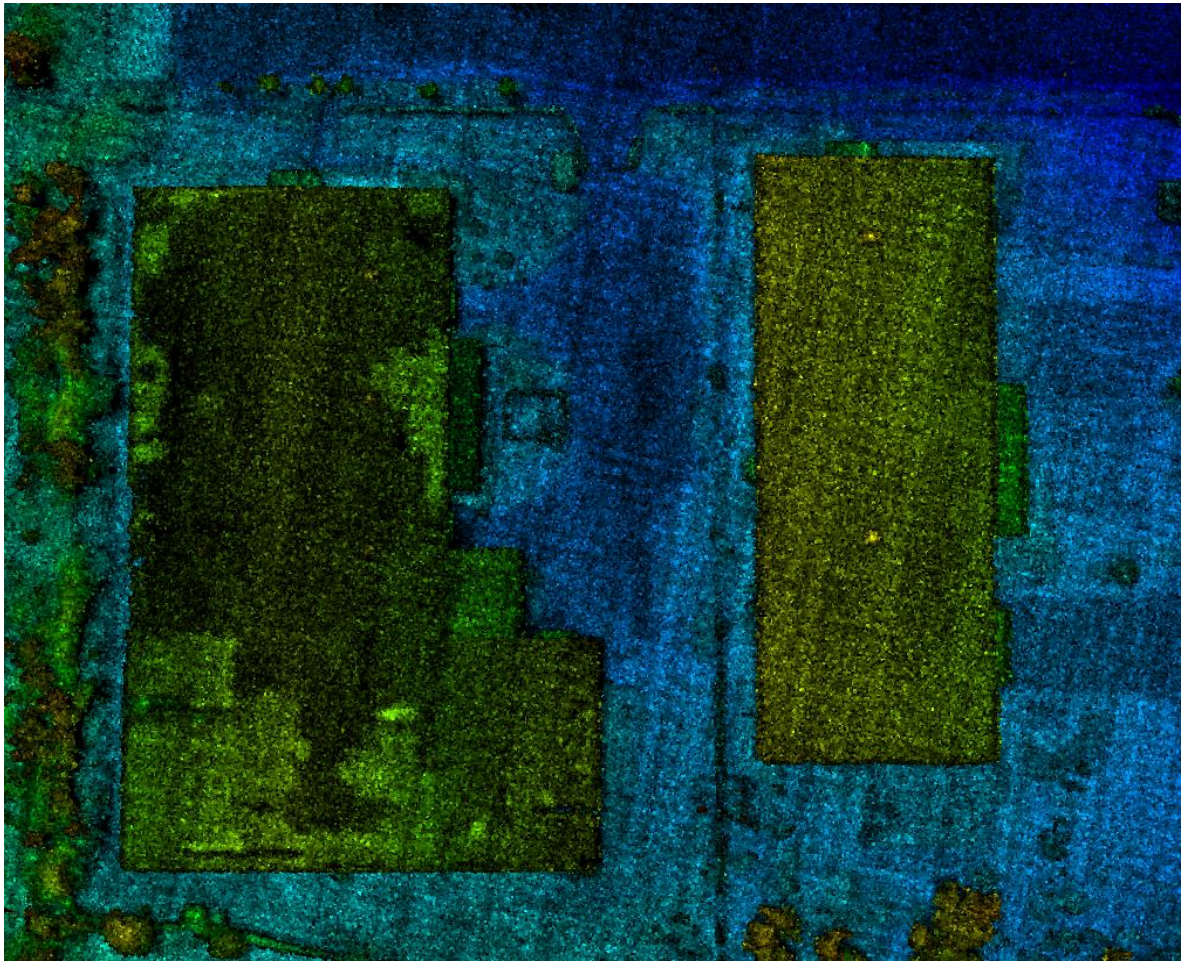
Figure 54. Example identification of roof damage by changes in height-above-ground (shown here as a color-scale) of roof surface in leftmost building. Compare to intact building roof's regular coloration on right.

Commonwealth Sector GM-LIDAR Fact Sheet

GM-LIDAR Capabilities: Commonwealth Sector

- Visualize structures correlated with GIS vector/point data
- Visual identification of damage to structures and infrastructure
- Measurements of damage:
    - Length
    - Width
    - Height
    - Volume

GM-LIDAR Limitations: Commonwealth Sector

- Precise georegistration over broad areas is in progress
- The richness of GM-LIDAR data makes viewing very large geographic areas computationally challenging; data visualization at a municipality scale does not require excessive computation

| Reporting Requirements	GM-LIDAR Applicable	Notes
Mapping of assets (fire, police, hospitals, etc.)	Yes	It would be possible to identify structures in GM-LIDAR data based on importing GIS vector data, but there may be some georegistration required
Mapping land parcels	No	There is no way to discern property boundaries from GM-LIDAR data.
Evaluate accuracy of field measurements for Project Worksheets (see **Figure 55** and **Figure 56**)	Yes	A user trained in the use of GM-LIDAR and the methodologies of site inspection can replicate field measurements using the data to validate those measurements based on visible damage. Some aspects of field measurements may not visible in the data (e.g., roadway depressions that are only a few inches); as such, discrepancies should take both sources into account

PAST SUCCESSFUL USE CASES: COMMONWEALTH SECTOR
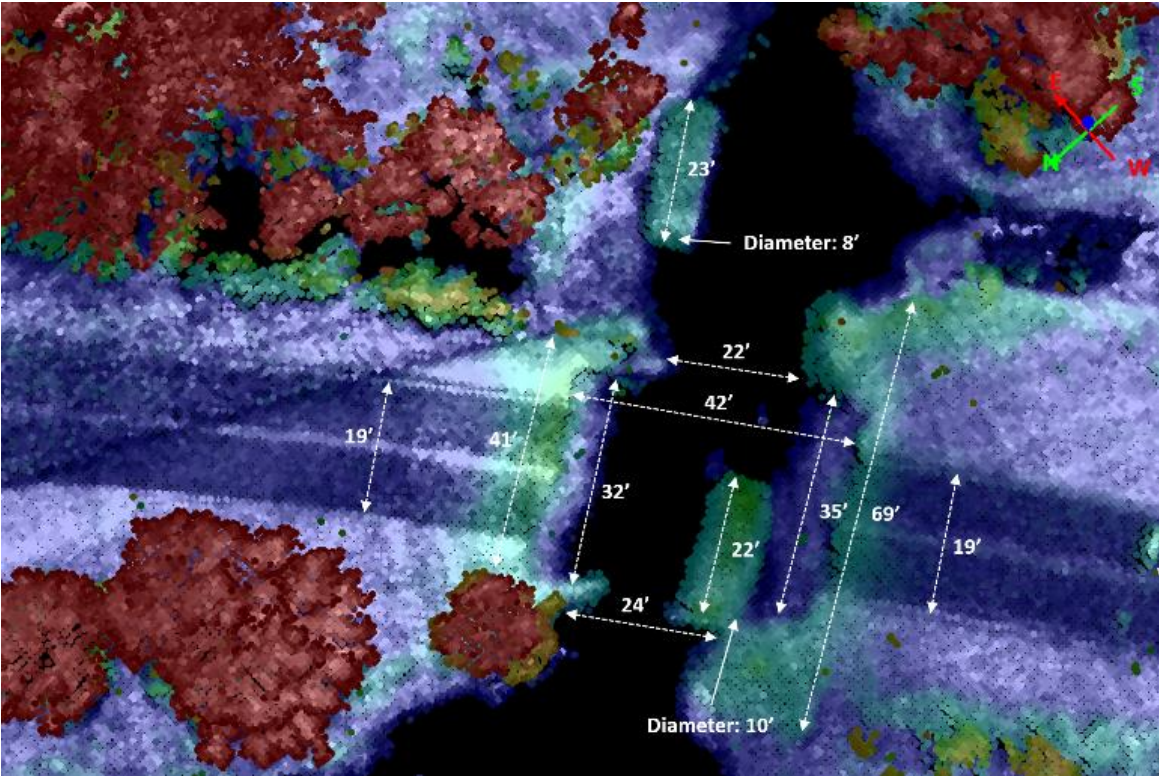
Figure 55. Documenting damage measurements.
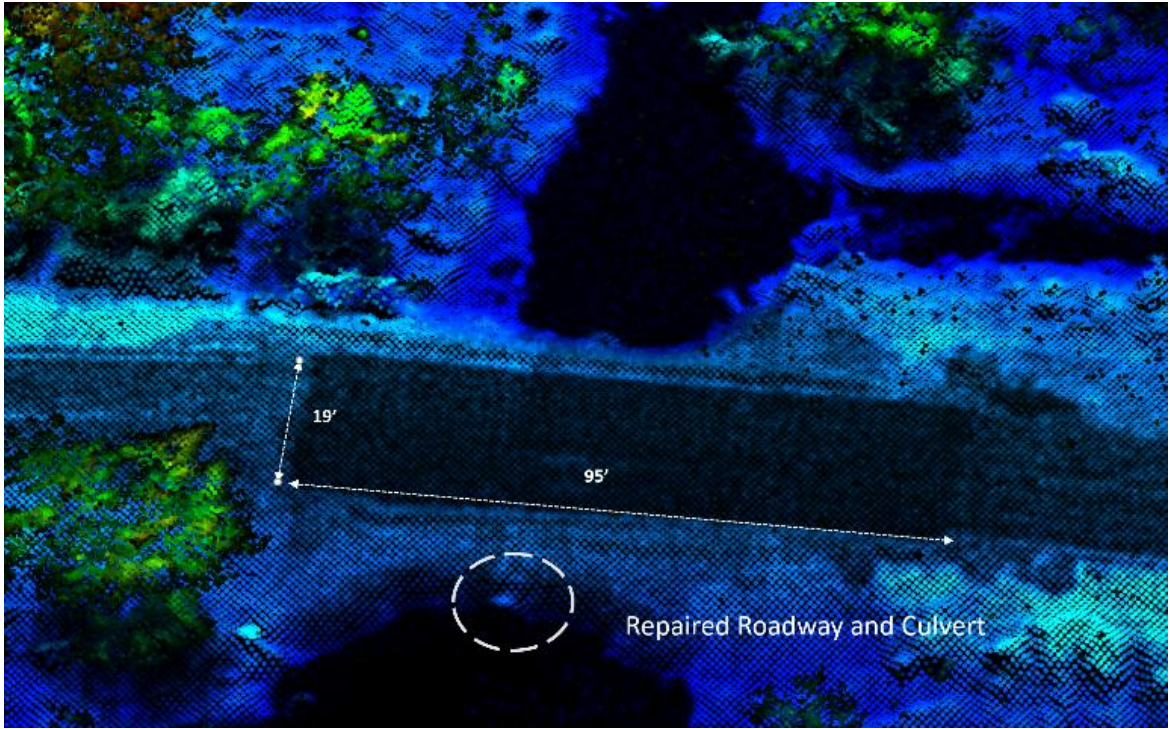
Figure 56. Documenting repair measurements.

Natural Culture Resources Sector GM-LIDAR Fact Sheet

GM-LIDAR Capabilities: Shoreline

- Visual identification of shoreline (see Figure 57)
- Measurements of shoreline and shoreline debris (see Figure 58)
  - o Length
  - o Width
  - o Height
  - o Volume
- Profile and cross-section analysis of shoreline
- Slope analysis
- Erosion and change detection (depending on data availability)

GM-LIDAR Limitations: Shoreline

- GM-LIDAR unable to penetrate water
- Slope or height changes that are small may not easily be detected (<25cm)
- Current data georegistration accuracy may not be high enough to compare with pre-event imagery, GM-LIDAR, or GIS vector data

Reporting Requirements	GM-LIDAR Applicable	Notes
Shoreline erosion	Yes	• Visual detection, confirmation and characterization of change detection (depending on data availability)
Shoreline debris	Yes	• Visual detection, confirmation and characterization • Volumetric measurements
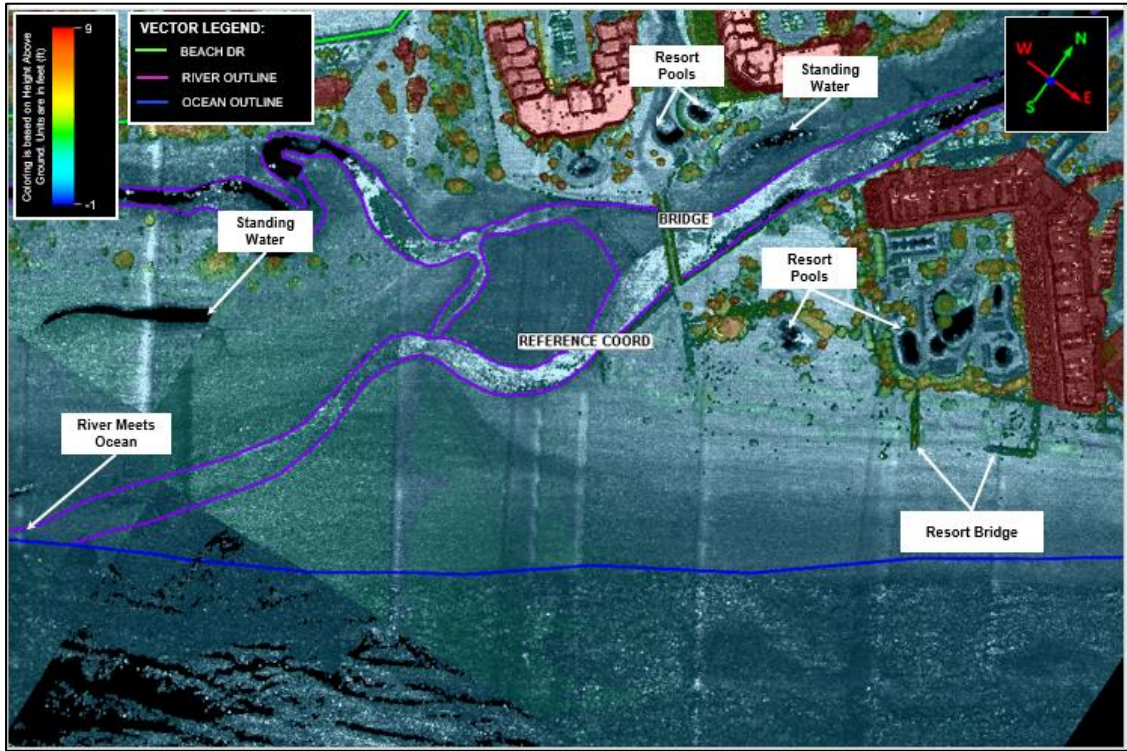
Figure 57. Visual detection, confirmation, and characterization of the shoreline.
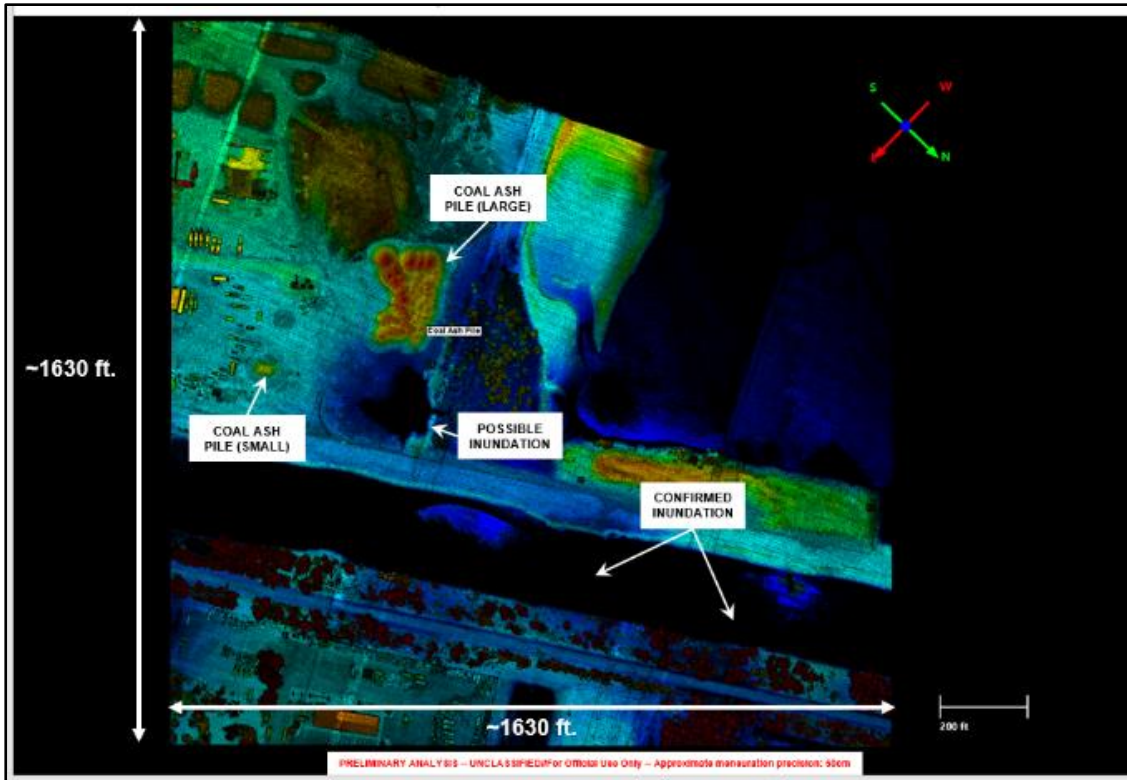
Figure 58. Measurements of shoreline features.

This page intentionally left blank.

APPENDIX B. ERSLA MESSAGE SPECIFICATION

Extended Remote Sensing Language (ERSLA) Message Specification

Humanitarian Assistance and Disaster Relief Systems Group
MIT Lincoln Laboratory
Version 0.1 [DRAFT]

BACKGROUND

The ERSLA message format was derived from the cursor on target (CoT) message format [1]. The CoT was designed to succinctly convey information regarding a point, a volume associated with that point, and attributes associated with that combination. This type of terse description and its associated format is valuable for emergency management in order to convey information about locations or entities that have been affected or damaged. The CoT XML-based message format is modified to convey information from remote sensing sources or even crowd-sourced data.

GENERAL FORMAT

The ERSLA message uses the extensible markup language (XML). The XML format allows for the message contents to be self-describing, enabling other tools to generate or parse an ERSLA message. The message is designed to convey those aspects from imagery or other "sensor" analysis products that are relevant for Humanitarian Assistance and Disaster Relief (HADR). The ERSLA message will contain attributes from a Base Message Schema Specification and, if appropriate, from a Details Sub-Schema Specification. The sub-schema is used to elaborate on the information contained in the base schema. Additionally, the ERSLA message shall be populated with a required set of attributes; these will be denoted by the value of **YES** in the *Required in Initial Message field* portion of the Attribute specification.

The general structure of an ERSLA Message follows:

```
<ERSLA_message>
    <base_message> base message schema </base_message>
    details subschema
</ERSLA_message>
```

The remainder of this specification details the attributes in the Base message schema and Details subschema.

ERSLA BASE SCHEMA

Attribute: **Unique Source ID**
Required in Message: **YES**
Default Value: None
Required in Update Message: No
Description: A unique ID generated by the Analytics Producer. This may be any alphanumeric string that uniquely describes the analysis product associated with this message. This string/ID will be used by ERSAT and the Analysis Producer in this and future messages to reference the Analysis Product that created the Initial ERSLA message. For example, if the MIT LL Airborne Optical Sensor platform collected GM-LIDAR over North Carolina on 23 September 2018 in support of Hurricane Florence and then subsequently conducted road damage and debris analysis, the road damage and debris analysis results would be communicated via ERSLA message, using the Unique Source Id = "*MITLLAOSTB_Florence_*23_SEP_2018".

Attribute: **Entity**
Required in Message: **YES**
Default Value: None
Required in Update Message: No
*Description***:** The observed entity type. One of the following entity types will be chosen from the dictionary below. Depending on the type of analysis product that is driving the report, certain pairs of Entity and Impact are generated. Depending on the Entity, an appropriate Impact and Magnitude dictionary will be selected to populate these attributes/elements of the point. The dictionary for Entity is currently limited to the high-level object types. For example, imagery may be able to inform that the damage is a "structure", but a second analysis is required to determine if that structure is a police station, hospital, shelter, etc.
Dictionary: {Unknown | Road | Structure | Debris | Dams | Energy | Water | Other}

Attribute: **Impact**
Required in Message: **No**
Default Value: None
Required in Update Message: No
*Description***:** The type or classification of the impact observed. One of the following entity types will be chosen from the dictionary below. Depending on the type of analysis product that is driving the report, certain pairs of Entity and Impact are generated. Depending on the Entity, an appropriate Impact and Magnitude dictionary will be selected to populate these attributes/elements of the point.
Dictionary: {N/A | Damage | Washout | Debris}

Attribute: **Magnitude**
Required in Message: **No**
Default Value: None

Required in Update Message: No
Description: The amount or degree of damage. It may be listed in one of the following categories or a numerical value may point to a separate "Magnitude Dictionary".
Dictionary: {No Damage | Destroyed | Major | Minor | Affected | Low | Medium | High}

*Attribute***: Collect Time**
Required in Message: **YES**
Default Value: None
Required in Update Message: No
Description: Time of collection in UTC: YYYY-MM-DD HH:MM:SS. For example, "2009-10-12 14:52:23"

Attribute: **Start Time**
Required in Message: **YES**
Default Value: None
Required in Update Message: No
Description: Time of message delivery in UTC: YYYY-MM-DD HH:MM:SS

Attribute: **Stale Time**
Required in Message: **No**
Default Value: None
Required in Update Message: No
Description: Optional, used for analytics with a cadence, i.e., flood extent UTC: YYYY-MM-DD HH:MM:SS

Attribute: **Point (lat/lon, [HAE, CE, LE])**
Required in Message: **YES**
Default Value: None
Required in Update Message: No
Description: Use the following set of "If statements" to determine how to populate this attribute.

- If a point-for-point located damage, each point will be a unique message:
  - lat/lon
  - HAE – 0.0 ?
  - CE - non-zero buffer area – default 1.0 meter?
  - LE – 0.0?

- If a Line segment:
  - lat/lon of segment center

- o HAE – 0.0
- o CE – 0.0
- o LE – 0.0
- o The endpoints of the segment will be described in the "*Details"* subschema section

- • If a polygon:
  - o lat/lon of complex hull surrounding the polygon centroid
  - o HAE – 0.0
  - o CE – 0.0
  - o LE – 0.0
  - o The polygon coordinates will be defined in the *"Details"* subschema section

- • If a raster:
  - o lat/lon of complex hull centroid of the raster data's footprint
  - o HAE – 0.0
  - o CE – 0.0
  - o LE – 0.0
  - o The polygon of the raster boundary will be defined in the *"Details"* subschema section

ERSLA DETAILS SUB-SCHEMA

Attribute: **Geometry Extension Type**
Required in Message: **Only if geometry is not a point type**
Default Value: None
Required in Update Message: No
Description:
If the geometry is other than a point, then use the following guide to determine how to populate this attribute.

- • For a polyline
  - o Two-element list containing the lat/lon of each of the endpoints
- • Polygon: stored as a geometric primitive or as a list containing the vertices coordinates

EITHER

- o A geometric primitive denoted with one of two keywords, followed by a list that describes the geometry

    - ellipse

        - [lat/lon, semi-minor len., semi-major len, angle]

    - rectangle

        - [lat/lon, lat/lon, lat/lon, lat/lon]

OR

- o [lat/lon, lat/lon, … lat/lon]

- Raster: list of the raster bounding box or vertices

    - o [lat/lon, lat/lon, … lat/lon]

Attribute: **Incident**
Required in Message: **No**
Default Value: None
Required in Update Message: No
Description: The event or incident name.

Attribute: **Sensor ID**
Required in Message: **No**
Default Value: None
Required in Update Message: No
Description: A unique ID (an alphanumeric string) to identify the sensor, i.e., name – serial number.

Attribute: **Platform**
*Required in Message***: No**
Default Value: None
Required in Update Message: No
Description: A description of the platform that collected the initial data.
Dictionary: {Airborne | Space | Ground | On Water | Under Water | Crowd-Sourced}

Attribute: **Analytics**
Required in Message: **No**
Default Value: None
Required in Update Message: No
Description: How analysis was done.
Dictionary: {Automated | Manual | Interferometry | Change Detection | Other: Specific}

Attribute: **Confidence**
Required in Initial Message: **No**
Default Value: None
Required in Update Message: No
Description: The percent certainty (numeric value 0–100), for example, the area under the ROC curve.

Attribute: **Confirmed**
Required in Initial Message: **No**
Default Value: None
Required in Update Message: No
Description: Human-in-the-loop confirmation of detection; validated or not. When this flag is set, all of the other attributes remain the same.
Dictionary: {True | False}

Attribute: **Format**
Required in Initial Message: **No**
Default Value: None
Required in Update Message: No
Description: The original type of data that served as the source of the message.
Dictionary: {las | ept | | tiff | jpg | obj | blend | fbx | gltf | dxf | stl | wrl | other }

Attribute: **Access**
Required in Initial Message: **No**
Default Value: None
Required in Update Message: No
Description: URL/path to get source. Use Source/Access to determine where to get the remotely sensed data and which visualization tool to use to view/interact to allow user to set Confirmed value. NOTE: This may be the same as the Unique Source ID. This Attribute has the following Credentials sub-attribute and the supporting attributes. If credentials are required to access the resource, then the credentials are listed in this section.
Credentials: This is the information required to access the source data at the URL/path in **Access Credentials**

> **Username –** To access the URL
> **Password –** Associated with the username
> **Additional_Info –** Any additional information that is needed to access the source URL

Attribute: **Additional Details**
*Required in Initial Message***: No**
Default Value: None
Required in Update Message: No
Description: These details will be based on the **Type:Entity** as defined in the ERSLA base schema.)

- Road – {Name, Width, Surface}

- Bridge – {Name, Width, Type, Load Capacity, Surface}

- Levee – {Name, Width, Height, Construction Material}

- Runway – {Name, Width, Length, Surface, Heading, Lowest Elevation}

- Railroad Tracks – {Name, Gauge/Width}

- Utility Lines – {Name, Number(?), Power, Voltage, AC | DC, Type: Power | Telecom | Fiber}

- Pipeline – {Name, Diameter, Type: Water | Sewer | Liquid Petroleum | Natural Gas | Unknown}

- Debris Pile – {Name, Type: Landfill | Construction | Other | Unknown}

- Structure – {Name, Height, Construction: Wood | Concrete | Steel | Unknown}

Attribute: **Notes**
Required in Message: **No**
Default Value: None
Required in Update Message: No
Description: Free text field, but limited in size (255 chars) in order to minimize message size.

SAMPLE MESSAGE

The following is an example of a well-formed ERSLA message:

```
<?xml version="1.0" standalone="yes"?>
<ERSLA_message>
    <base_message collect_time="2020-02-20 12:00:00.00" entity="Debris" message_type="initial"
    start_time="2020-02-20                12:00:00.00"                unique_source_id="AOSTB_2019-c3-
    ma_sortie0127_tile_X689_Y873" />
    <point ce="32" hae="2" lat="42.309734520499056" le="0" lon="-71.35983231328902" />
    <geometry_extension description_list="42.30972394813766,-71.3598272387995 42.309726592661356,-
    71.3598272387995  42.30972923718505,-71.3598272387995  42.30973188170874,-71.3598272387995
    42.30973452623244,-71.3598272387995                        42.30973717075614,-71.3598272387995
    42.30973981527983,-71.3598272387995                        42.30974245980353,-71.3598272387995
    42.30974510432723,-71.3598272387995                        42.309747748850924,-71.3598272387995
    42.309747790333645,-71.35982728028223                      42.309747790333645,-71.35982992480592
    42.309747790333645,-71.35983256932961                      42.30974780045138,-71.35983521385332
    42.309747748850924,-71.35983542541521                      42.30974753728903,-71.35983521385332
    42.30974510432723,-71.35983278089151                       42.30974245980353,-71.35983267511057
    42.30973981527983,-71.3598326375754                        42.30973717075614,-71.35983262093008
    42.30973452623244,-71.35983262093008                       42.30973188170874,-71.3598326375754
    42.30972923718505,-71.35983267511057                       42.309726592661356,-71.35983278089151
    42.309724159699556,-71.35983521385332                      42.30972405391861,-71.359837858377
    42.30972394813766,-71.3598380699389 42.30972389653719,-71.359837858377 42.30972389653719,-
```

71.35983521385332 42.30972390665493,-71.35983256932961 42.30972390665493,-71.35982992480592 42.30972390665493,-71.35982728028223 42.30972394813766,-71.3598272387995" geom_type="polygon" primative="" />
<message_details access="access_1" additional_details="" analytics="CNN" confidence="-1" confirmed="False" impact="Damage" incident="Incident 1" magnitude="Affected" message_id="3129" platform="Airborne" published="False" sensor_id="1" source="Point Cloud" stale_time="2020-02-20 12:00:00.00" />
<additional_details name="foo_pile" type="landfill" />
</ERSLA_message>

REFERENCES

1. U. G. Survey, "3DEP LIDAR Base Specification 2020 Rev. A," September 2020. [Online]. Available: https://www.usgs.gov/core-science-systems/ngp/ss/lidar-base-specification-table-contents. [Accessed 15 December 2020].

2. NOAA , "National Geodetic Survey," [Online]. Available: https://www.ngs.noaa.gov/datums/vertical/puerto-rico-vertical-datum-2002.shtml.

3. NGA, "Geospatial Repository and Data (GRiD) Management System," [Online]. Available: https://grid.nga.mil/devgrid/accounts/login/.

4. Entwine, [Online]. Available: https://entwine.io/.

5. Potree, "Potree," [Online]. Available: http://www.potree.org/.

6. Unity, "Unity Game Engine," [Online]. Available: https://unity.com/.

7. National Institute of Standards and Technology, "Learning from Hurricane Maria's Impacts on Puerto Rico," January 2021. [Online]. Available: https://www.nist.gov/topics/disaster-failure-studies/hurricane-maria/progress. [Accessed 2021].

8. OGC, "OGC 12-007r2," 3 December 2020. [Online]. Available: http://docs.opengeospatial.org/is/12-007r2/12-007r2.html.

9. NGA, "Binary Point File 3 (BPF3), BPF Public License File Format Definition, Implementation Guide v1.1," 3 December 2020. [Online]. Available: https://nsgreg.nga.mil/doc/view?i=4220..

10. J.-E. D. B. M. F. G. Y. L. G. Hughes Thomas, "Semantic Classification of 3D Point Clouds with Multiscale Spherical Neighborhoods," 1 August 2018. [Online]. Available: https://arxiv.org/pdf/1808.00495.pdf. [Accessed November 2019].

11. NOAA, "The NOAA Continuously Operating Reference Stations (CORS) Network," [Online]. Available: https://geodesy.noaa.gov/CORS/.

12. Federal Aviation Administration, "Advisory Circular: Survey and Data Standards for Submission of Aeronautical Data Using Airports GIS," 30 09 2015. [Online]. Available: https://www.faa.gov/documentLibrary/media/Advisory_Circular/150-5300-18C.pdf. [Accessed 2019].

13. U.S. Department of Transportation Federal Highway Administration, "Standard Specifications for Construction of Roads and Bridges onFederal Highway Projects (FP-14)," 2014. [Online]. Available: https://highways.dot.gov/federal-lands/specs. [Accessed 2019].

14. MITRE , "Cursor On Target Specification," [Online]. Available: https://www.mitre.org/sites/default/files/pdf/09_4937.pdf.

15. Wikipedia, "Emergency Data Exchange Language (EDXL)," [Online]. Available: https://en.wikipedia.org/wiki/EDXL.

16. Keycloak, "Open Source Identity and Access Management," [Online]. Available: https://www.keycloak.org/.

17. GeoServer, [Online]. Available: http://geoserver.org/.

18. PostgreSQL, "PostgreSQL: The World's Most Advanced Open Source Relational Database," [Online]. Available: https://www.postgresql.org/.

19. NGINX, "NGINX," [Online]. Available: https://nginx.org/en/.

20. CentOS, "The CentOS Project," [Online]. Available: https://www.centos.org/.

21. Ubuntu, "Ubuntu: The new standard secure enterprise Linux for servers, desktops, clouds, developers and things," [Online]. Available: https://ubuntu.com/.

22. Amazon, "Amazon Elastic Compute Cloud (EC2)," [Online]. Available: https://aws.amazon.com/ec2/.